Master thesis and internship[BR]- Master's thesis : Assessing the robustness of the acceleration surface method[BR]- Internship

Auteur : Ghysens, François
Promoteur(s) : Kerschen, Gaëtan
Faculté : Faculté des Sciences appliquées
Diplôme : Master en ingénieur civil en aérospatiale, à finalité spécialisée en "aerospace engineering"
Année académique : 2023-2024
URI/URL : http://hdl.handle.net/2268.2/20237

UNIVERSITY OF LIÈGE
SCHOOL OF ENGINEERING AND COMPUTER SCIENCE

Assessing the robustness of the acceleration surface method

Master's thesis completed in order to obtain the degree of Master of Science in Aerospace Engineering by

GHYSENS François

Supervisor: KERSCHEN Gaëtan

Academic year 2023-2024

Abstract

Nonlinearities are an important aspect to consider in the study of the vibrations of a structure, as they can influence the dynamics of the analysed system, resulting in unexpected behaviours. Nonlinear system identification aims at finding a mathematical model of the structure taking into account the nonlinear forces. One method used in the nonlinear system identification is the acceleration surface method, which helps at determining the functional form of these nonlinear forces by creating stiffness and damping curves. While the method has proven to work well in real-life applications, some artefacts sometimes appear in the stiffness and damping curves, making it more difficult to correctly interpret these curves. The aim of this work is thus to understand their origin and determine how the curves can be improved.

For this purpose, the acceleration surface method is applied to systems composed of 1, 2 and 10 degrees of freedom, whose response to sine sweep excitations is obtained through numerical integration. The nonlinearities consist of a cubic stiffness, a piecewise linear stiffness and Coulomb friction, which are all common types of nonlinearities encountered in real-life structures.

The analysis of the stiffness and damping curves obtained for the different systems reveals that the presence of harmonic components in the response of the system to the excitation can impact the curves, such that the curves can be composed of different lines, which can complicate the determination of the functional form of the nonlinear forces. Such phenomena particularly occur at superharmonic resonances and modal interactions. An effective way to improve the curves in such cases is the use of filters to remove the harmonic components from the response of the system to the excitation. Furthermore, in multiple degree of freedom systems, the linear forces that have been ignored in the equation of the acceleration surface method are responsible for the quality of the stiffness and damping curves. Applying the method to modes for which these forces are small thus yields better results. In particular, modes for which the neighbouring degrees of freedom of the linear connections oscillate in phase with the degree of freedom to which the acceleration surface method is applied have shown to produce better results. The position of the excitation and the extremity of the nonlinear connection to consider in the acceleration surface method also influence the quality of the stiffness and damping curves.

While the identification of the stiffness force can be done successfully in most cases, the functional form of the damping force remains difficult to determine with the acceleration surface method and it can only be found in some specific cases. The artefacts in the stiffness and damping curves can be explained by several phenomena, but are always due to the terms neglected in the equation of the acceleration surface method.

Acknowledgements

First of all, I would like to thank Professor Gaëtan Kerschen for allowing me to do this thesis at the University of Liège and for his precious advice throughout this work.

I would also like to thank all the other members of the Space Structures and Systems Laboratory for their advice and help.

Finally, I would like to thank my family who supported me during my thesis as well as during all my studies.

Contents

List of Figures

List of Tables

Chapter 1

Introduction

Nonlinearities are becoming more and more important in the study of aerospace and mechanical structures. They can occur for various reasons, such as large displacements, material properties, friction or boundary conditions [1]. Nonlinear vibrations can result in unexpected behaviours of the structure, such as a shift in the resonance frequencies or even the appearance of new resonances. The behaviour of a nonlinear structure can therefore be difficult to analyse and predict using a linear model of the structure, for which the equations governing the dynamics of the system are given by

$$\mathbf{M}\ddot{\mathbf{q}} + \mathbf{C}\dot{\mathbf{q}} + \mathbf{K}\mathbf{q} = \mathbf{p}(t), \tag{1.1}$$

where $\mathbf{M}$, $\mathbf{C}$ and $\mathbf{K}$ are respectively the mass, damping and stiffness matrices of the system, $\mathbf{q}$ is the displacement vector and $\mathbf{p}(t)$ the vector of the applied force varying with the time t. If the dynamics of the system is nonlinear, the equations become

$$\mathbf{M}\ddot{\mathbf{q}} + \mathbf{C}\dot{\mathbf{q}} + \mathbf{K}\mathbf{q} + \mathbf{f}_{\text{nl}}(\mathbf{q}, \dot{\mathbf{q}}) = \mathbf{p}(t), \tag{1.2}$$

where $\mathbf{f}_{\text{nl}}(\mathbf{q}, \dot{\mathbf{q}})$ is the vector of nonlinear forces depending on the displacement $\mathbf{q}$ and the velocity $\dot{\mathbf{q}}$. As this considerably changes the behaviour of the structure, methods used to analyse and predict the motion of linear systems cannot be applied to nonlinear systems. The use of specific tools to study the nonlinearities is thus required.

1.1 Nonlinear system identification

An important aspect of the study of nonlinear dynamics is the identification of nonlinear systems, which aims at creating a mathematical model of the real structure under study. The goal is therefore to find an analytical expression of the nonlinear forces $\mathbf{f}_{\text{nl}}(\mathbf{q}, \dot{\mathbf{q}})$, such that the behaviour of the system can be accurately predicted with a numerical model of the structure. This nonlinear system identification (NSI) is achieved through the analysis of experimental measurements and is done in three steps [1].

The first step is the nonlinearity detection step, whose goal is to determine whether the structure behaves in a nonlinear way or not. This can be done by applying a sine sweep excitation to the structure, which consists of a sine excitation whose frequency varies with time. A visual analysis of the time series of the response can already reveal a nonlinear behaviour of the system [2]. Indeed, a nonlinear system may exhibit a jump phenomenon, the amplitude of

the displacement suddenly decreasing. Furthermore, the principle of superposition does not hold true anymore for nonlinear systems and the resonance frequency is dependent on the forcing level. Other hints at a nonlinear behaviour of the structure are the presence of harmonics in the response, a difference in the response envelope between sine sweep excitations with an increasing frequency and a decreasing frequency or even the appearance of a new resonance [3]. The detection of a nonlinearity is thus not especially difficult, but is of high importance, as it determines whether the construction of a nonlinear model of the structure is necessary, such a model being more challenging to obtain.

The second step of NSI is the characterisation step. It follows the determination of the fact that the system is nonlinear through the detection step. It aims at finding the location of the nonlinearity, understanding the physics behind it and finding a functional form of the nonlinear forces $\mathbf{f}_{\text{nl}}(\mathbf{q}, \dot{\mathbf{q}})$. One of the tools used to find the functional form of the nonlinear forces is the acceleration surface method (ASM), which is a simplified version of the restoring force surface (RFS) method [4]. It only requires acceleration measurements at both extremities i and j of a nonlinear connection, which is illustrated in Figure 1.1.

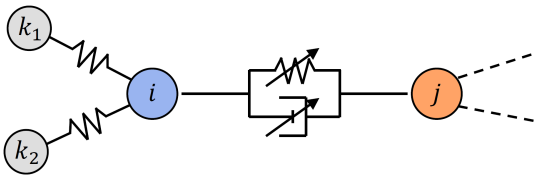

Figure 1.1: Nonlinear connection and its extremities i and j [5].

From the acceleration, the velocity and the displacement can be obtained by integration using the trapezium rule and high-pass filtering [6]. The acceleration surface method then results from Newton's second law applied to the degree of freedom (DOF) i, which is given by

$$\sum_k m_{i,k}\,\ddot{q}_k + g_i(q,\dot{q}) = p_i \tag{1.3}$$

where $m_{i,k}$ is the element (i,k) of the mass matrix $\mathbf{M}$, q_k is the displacement of degree of freedom k, g_i is the internal force exerted on degree of freedom i and p_i is the external force applied to degree of freedom i. In this equation, only the terms related to the nonlinear connection between degrees of freedom i and j are retained, which results in the equation

$$m_{i,i}\,\ddot{q}_i + g_i\left(q_i - q_j, \dot{q}_i - \dot{q}_j\right) \cong p_i. \tag{1.4}$$

The external force is also neglected and the mass $m_{i,i}$ is dropped as it can be seen as a simple scaling factor, which gives the equation

$$g_i\left(q_i - q_j, \dot{q}_i - \dot{q}_j\right) \cong -\ddot{q}_i. \tag{1.5}$$

The force g_i, which is the sum of the stiffness and damping forces between degrees of freedom i and j and is supposedly nonlinear, can thus be approximated by the opposite of the acceleration at degree of freedom i. The acceleration surface method then consists in representing $-\ddot{q}_i$ as a function of the relative displacement $q_i - q_j$ and the relative velocity $\dot{q}_i - \dot{q}_j$, creating a three-dimensional surface of the acceleration, hence the name of the method. This surface can also be represented in a two-dimensional way by plotting $-\ddot{q}_i$ as a function of the relative

displacement for $\dot{q}_i - \dot{q}_j = 0$ and as a function of the relative velocity for $q_i - q_j = 0$. The resulting curves are called the stiffness curve and the damping curve respectively, as they allow to visualise the functional form of the stiffness and damping forces of the nonlinear connection. These curves can then be used to determine whether the stiffness or the damping force is nonlinear and how it can be modelled by mathematical functions.

The last step of the nonlinear system identification is the parameter estimation, which can be achieved using the restoring force surface method [7]. This method is the general form of the ASM method, which is derived from it. Its goal is to find the parameters of the nonlinear model using the functional form of the nonlinear forces determined in the previous step. Newton's second law states that

$$\mathbf{M}\ddot{\mathbf{q}} + \mathbf{f}(\mathbf{q}, \dot{\mathbf{q}}) = \mathbf{p}(t), \tag{1.6}$$

where $\mathbf{f}(\mathbf{q}, \dot{\mathbf{q}})$ is the restoring force composed of the stiffness and damping forces of the system. This equation can be rewritten as

$$\mathbf{f}(\mathbf{q}, \dot{\mathbf{q}}) = \mathbf{p}(t) - \mathbf{M}\ddot{\mathbf{q}}. \tag{1.7}$$

Knowing $\mathbf{M}$ and obtaining $\mathbf{p}(t)$ and $\ddot{\mathbf{q}}$ from experimental measurements, the restoring force $\mathbf{f}(\mathbf{q}, \dot{\mathbf{q}})$ can also be obtained. Assuming a functional form of the nonlinear restoring force obtained from the characterisation step, an estimation of this nonlinear force is given by

$$\hat{\mathbf{f}}_{\mathrm{nl}}(\mathbf{q}, \dot{\mathbf{q}}) = \sum_{i=1}^{M} k_i \, \mathbf{f}_i(\mathbf{q}, \dot{\mathbf{q}}), \tag{1.8}$$

where $\mathbf{f}_i(\mathbf{q}, \dot{\mathbf{q}})$ are the M assumed functional forms of the nonlinear force and k_i are the M parameters to be estimated with the RFS method. From this expression of the nonlinear force, the equation

$$[\mathbf{f}_1(\mathbf{q}, \dot{\mathbf{q}}) \ \cdots \ \mathbf{f}_M(\mathbf{q}, \dot{\mathbf{q}})] \begin{bmatrix} k_1 \\ \vdots \\ k_M \end{bmatrix} = \mathbf{p}(t) - \mathbf{M}\ddot{\mathbf{q}} - \mathbf{C}\dot{\mathbf{q}} - \mathbf{K}\mathbf{q} \tag{1.9}$$

can be obtained. Knowing the external force $\mathbf{p}(t)$ and the displacement $\mathbf{q}$, velocity $\dot{\mathbf{q}}$ and acceleration $\ddot{\mathbf{q}}$ at Q different times $t_i, \ldots, t_Q$, with $Q > M$, one obtains an overdetermined system of equations

$$\begin{bmatrix} \mathbf{f}_1(\mathbf{q}(t_1), \dot{\mathbf{q}}(t_1)) & \cdots & \mathbf{f}_M(\mathbf{q}(t_1), \dot{\mathbf{q}}(t_1)) \\ & \vdots & \\ \mathbf{f}_1(\mathbf{q}(t_Q), \dot{\mathbf{q}}(t_Q)) & \cdots & \mathbf{f}_M(\mathbf{q}(t_Q), \dot{\mathbf{q}}(t_Q)) \end{bmatrix} \begin{bmatrix} k_1 \\ \vdots \\ k_M \end{bmatrix} = \begin{bmatrix} \mathbf{p}(t_1) - \mathbf{M}\ddot{\mathbf{q}}(t_1) - \mathbf{C}\dot{\mathbf{q}}(t_1) - \mathbf{K}\mathbf{q}(t_1) \\ \vdots \\ \mathbf{p}(t_Q) - \mathbf{M}\ddot{\mathbf{q}}(t_Q) - \mathbf{C}\dot{\mathbf{q}}(t_Q) - \mathbf{K}\mathbf{q}(t_Q) \end{bmatrix}, \tag{1.10}$$

for which the parameters k_i are the unknowns. The least-squares solution of this system of equations is given by

$$\begin{bmatrix} k_1 \\ \vdots \\ k_M \end{bmatrix} = \begin{bmatrix} \mathbf{f}_1(\mathbf{q}(t_1), \dot{\mathbf{q}}(t_1)) & \cdots & \mathbf{f}_M(\mathbf{q}(t_1), \dot{\mathbf{q}}(t_1)) \\ & \vdots & \\ \mathbf{f}_1(\mathbf{q}(t_Q), \dot{\mathbf{q}}(t_Q)) & \cdots & \mathbf{f}_M(\mathbf{q}(t_Q), \dot{\mathbf{q}}(t_Q)) \end{bmatrix}^{\dagger} \begin{bmatrix} \mathbf{p}(t_1) - \mathbf{M}\ddot{\mathbf{q}}(t_1) - \mathbf{C}\dot{\mathbf{q}}(t_1) - \mathbf{K}\mathbf{q}(t_1) \\ \vdots \\ \mathbf{p}(t_Q) - \mathbf{M}\ddot{\mathbf{q}}(t_Q) - \mathbf{C}\dot{\mathbf{q}}(t_Q) - \mathbf{K}\mathbf{q}(t_Q) \end{bmatrix}. \tag{1.11}$$

This method can result in an accurate determination of the nonlinear parameters [3]. However, it requires the knowledge of the entire mass, stiffness and damping matrices of the structure, which may be difficult to obtain in practice for a real-life structure. Furthermore, its results depend on the correct estimation of the functional form of the nonlinear force done in the characterisation step. This second step is thus of crucial importance and the acceleration surface method needs to enable a precise determination of this functional form. Once the parameters have been computed, the nonlinear system identification is complete and an accurate mathematical model of the nonlinear structure can be built.

1.2 Acceleration surface method applied to real structures

The acceleration surface method has already been successfully applied to simple real-life nonlinear systems, such as a cantilever beam [8] and a clamped-clamped beam [9] having a polynomial stiffness. It has also been applied to more complex aerospace structures, such as the SmallSat spacecraft structure [2], aircraft such as the F-16 aircraft [10] and the Morane-Saulnier Paris aircraft [11] or an aircraft Piccolo tube [12], for which nonlinearities were detected at the connection between two substructures. Applying the ASM to the nonlinear connections of these systems revealed the presence of a piecewise linear stiffness and the clearance of the connection could be estimated from the stiffness curve. The presence of Coulomb friction was also detected with the ASM for the F-16 aircraft [10].

However, the ASM may sometimes lead to unwanted artefacts in the stiffness and damping curves, which can make the characterisation of the nonlinearity more difficult. In particular, for the case of the SmallSat structure, the stiffness curve depicted in Figure 1.2 presents some unexpected artefacts. Indeed, while the slope of the curve increases at a positive displacement corresponding to the clearance of the connection, a part of the curve that is decreasing also appears at such a displacement. A similar observation can also be made at negative displacements. Furthermore, such an artefact is also visible in the case of the aircraft Piccolo tube [12].

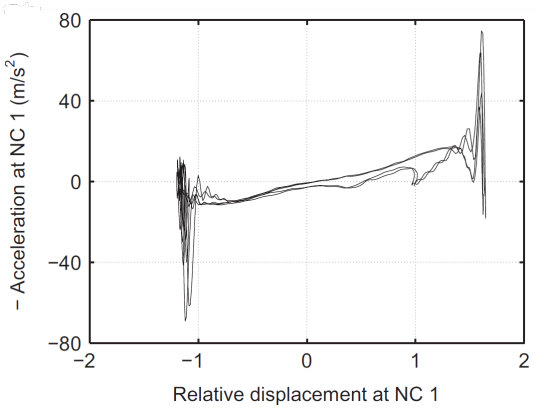

Figure 1.2: Stiffness curve of the nonlinear connection of the SmallSat structure [2].

Applying a qualitative version of the RFS method similar to the ASM to two different modes of the spacecraft structure simultaneously, the stiffness curve in Figure 1.3 is obtained. It can be seen that the two modes result in curves with different slopes, both being inexact.

Furthermore, the curve with the highest slope is composed of two separate lines connecting together at the maximum relative displacement.

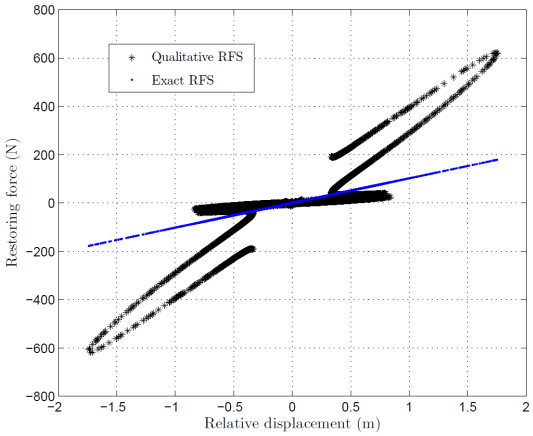

Figure 1.3: Stiffness curve for two different modes of the SmallSat structure [13].

With the experimental data of the ground vibration testing of the F-16 aircraft for a forcing level of 67 N [14], the ASM can be applied to both extremities of the nonlinear connection between the wing and the payload and to different modes. It is first applied to the third vibration mode and to the extremity of the nonlinear connection corresponding to the payload. The stiffness and damping curves are represented in Figure 1.4.

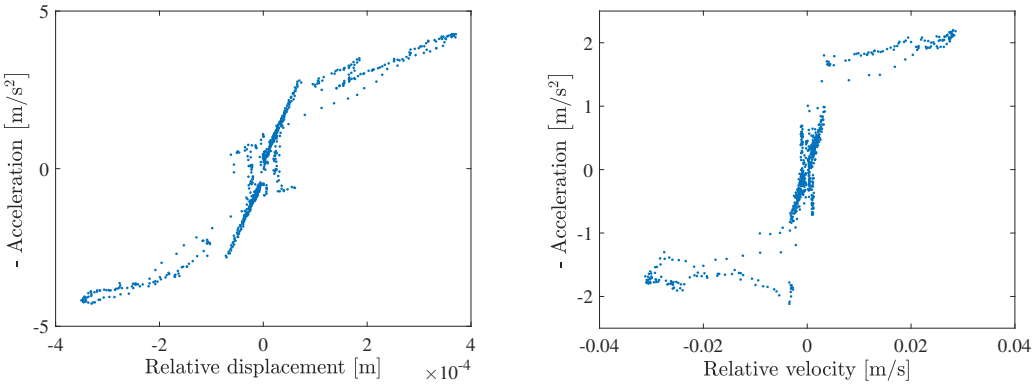

(a) Stiffness curve. (b) Damping curve.

Figure 1.4: Stiffness and damping curves of the third mode of the F-16 aircraft for which the ASM is applied to the payload.

As can be seen, both the presence of a piecewise linear stiffness and Coulomb friction can easily be deduced from the curves and the ASM produces good results. However, applying the method to other modes may not always yield such good results. Indeed, for the second mode, the stiffness and damping curves shown in Figure 1.5 are obtained. From these curves, nothing can be concluded about the functional form of the stiffness and damping forces at the connection between the wing and the payload.

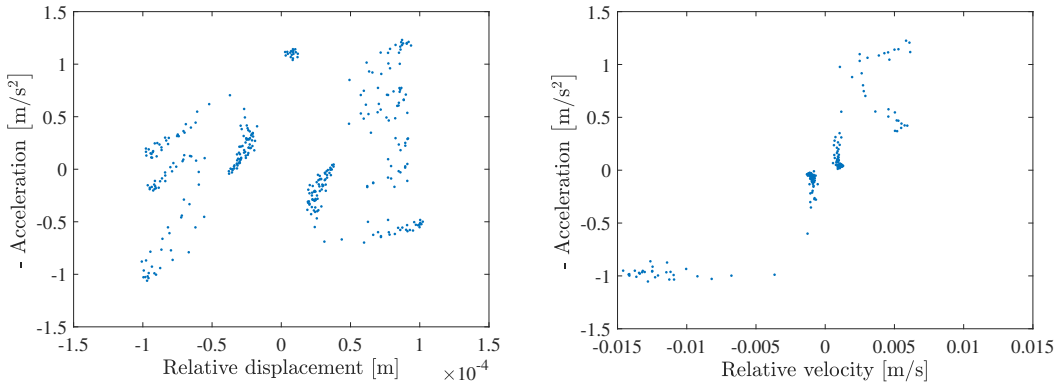

(a) Stiffness curve. (b) Damping curve.

Figure 1.5: Stiffness and damping curves of the second mode of the F-16 aircraft for which the ASM is applied to the payload.

The ASM is now applied to the wing side of the nonlinear connection and to mode 3. The obtained stiffness and damping curves are depicted in Figure 1.6. The stiffness curve is similar as when the ASM is applied to the payload side of the connection, but the curve decreases as the relative displacement increases. The stiffness may thus be interpreted as a negative stiffness, while it is in reality positive. Furthermore, the damping curve exhibits a different behaviour as for the previous cases and from which the presence of Coulomb friction cannot be inferred.

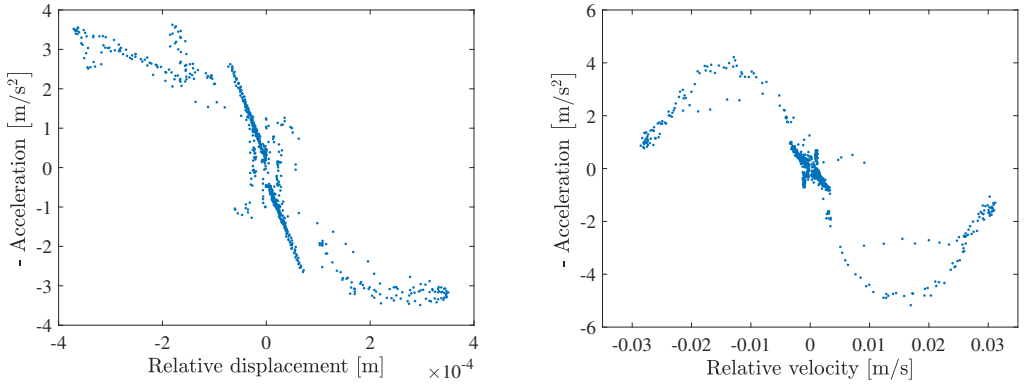

(a) Stiffness curve. (b) Damping curve.

Figure 1.6: Stiffness and damping curves of the third mode of the F-16 aircraft for which the ASM is applied to the wing.

As illustrated above, while the acceleration surface method works well in most cases, some unexpected results may appear in the stiffness and damping curves due to the simplifications made when using the method. To understand the origin of these results, the ASM is applied in the following chapters to simple systems with a cubic stiffness, a piecewise linear stiffness and Coulomb friction. First, 1 DOF systems are considered, then systems consisting of two degrees of freedom and finally more complex systems composed of 10 degrees of freedom are studied. Some ways to improve the curves, enabling a better identification of the nonlinear forces, will also be presented.

Chapter 2

1 DOF systems

The acceleration surface method is first applied to 1 DOF systems with different nonlinearities, which consist of a cubic stiffness and a piecewise linear stiffness representing an impact. Unless specified otherwise, all the results presented in this chapter are obtained with a system described by the equation

$$\ddot{x} + 0.01\,\dot{x} + x + f_{\text{nl}}(x,\dot{x}) = p(t), \tag{2.1}$$

where x is the displacement, t the time, $f_{\text{nl}}(x,\dot{x})$ the nonlinear force and $p(t)$ the external force applied to the system. The natural frequency of the linear system is equal to 0.159 Hz. The applied force $p(t)$ consists of a linear sine sweep excitation, as such an excitation produces good data for the restoring force surface method and thus also the ASM [15]. Its expression is given by

$$p(t) = A\sin\left(2\pi f_0 t + 2\pi\frac{r}{2}t^2\right), \tag{2.2}$$

where A is the forcing amplitude, f_0 the starting frequency and r the sweep rate. The response is computed by the NI2D software [16] using a Newmark integration scheme [17]. The time step of the Newmark integration scheme is equal to 0.001 s, resulting in a sampling frequency of 1000 Hz, and its parameters γ and β are equal to $\gamma = \frac{1}{2}$ and $\beta = \frac{1}{4}$, the Newmark integration scheme being unconditionally stable for these parameters [18].

After the simulation of the response of the system to the excitation has been carried out, the acceleration surface method implemented in MATLAB is applied to the results. The displacement and acceleration values of the stiffness curve are obtained by performing a linear interpolation between two consecutive values of the time series corresponding to velocity values of opposite signs, the change in sign indicating the presence of a point where the velocity is equal to zero between the two data points. The damping curve is computed in a similar way.

2.1 Cubic stiffness

In this section, a Duffing oscillator [19] is considered, which is described by the equation

$$\ddot{x} + 0.01\,\dot{x} + x + x^3 = p(t), \tag{2.3}$$

the nonlinear force consisting of a cubic stiffness. The results for different forcing amplitudes are shown below.

2.1.1 Forcing amplitude of 0.1 N

A sine sweep excitation with an amplitude of 0.1 N, a starting frequency of 0 Hz, an ending frequency of 1 Hz and a sweep rate of 0.01 Hz/min is applied to the system. At this forcing level, the behaviour of the system is strongly nonlinear. To determine the degree to which the response of the system is nonlinear, the ratio of the root mean square (RMS) value of the nonlinear force, which is here equal to x^3, to the RMS value of the inertia force of the system, given by $m\ddot{x}$, can be computed. It is expressed as

$$r_{\text{nl}} = \frac{\text{RMS}\left(f_{\text{nl}}\left(x,\dot{x}\right)\right)}{\text{RMS}\left(m\ddot{x}\right)}, \tag{2.4}$$

where m is the mass of the system, which is equal to 1 kg here. A high ratio indicates a strongly nonlinear system while a low ratio indicates a system with a linear behaviour. This ratio is equal to 86.3 % in this case, meaning that the system already behaves in a strongly nonlinear way. The acceleration surface and the stiffness and damping curves obtained when applying the acceleration surface method to the results are represented in Figure 2.1.

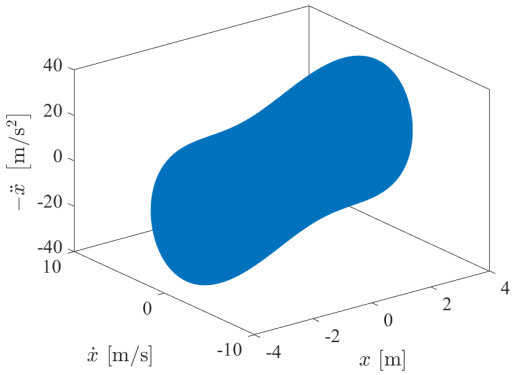

(a) Acceleration surface.

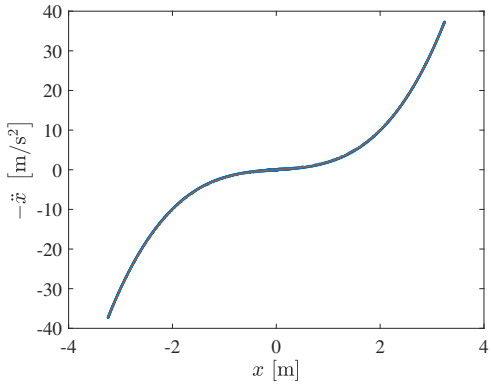

(b) Stiffness curve.

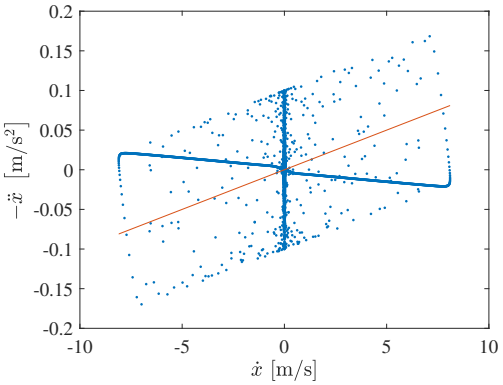

(c) Damping curve.

Figure 2.1: Acceleration surface and stiffness and damping curves of the 1 DOF system with a cubic stiffness and for a forcing amplitude of 0.1 N. The curve obtained from the simulated measurements is shown in blue and the exact curve is depicted in orange.

The stiffness curve is cubic and in good accordance with the theoretical curve, the points being however not exactly located on it. This can be explained by the forcing term that is

ignored in the acceleration surface method, but influences the acceleration of the mass and therefore also the stiffness and damping curves. The small value of the error is due to the fact that the error in the acceleration of the stiffness curve can never be larger than the acceleration the force produces to the mass of the system, obtained from Newton's second law

$$p = m\ddot{x} \Leftrightarrow \ddot{x} = \frac{p}{m}, \tag{2.5}$$

where m is the mass of the system, which is equal to $m = 1$ kg for this system. The error resulting from the applied force that is neglected is thus never larger than its forcing amplitude. However, this forcing amplitude is equal to 0.1 N and the acceleration takes values up to 37 $\mathrm{m/s^2}$, which is much greater than 0.1 $\mathrm{m/s^2}$. The influence of the external force can thus be neglected for this forcing level.

The damping curve does not correspond to a linear curve, as it is expected to be. This is due to the external force. Indeed, while the nonlinear stiffness force is dominant compared to the external force, the damping force is lower than the amplitude of the applied force. Similarly as for the stiffness curve, the contribution of the force to the acceleration can be as high as its forcing amplitude, the mass of the system being equal to 1 kg. However, the highest acceleration value of the damping curve is equal to 0.17 $\mathrm{m/s^2}$ and the force amplitude is equal to 0.1 N, indicating that the acceleration in the damping curve is mostly due to the external force and not the damping force itself, which is only responsible for the linear increase trend visible in the curve. Disregarding the linear increase trend, the damping curve is composed of points that seem randomly distributed. A curve going from the origin towards a positive acceleration for positive displacements and a negative acceleration for negative displacements can also be observed. This curve is due to the measurement points before the occurrence of the resonance peak, the other points randomly distributed being the result of the data points located after the resonance peak. Indeed, before the resonance peak, the displacement of the system is first in phase with the external force, then becomes progressively out-of-phase when the maximum displacement amplitude is reached, as shown in Figure 2.2.

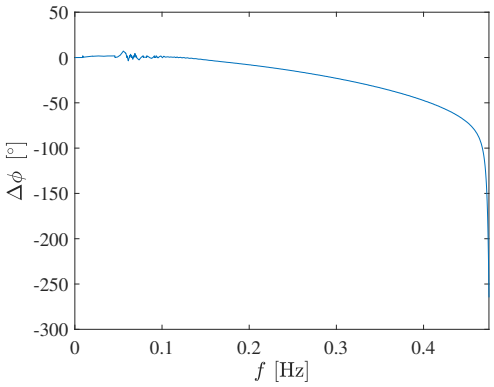

Figure 2.2: Phase difference up to the resonance between the displacement and the external force of the 1 DOF system with a cubic stiffness and for a forcing amplitude of 0.1 N.

As the velocity always has a phase difference of $\frac{\pi}{2}$ with the displacement, the velocity first has a phase difference of $\frac{\pi}{2}$ with the external force, thus leading to values close to 0 of the acceleration for small values of the velocity, the points of the damping curve occurring at the extrema of the velocity. The velocity and the external force then become briefly in

phase, leading to the points with the highest amplitude in acceleration, before having a phase difference of $\frac{3\pi}{2}$ at the resonance peak, leading to an acceleration close to 0 for the highest amplitude in velocity. After the resonance peak, the phase difference changes more rapidly, which explains the appearance of points in the damping curve that seem randomly distributed. This is depicted in Figure 2.3b.

The influence of the phase difference between the displacement and the applied force is also visible on the stiffness curve. Indeed, for small displacements before the resonance peak, the displacement and the force are in phase, such that they reach their maximum amplitude simultaneously. For these points, the points in the stiffness curve have a lower acceleration amplitude than the curve predicted theoretically, the obtained curve being below the exact curve for positive displacements and above for negative displacements. After the resonance peak on the other hand, the obtained curve is above the exact curve for positive displacements and below it for negative displacements, since the displacement and the acceleration are out-of-phase. As the displacement amplitude decreases after the resonance peak, the displacement becomes out-of-phase with the external force. Due to this, the points of the stiffness curve corresponding to this part of the data are mainly located above the exact curve for positive displacements and below for negative displacements. This is illustrated in Figure 2.3a.

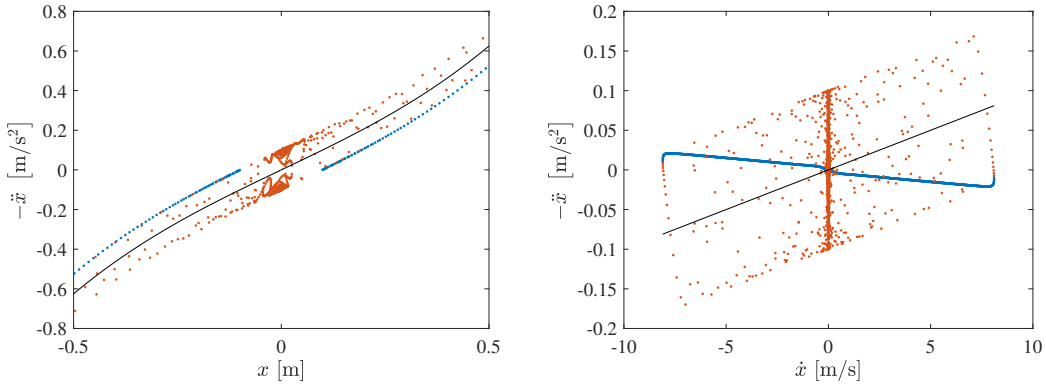

(a) Close-up of the stiffness curve.

(b) Damping curve.

Figure 2.3: Stiffness and damping curves of the 1 DOF system with a cubic stiffness and for a forcing amplitude of 0.1 N. The points occurring before the resonance peak are indicated in blue, those occurring after the resonance peak are indicated in orange and the exact curve is depicted in black.

Although the stiffness curve produces good results, the damping curve does not correspond to a linear curve, as it is expected to be. This is due to the excitation $p(t)$ that is the only term that has been discarded from Equation 2.3. Representing $-\ddot{x}+p$ as a function of the displacement and velocity in the stiffness and damping curves respectively instead of $-\ddot{x}$, the obtained curves correspond perfectly to the expressions of the stiffness and damping forces, since Equation 2.3 can be rewritten as

$$0.01\,\dot{x}+x+x^3=-\ddot{x}+p. \tag{2.6}$$

The stiffness force being $f_\mathrm{s}=x+x^3$ and the damping force being $f_\mathrm{d}=0.01\,\dot{x}$, the equation becomes

$$f_\mathrm{s}+f_\mathrm{d}=-\ddot{x}+p. \tag{2.7}$$

The stiffness and damping curves obtained when taking into account the forcing term are depicted in Figure 2.4.

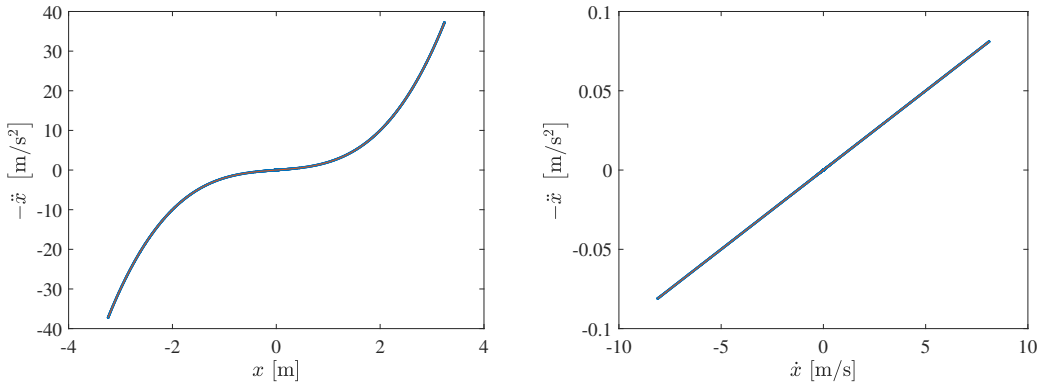

(a) Stiffness curve. (b) Damping curve.

Figure 2.4: Stiffness and damping curves of the 1 DOF system with a cubic stiffness and for a forcing amplitude of 0.1 N, taking into account the applied force. The curve obtained from the simulated measurements is shown in blue and the exact curve is depicted in orange.

It can be seen that both the stiffness and damping curves perfectly correspond to the theoretical expression of the stiffness and damping forces when taking the excitation force into account, which confirms that the inexact curves are due to the fact that the forcing term is ignored in the acceleration surface method. This observation can also be made for all the following results of 1 DOF systems, for all the types of nonlinearities studied.

2.1.2 Forcing amplitude of 10 N

The forcing level is now increased to reach 10 N. The nonlinearity ratio r_{nl} is equal to 99.7 %, which indicates that the nonlinear stiffness force is large, the linear stiffness and damping forces and the external force being negligible with respect to it. Due to the strong nonlinearities created at such a high forcing, the resonance peak occurs at a frequency higher than 1 Hz, namely at around 3.09 Hz, as can be seen in Figure 2.5.

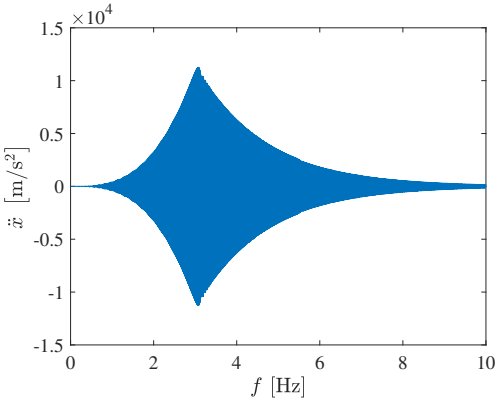

Figure 2.5: Acceleration as a function of the excitation frequency for the 1 DOF system with a cubic stiffness and for a forcing amplitude of 10 N.

The ending frequency of the sine sweep excitation is thus set to 10 Hz and the sweep rate is modified to 1 Hz/min. The acceleration surface method is applied to the entire frequency window of the sine sweep excitation ranging from 0 to 10 Hz. The ASM is also applied to the entire frequency range of the excitation for all the other 1 DOF systems studied, unless specified otherwise. The stiffness curve and the damping curve obtained for these data can be seen in Figure 2.6.

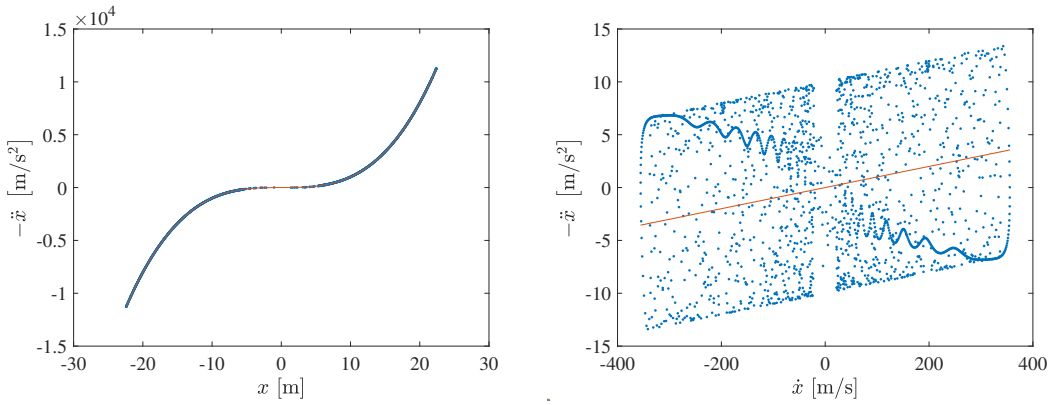

(a) Stiffness curve. (b) Damping curve.

Figure 2.6: Stiffness and damping curves of the 1 DOF system with a cubic stiffness and for a forcing amplitude of 10 N. The curve obtained from the simulated measurements is shown in blue and the exact curve is depicted in orange.

The stiffness curve is very similar to the one obtained for a force amplitude of 0.1 N, except that the displacement and acceleration amplitudes are higher, which is simply due to the higher forcing level. The curve has a cubic shape and corresponds to the analytical expression of the stiffness force.

The damping curve however has a difference with those obtained previously for lower forcing levels. There are indeed oscillations in the part of the curve composed of the data points occurring before the resonance peak. These oscillations can be linked to oscillations appearing in the phase difference between the displacement and the external force, which are depicted in Figure 2.7.

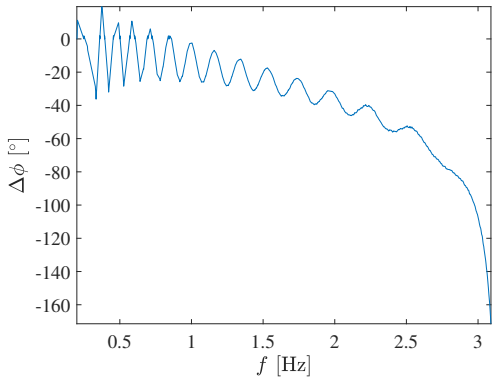

Figure 2.7: Phase difference between the displacement and the external force of the 1 DOF system with a cubic stiffness and for a forcing amplitude of 10 N from 0.2 Hz to the resonance frequency of 3.09 Hz.

As the points of the damping curve correspond to measurement points for which the displacement is equal to 0 m, if the displacement and the force are not perfectly in phase, the force will be non-zero at the points where the damping curve is obtained. Oscillations in the phase difference between the displacement and the external force around and below 0° thus lead to oscillations in the force at the points corresponding to the damping curve, which themselves are responsible for the oscillations observed in the damping curve. One possibility to reduce the impact of these oscillations in the damping curve is to use a lower sweep rate for the sine sweep excitation. The damping curve for a sweep rate of 0.1 Hz/min instead of 1 Hz/min is illustrated in Figure 2.8.

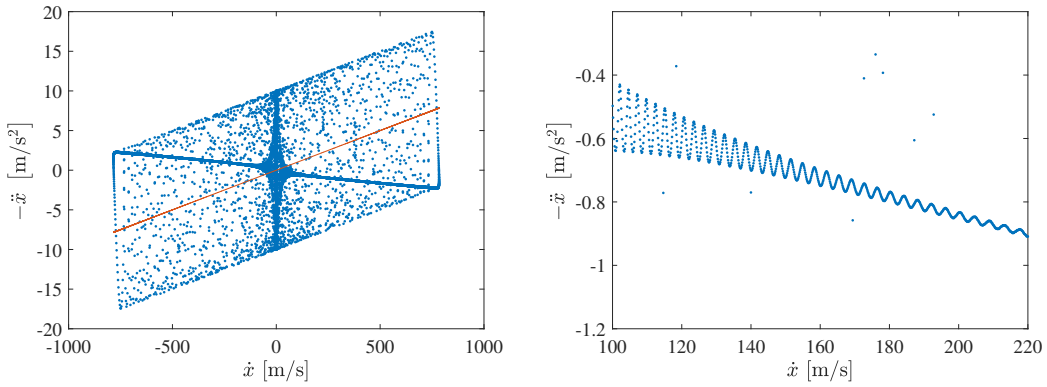

(a) Damping curve.

(b) Zoom on the oscillations of the curve.

Figure 2.8: Damping curve of the 1 DOF system with a cubic stiffness and for a forcing amplitude of 10 N and a sweep rate of 0.1 Hz/min. The curve obtained from the simulated measurements is shown in blue and the exact curve is depicted in orange.

It can be seen that when using a lower sweep rate, the oscillations are not visible anymore in the damping curve. However, when zooming on the curve such as in Figure 2.8b, it can be observed that these oscillations are still present, with a higher frequency than previously but a lower amplitude, which is the reason why they are not visible at first glance.

2.1.3 Superharmonic resonances

In order to study superharmonic resonances of a 1 DOF system with a cubic stiffness, another system is considered, for which superharmonic resonances are easier to detect. It is described by the equation

$$0.289\ddot{x} + 0.1357\dot{x} + 11009x + 2.37 \times 10^9 x^3 = p(t), \tag{2.8}$$

which is a 1 DOF model of the first mode of a cantilever beam with a very thin beam at the tip [5]. A sine sweep excitation is applied to the system with an amplitude of 10 N, a starting frequency of 0 Hz, an ending frequency of 15 Hz and a sweep rate of 0.1 Hz/min. The evolution of the acceleration with the excitation frequency is depicted in Figure 2.9.

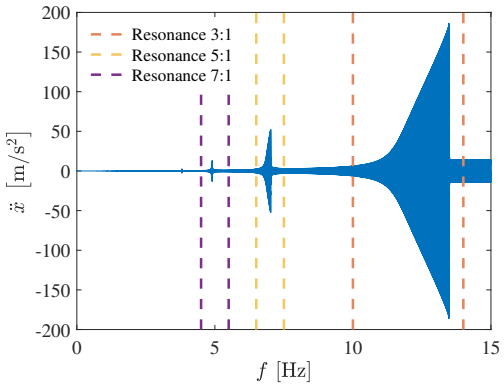

Figure 2.9: Acceleration as a function of the excitation frequency for the 1 DOF system with a cubic stiffness with the presence of superharmonic resonances and the frequency windows of the 3:1, 5:1 and 7:1 superharmonic resonances.

It can be seen that there are different peaks in the acceleration time series at 13.5 Hz, 7.02 Hz, 4.90 Hz and even a small peak at 3.80 Hz. The natural frequency of the linear system being equal to 31.1 Hz, it can be deduced that these peaks correspond respectively to the 3:1, 5:1, 7:1 and 9:1 superharmonic resonances. Indeed, the peaks occur at frequencies close to $\frac{1}{3}$, $\frac{1}{5}$, $\frac{1}{7}$ and $\frac{1}{9}$ of the natural frequency of the linear system. The shift of these peaks towards higher frequencies than expected is simply the result of the hardening nonlinearity, which makes the system reach resonance at higher frequencies than in the linear case. Furthermore, for each of these peaks, the analysis of the evolution of the displacement with time reveals the presence of harmonics of order n for the $n:1$ superharmonic resonance, as for each period of the signal, there are n maxima and n minima visible in the time series. This is shown in Figure 2.10.

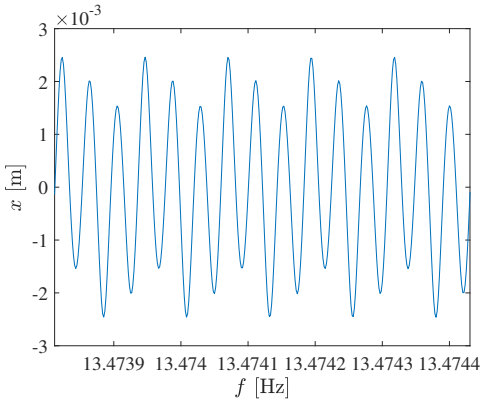

(a) 3:1 superharmonic resonance.

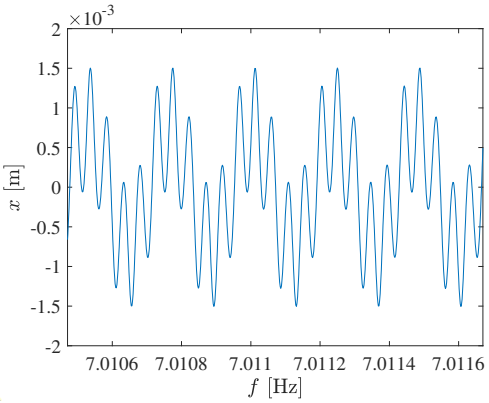

(b) 5:1 superharmonic resonance.

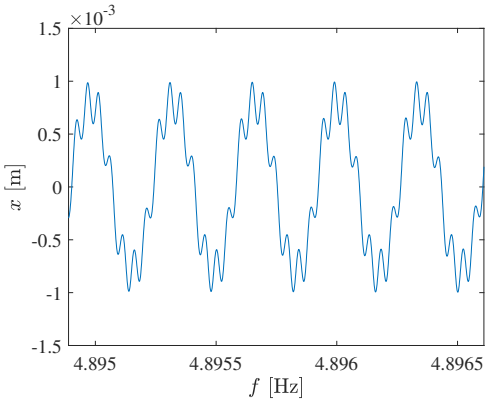

(c) 7:1 superharmonic resonance.

Figure 2.10: Displacement as a function of the excitation frequency for the 1 DOF system with a cubic stiffness at the 3:1, 5:1 and 7:1 superharmonic resonances.

The acceleration surface method is applied to the 3:1, 5:1 and 7:1 superharmonic resonances, the frequency windows to which the method is applied being represented in Figure 2.9. The stiffness curves obtained for each of these resonances are illustrated in Figure 2.11.

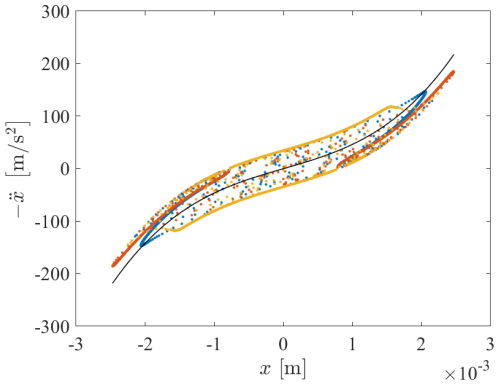

(a) 3:1 superharmonic resonance.

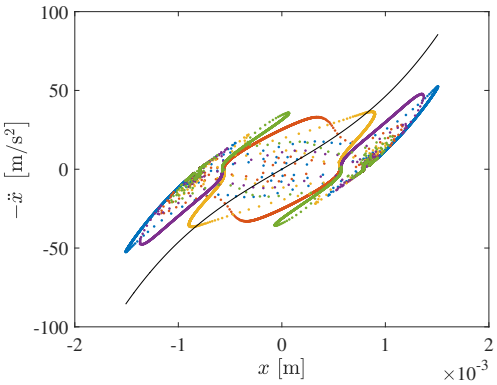

(b) 5:1 superharmonic resonance.

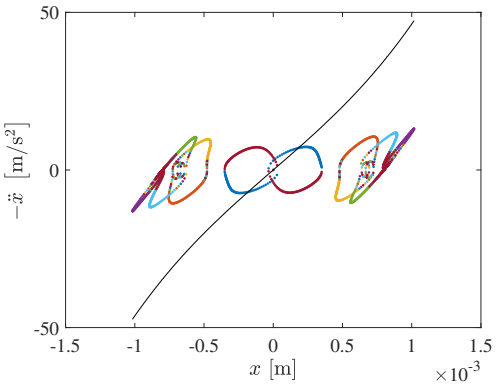

(c) 7:1 superharmonic resonance.

Figure 2.11: Stiffness curves of the 1 DOF system with a cubic stiffness for the 3:1, 5:1 and 7:1 superharmonic resonances. The different pairs of lines are represented in different colours and the exact curve is depicted in black.

While the cubic nature of the stiffness force can still be deduced from the curve obtained for the 3:1 superharmonic resonance, it becomes impossible to recognise a cubic stiffness in the stiffness curves of the two other superharmonic resonances. While the three curves are different from each other, they share some common characteristics. Indeed, the curves of the 3:1 and 5:1 superharmonic resonances and those of the 5:1 and 7:1 superharmonic resonances are to some extent similar to each other. This indicates that the obtained stiffness curves progressively change as superharmonic resonances of higher order are considered. Furthermore, for each stiffness curve, a certain number of distinct lines are visible. The number of pairs of lines is equal to the order of the harmonic component that is dominant in the analysed response signal. There are thus 3, 5 and 7 pairs of lines respectively for the 3:1, 5:1 and 7:1 superharmonic resonances. Each pair of lines can be related to one maximum and one minimum of each period of the displacement time series. Indeed, the points of the stiffness curve are taken at the extrema of the displacement, since the velocity is equal to 0 m/s when the displacement reaches an extremum. Since the different extrema over one period do not have the same displacement and acceleration, this results in different curves that can be distinguished from each other in the stiffness curve. The curves related to the different extrema have been represented in different colours in Figure 2.11. The points that are not located on any of the lines in Figure 2.11a and Figure 2.11b are linked to data points occurring after the resonance peak,

where the system jumps from the upper branch of the nonlinear frequency response curve to the lower branch, resulting in a transient response.

The damping curves obtained for the 3:1, 5:1 and 7:1 superharmonic resonances are depicted in Figure 2.12.

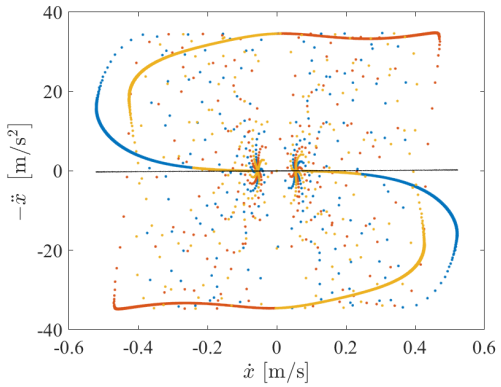

(a) 3:1 superharmonic resonance.

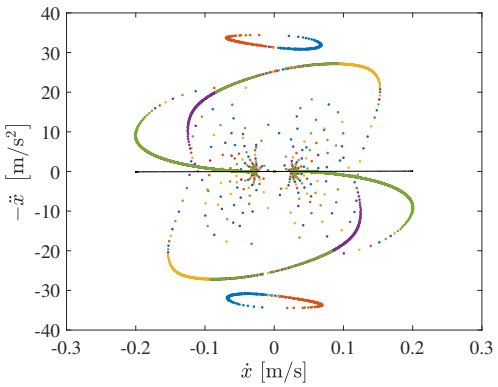

(b) 5:1 superharmonic resonance.

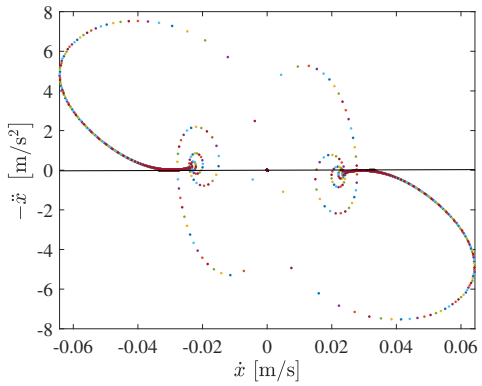

(c) 7:1 superharmonic resonance.

Figure 2.12: Damping curves of the 1 DOF system with a cubic stiffness for the 3:1, 5:1 and 7:1 superharmonic resonances. The different pairs of lines are represented in different colours and the exact curve is depicted in black.

At the 3:1 and 5:1 superharmonic resonances, there are respectively 3 and 5 pairs of lines in the damping curve, such as in the stiffness curve. The origin of these lines is similar to those of the stiffness curve, as each of these lines correspond to a different moment of every period at which the displacement is equal to 0 m. As can be seen in Figure 2.10, the displacement crosses the horizontal axis $2n$ times per period for the $n:1$ superharmonic resonance, half of them corresponding to a positive velocity and the other half to a negative velocity, the velocity being equal to the slope of the curve. These different points where $x = 0$ m thus create different lines in the damping curve, the velocity and the acceleration being different for each of these points. This also explains why there is only one pair of lines for the 7:1 superharmonic resonance. As shown in Figure 2.10c, while there are 7 maxima and 7 minima of the displacement, there are only two points per period where $x = 0$ m, thus only creating 2 lines, one for which the velocity is positive and one for which it is negative.

One possible solution to improve the results, especially the stiffness curve, is to filter the

displacement, velocity and acceleration signals to only keep the n-th harmonic component, which corresponds to the eigenfrequency of the system. This harmonic component is indeed the dominant harmonic component in the response, but there is also a large contribution of the fundamental frequency and even some influence of the other harmonics that are also present. To do so, a low-pass filter is first applied to remove the fundamental frequency as well as the harmonics of lower order. Then, a high-pass filter is applied to remove the harmonics of higher order. The stiffness curves obtained after filtering the results are shown in Figure 2.13.

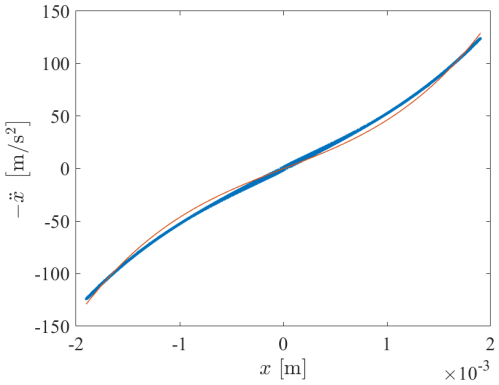

(a) 3:1 superharmonic resonance.

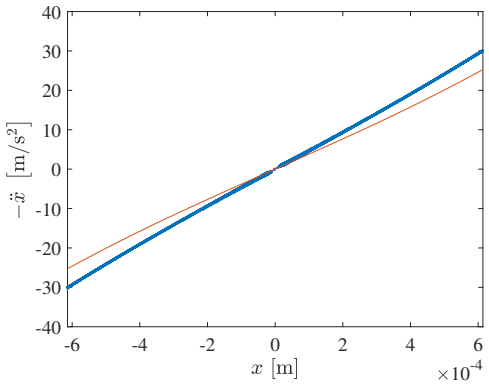

(b) 5:1 superharmonic resonance.

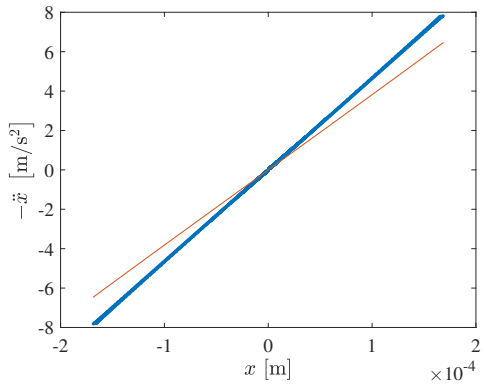

(c) 7:1 superharmonic resonance.

Figure 2.13: Stiffness curves of the 1 DOF system with a cubic stiffness for the 3:1, 5:1 and 7:1 superharmonic resonances obtained after filtering the data. The curve obtained from the simulated measurements is shown in blue and the exact curve is depicted in orange.

It can be seen that filtering the measurement data greatly improves the stiffness curves. For the 3:1 superharmonic resonance, the cubic shape of the curve is now clearly visible and for the two other superharmonic resonances, the curve is linear as it should be due to the low displacements, at which the nonlinearities are not significantly activated. However, the curves do not exactly correspond to the analytical curve derived from the expression of the stiffness force, but this is not problematic, since the acceleration surface method is a qualitative method aimed at finding the functional form of the nonlinear force and is not used to estimate the parameters of this nonlinear force, which have to be determined with another method.

The damping curves obtained after filtering the displacement, velocity and acceleration for each superharmonic resonance are illustrated in Figure 2.14.

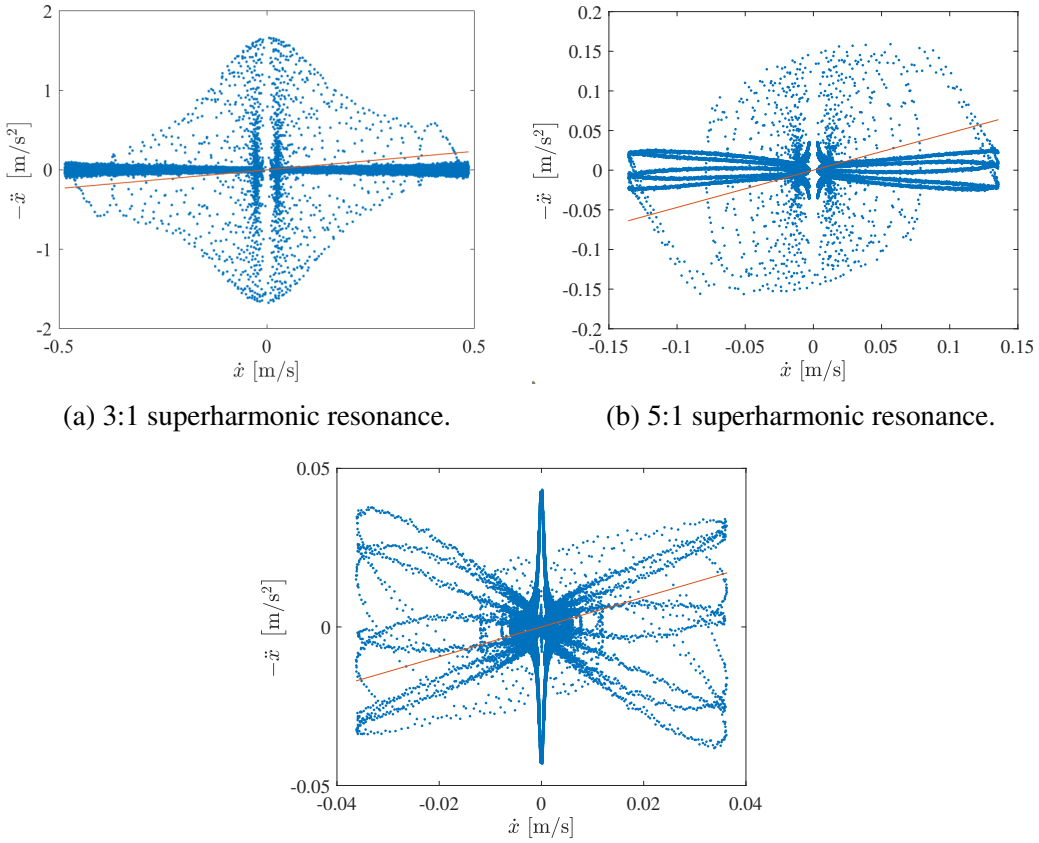

(a) 3:1 superharmonic resonance.

(b) 5:1 superharmonic resonance.

(c) 7:1 superharmonic resonance.

Figure 2.14: Damping curves of the 1 DOF system with a cubic stiffness for the 3:1, 5:1 and 7:1 superharmonic resonances obtained after filtering the data. The curve obtained from the simulated measurements is shown in blue and the exact curve is depicted in orange.

While filtering improves the stiffness curve, it does not improve the damping curve and the functional form of the damping force remains difficult to estimate with the acceleration surface method.

2.2 Piecewise linear stiffness

In this section, the nonlinearity takes the form of a trilinear stiffness, which can exist in real-life structures for which there is an impact happening at the connection between two substructures, leading to an increase in stiffness when the displacement amplitude reaches the clearance of the connection. The studied system is described by the equation

$$\begin{cases} \ddot{x} + 0.01\dot{x} + x = p(t) & \text{if } |x| \leq 1 \text{ m} \\ \ddot{x} + 0.01\dot{x} + 3x = p(t) & \text{if } |x| > 1 \text{ m} \end{cases}. \tag{2.9}$$

2.2.1 Forcing amplitude of 0.1 N

The system is subjected to a sine sweep excitation having an amplitude of 0.1 N, a starting frequency of 0 Hz, an ending frequency of 1 Hz and a sweep rate of 0.01 Hz/min. This yields a

nonlinearity ratio of 54.0 %, meaning that the system is nonlinear, but the linear forces and the excitation force are not negligible compared to the nonlinear force. The stiffness and damping curves are obtained by applying the acceleration surface method to the results computed by numerical integration. They are depicted in Figure 2.15.

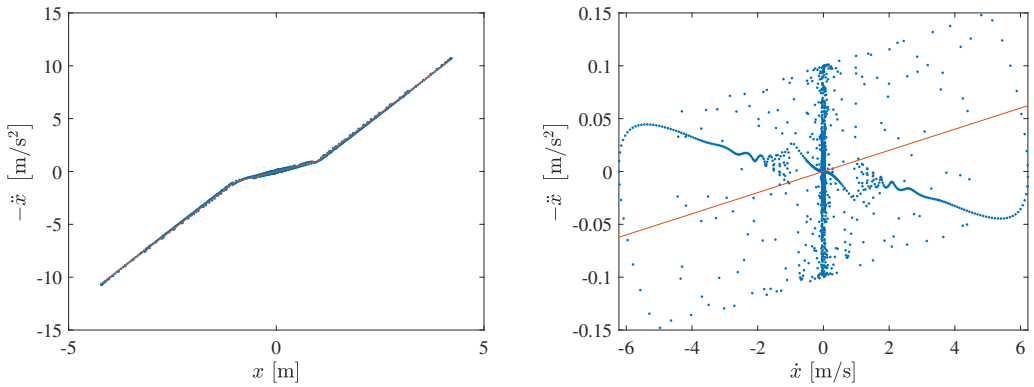

(a) Stiffness curve.

(b) Damping curve.

Figure 2.15: Stiffness and damping curves of the 1 DOF system with a trilinear stiffness and for a forcing amplitude of 0.1 N. The curve obtained from the simulated measurements is shown in blue and the exact curve is depicted in orange.

Similarly as for the cubic stiffness, the acceleration surface method produces good results for the stiffness curve, the piecewise linear form of the stiffness force being easy to identify. Furthermore, for small values of the displacement, the stiffness curve has a similar behaviour as for the cubic stiffness, which is shown in Figure 2.3a. Indeed, there is a linear part located below the exact curve for positive displacements and other points situated above it. The origin of these points is again due to the phase difference between the displacement and the applied force, which are in phase before the resonance and then become out-of-phase.

The damping curve is almost identical to that of the system having a cubic stiffness. There is a line due to data points located before the resonance peak, which also has some oscillations at small velocities. The presence of this line and its oscillations is explained in the same way as for the cubic stiffness by the phase difference between the displacement and the external force.

2.2.2 Forcing amplitude of 1 N

A sine sweep excitation with a forcing amplitude of 1 N is now applied, the other parameters remaining unchanged. This results in a nonlinearity ratio of 64.4 %, the nonlinear force being thus more important than for a forcing level of 0.1 N. The stiffness and damping curves obtained for this external force are indicated in Figure 2.16.

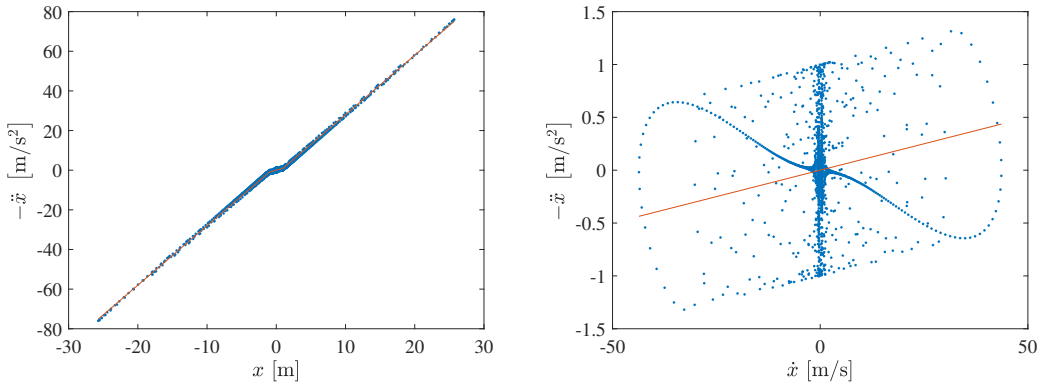

(a) Stiffness curve. (b) Damping curve.

Figure 2.16: Stiffness and damping curves of the 1 DOF system with a trilinear stiffness and for a forcing amplitude of 1 N. The curve obtained from the simulated measurements is shown in blue and the exact curve is depicted in orange.

Both the stiffness curve and the damping curve are very close to those obtained for a forcing amplitude of 0.1 N. The only difference in the stiffness curve is the higher displacement amplitude which is reached due to the higher forcing level. The observations made in Figure 2.3a and for a forcing level of 0.1 N can also be made here. The main difference with the previous case are the oscillations that have almost disappeared from the damping curve. There are still some oscillations, which have however a small amplitude such that they are barely not visible, as can be seen in Figure 2.17. This is due to the fact that the oscillations in the phase difference are also smaller.

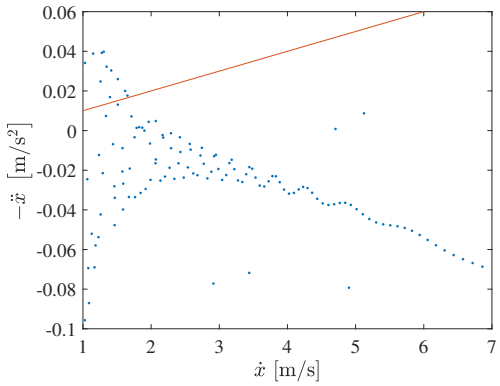

Figure 2.17: Close-up on the oscillations of the damping curve of the 1 DOF system with a trilinear stiffness and for a forcing amplitude of 1 N. The curve obtained from the simulated measurements is shown in blue and the exact curve is depicted in orange.

The results obtained when applying the ASM to a 1 DOF system with a cubic stiffness and a trilinear stiffness are very similar, the functional form of the stiffness force being easy to identify, while it produces identical damping curves for both types of nonlinearities and does not allow the detection of the linear expression of the damping force.

2.3 Conclusion

To conclude, simple nonlinear 1 DOF systems can already produce unexpected results when using the acceleration surface method. However, the stiffness curves always allow to determine the functional form of the stiffness force. On the other hand, due to its small amplitude, the damping force remains difficult to characterise.

Furthermore, in the case of a strong presence of harmonics in the response of the system, such as during superharmonic resonances, filtering the displacement, velocity and acceleration signals can greatly improve the stiffness curve. The best way to improve the stiffness and damping curves is however to take the external force into account and replace $-\ddot{x}$ by $-m\ddot{x}+p$. The obtained curves then always correspond exactly to the stiffness and damping forces, as p is the only term neglected in the acceleration surface method. Doing this is equivalent to using the restoring force surface method and requires the knowledge of the applied force at every instant the acceleration is recorded, which can be difficult to achieve in practice.

While 1 DOF systems allow a first analysis of the results obtained when using the acceleration surface method, most structures encountered in real-life applications are more complex and need to be modelled by a system composed of multiple degrees of freedom. In the next chapter, 2 DOF systems will thus be studied, for which more complex phenomena can occur.

Chapter 3

2 DOF systems

In this chapter, the acceleration surface method is applied to 2 DOF systems, the nonlinearities consisting of a cubic stiffness, a piecewise linear stiffness and Coulomb friction, which belong to the most common types of nonlinearity [20]. A cubic stiffness can for example be encountered for clamped plates and beams. A piecewise linear stiffness and Coulomb friction on the other hand are often present at the connection between two substructures having a clearance. These nonlinear forces are located on the connection between DOF 1 and the ground. A sine sweep excitation is applied to DOF 2. The system of equations governing the motion of the system is given by

$$\mathbf{M}\ddot{\mathbf{q}} + \mathbf{C}\dot{\mathbf{q}} + \mathbf{K}\mathbf{q} + \mathbf{f}_{\text{nl}}(\mathbf{q}, \dot{\mathbf{q}}) = \mathbf{p}(t), \tag{3.1}$$

where $\mathbf{M}$, $\mathbf{C}$ and $\mathbf{K}$ are respectively the mass, damping and stiffness matrices of the system, $\mathbf{q} = \begin{pmatrix} q_1 \\ q_2 \end{pmatrix}$ is the displacement vector, $\mathbf{f}_{\text{nl}}(\mathbf{q}, \dot{\mathbf{q}})$ the vector of the nonlinear forces and $\mathbf{p}(t)$ the vector of the applied force. Knowing the matrices $\mathbf{M}$, $\mathbf{C}$ and $\mathbf{K}$ and taking into account that the nonlinear force is located on DOF 1 and the excitation force on DOF 2, the system of equations becomes

$$\begin{bmatrix} 1 & 0 \\ 0 & 1 \end{bmatrix} \begin{pmatrix} \ddot{q}_1 \\ \ddot{q}_2 \end{pmatrix} + 0.01 \begin{bmatrix} 2 & -1 \\ -1 & 2 \end{bmatrix} \begin{pmatrix} \dot{q}_1 \\ \dot{q}_2 \end{pmatrix} + \begin{bmatrix} 8 & -7 \\ -7 & 8 \end{bmatrix} \begin{pmatrix} q_1 \\ q_2 \end{pmatrix} + \begin{pmatrix} f_{\text{nl}}(q_1, \dot{q}_1) \\ 0 \end{pmatrix} = \begin{pmatrix} 0 \\ p(t) \end{pmatrix}. \tag{3.2}$$

Unless specified otherwise, the systems studied in this chapter are governed by Equation 3.2 and the starting frequency and the ending frequency of the sine sweep excitation $p(t)$, whose expression is given by Equation 2.2, are 0 Hz and 1 Hz respectively, the natural frequencies of the linear system being equal to 0.159 Hz and 0.616 Hz, and the sweep rate r is equal to 0.01 Hz/min, the forcing amplitude A being specified for each case.

Since the nonlinear force is located at the connection between DOF 1 and the ground and the external force is exerted on DOF 2, the ASM is applied to DOF 1 in order to be situated at one extremity of the nonlinear connection and avoid having an external force at the considered degree of freedom. The equation of motion of DOF 1 can be expressed as

$$0.01\,\dot{q}_1 + q_1 + 0.01\,(\dot{q}_1 - \dot{q}_2) + 7\,(q_1 - q_2) + f_{\text{nl}}(q_1, \dot{q}_1) = -\ddot{q}_1. \tag{3.3}$$

Using the acceleration surface method, the stiffness force $7\,(q_1 - q_2)$ and the damping force $0.01\,(\dot{q}_1 - \dot{q}_2)$ at the linear connection between DOF 1 and DOF 2 are discarded, which results in the equation

$$0.01\,\dot{q}_1 + q_1 + f_{\text{nl}}(q_1, \dot{q}_1) \cong -\ddot{q}_1. \tag{3.4}$$

Using a similar approach as for the 1 DOF systems, the response of the system to the applied force is computed on the NI2D software with a Newmark integration scheme and the stiffness and damping curves are obtained following the same methodology.

3.1 First system with a cubic stiffness

First, the system described by Equation 3.2 and a cubic stiffness whose expression is given by $f_{\text{nl}}(q_1, \dot{q}_1) = 0.5\, q_1^3$ are considered, such that Equation 3.4 becomes

$$0.01\, \dot{q}_1 + q_1 + 0.5\, q_1^3 \cong -\ddot{q}_1. \tag{3.5}$$

3.1.1 Forcing amplitude of 0.1 N

A forcing amplitude of 0.1 N is considered. The ratio of the nonlinear force to the inertia force of DOF 1 is computed similarly as for 1 DOF systems to assess whether the considered mode is nonlinear. It is given by

$$r_{\text{nl}} = \frac{\text{RMS}\left(f_{\text{nl}}(q_1, \dot{q}_1)\right)}{\text{RMS}\left(m_1 \ddot{q}_1\right)}, \tag{3.6}$$

where m_1 is the mass of DOF 1. This ratio is equal to 53.1 % for the first mode, this mode thus being already significantly nonlinear at a forcing amplitude of 0.1 N. On the other hand, the second mode has a nonlinearity ratio r_{nl} of 0.163 % and is thus only very weakly nonlinear.

The acceleration time series is depicted in Figure 3.1.

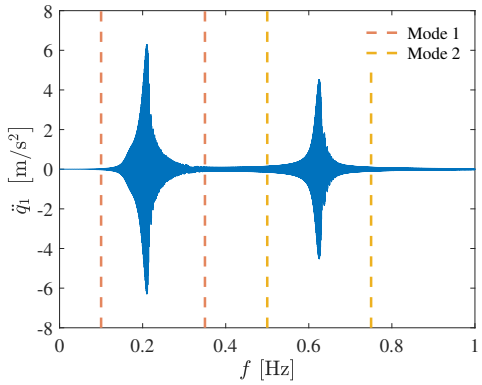

Figure 3.1: Acceleration of DOF 1 as a function of the excitation frequency for the 2 DOF system with a cubic stiffness and for a forcing amplitude of 0.1 N and the frequency windows of the first and second modes.

The stiffness and damping curves obtained for the first vibration mode are shown in Figure 3.2.

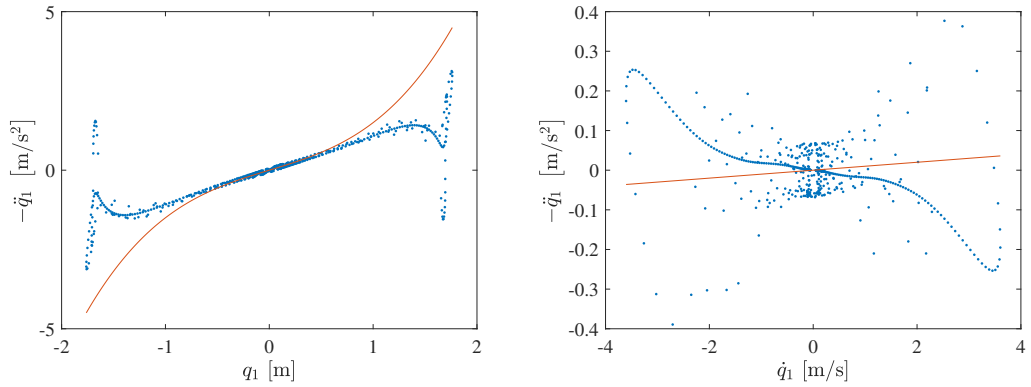

(a) Stiffness curve.

(b) Damping curve.

Figure 3.2: Stiffness and damping curves for the first mode of the 2 DOF system with a cubic stiffness and for a forcing amplitude of 0.1 N. The curve obtained from the simulated measurements is shown in blue and the exact curve is depicted in orange.

It can be seen that the damping curve is similar to those obtained for the 1 DOF systems. The part of the curve decreasing as the velocity increases originates from the points occurring before the resonance and the points that seem randomly distributed and are concentrated at the centre of the curve arise from the points located after the resonance peak. However, for the 2 DOF system, the shape of the damping curve, as well as of the stiffness curve, is not directly due to the external force, since the excitation force does not appear in Equation 3.3. It is rather due to the stiffness and damping forces at the connection between DOF 1 and DOF 2. Indeed, they are the only terms from the equation of motion of DOF 1 that are neglected in the ASM. Replacing in the stiffness and damping curves $-\ddot{q}_1$ by $-\ddot{q}_1 - 0.01\,(\dot{q}_1 - \dot{q}_2) - 7\,(q_1 - q_2)$, the exact shape of the stiffness and damping forces between DOF 1 and the ground are retrieved. This holds true for all the types of nonlinearities studied and for all the forcing levels. Furthermore, as the stiffness force is much larger than the damping force, the different shapes that may be encountered in the curves and that differ from the exact expression of the forces are mainly due to the stiffness force between DOF 1 and DOF 2, the damping force only weakly modifying the curves, even the damping curve.

While the stiffness curve is close to the exact curve at small displacements, it starts to differ as the displacement amplitude increases until it splits in different parts, one strongly increasing and one strongly decreasing. This can be explained by the presence of third order harmonics in the response. It leads to the appearance of three maxima and three minima per period of the displacement time series for sufficiently large displacements, as depicted in Figure 3.3.

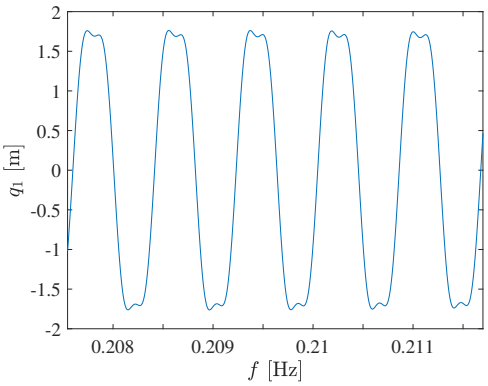

Figure 3.3: Displacement of DOF 1 as a function of the excitation frequency for the 2 DOF system with a cubic stiffness and a forcing amplitude of 0.1 N at the first resonance mode.

The stiffness curve only taking into account the points for which the velocity is null, this corresponds to the extrema of the displacement, the velocity being the derivative of the displacement. When only considering the extrema for which the displacement is positive, the presence of two maxima and one minimum can be observed. As the acceleration is the second derivative of the displacement, it is positive for a local minimum of the displacement and negative for a local maximum. The part of the stiffness curve increasing at large positive displacements is thus due to the two positive displacement maxima, for which $-\ddot{q}_1$ is positive, and the part of the curve decreasing is due to the local positive minimum, at which $-\ddot{q}_1$ is negative. A similar reasoning can explain the part of the stiffness curve for which the displacement is negative.

Furthermore, before the separation in two different lines, the stiffness curve stops following the exact curve at some point and even strongly decreases for positive displacements shortly before the curve gets separated in two. This is due to the difference in amplitude between q_1 and q_2 which increases when approaching the resonance frequency. The stiffness force between both degrees of freedom therefore also increases. Since the amplitude of q_2 is larger than that of q_1 and both degrees of freedom oscillate in phase, the stiffness force $7(q_1 - q_2)$ is negative and thus decreases the value of $-\ddot{q}_1$, according to Equation 3.3. The increase of this force as q_1 increases is thus responsible for the drop in the stiffness curve as the displacement increases. The sharp decrease right before the separation in different parts is due to the appearance of harmonics of order 3, which causes the maxima of q_1 to flatten and thus not increase with time as much as those of q_2, which does not have a harmonic component as important as q_1. The flattening of the peaks of q_1 then finally leads to the creation of two separate maxima and a minimum between them.

The appearance of an important harmonic component of third order is due to a 3:1 modal interaction. The presence of this 3:1 modal interaction can be determined by considering the frequency-energy plots (FEP) of both nonlinear normal modes of the system. These frequency-energy plots are computed with the NI2D software and are shown in Figure 3.4.

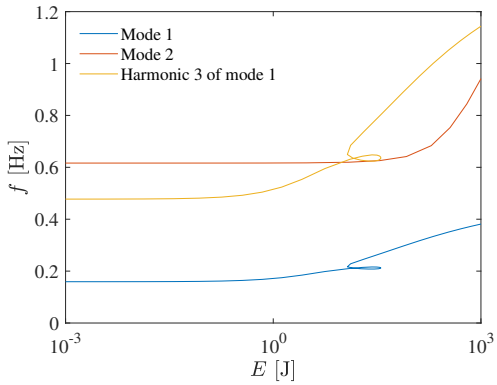

Figure 3.4: Frequency-energy plots of both nonlinear normal modes as well as the third harmonics of mode 1 of the 2 DOF system with a cubic stiffness.

It can be seen that the FEP of the third harmonics of mode 1, for which the frequency of mode 1 is multiplied by 3, crosses the FEP of mode 2 at a frequency of 0.624 Hz, which corresponds to a frequency of 0.208 Hz for mode 1. This frequency of 0.208 Hz at which the 3:1 modal interaction occurs is very close to that of the resonance of the first mode, which is equal to 0.211 Hz. This modal interaction thus explains the strong presence of third order harmonics and the stiffness curve resulting from it.

As the shape of the stiffness curve is due to the presence of harmonics, a possible solution to obtain a more accurate stiffness curve is to filter the displacement, velocity and acceleration time signals of both degrees of freedom. A low-pass filter is used to only keep the fundamental frequency and remove all the harmonic components. The ASM is then applied to the filtered data. The stiffness and damping curves are shown in Figure 3.5.

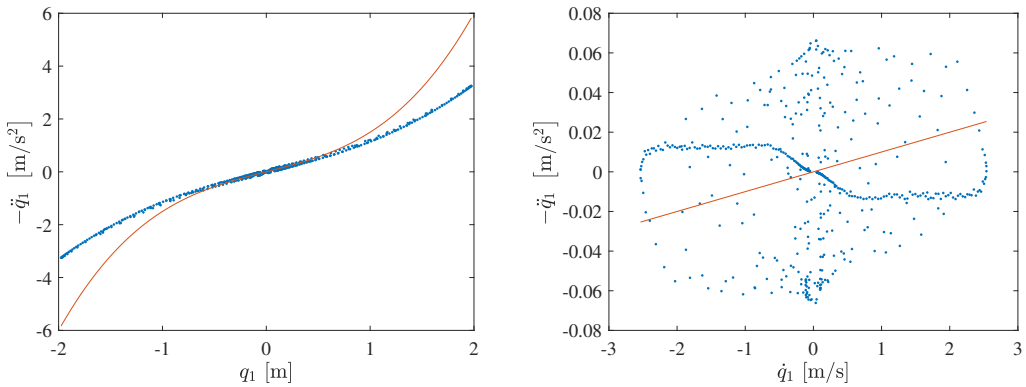

(a) Stiffness curve. (b) Damping curve.

Figure 3.5: Stiffness and damping curves for the first mode of the 2 DOF system with a cubic stiffness and for a forcing amplitude of 0.1 N obtained after filtering. The curve obtained from the simulated measurements is shown in blue and the exact curve is depicted in orange.

It can be seen that removing the harmonic components by filtering the data improves the stiffness curve, as the cubic expression of the stiffness force can now be clearly identified. However, it does not match with the analytical curve, but this is not problematic, as the ASM is mainly a qualitative method. While the stiffness curve is improved, the damping curve on

the other hand is not changed significantly by the application of a filter. This shows once again the difficulty of the characterisation of the damping force of a nonlinear system using the acceleration surface method.

The acceleration surface method is now applied to the second mode of the system. The stiffness and damping curves are illustrated in Figure 3.6.

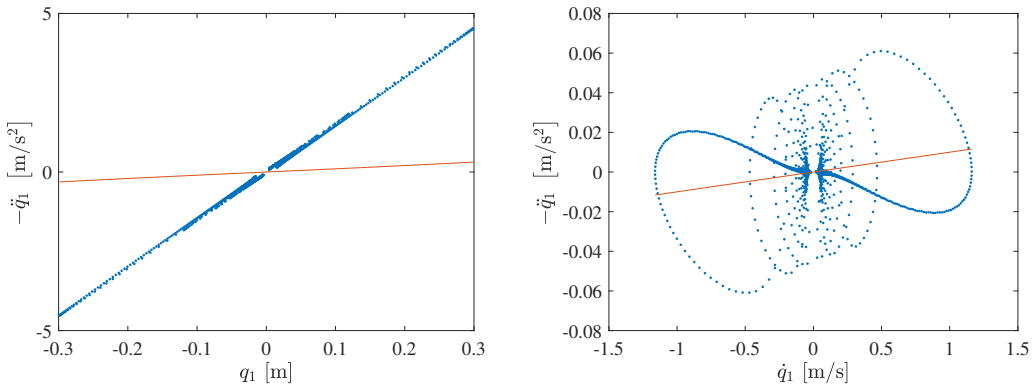

(a) Stiffness curve.

(b) Damping curve.

Figure 3.6: Stiffness and damping curves for the second mode of the 2 DOF system with a cubic stiffness and for a forcing amplitude of 0.1 N. The curve obtained from the simulated measurements is shown in blue and the exact curve is depicted in orange.

The displacement being smaller for this mode than for the first mode, the stiffness curve is linear and the cubic component of the stiffness is not visible, as already predicted by the low value of r_{nl}. However, the slope of the linear curve is higher than what it should be. Indeed, one might expect a slope of 1 $\left(\text{m/s}^2\right)/\text{m}$, the linear coefficient of the stiffness force between DOF 1 and the ground being equal to 1 N/m and the mass of DOF 1 being equal to 1 kg. However, the actual slope, computed with a least-squares estimation, is found to be equal to 14.96 $\left(\text{m/s}^2\right)/\text{m}$. This illustrates that different modes can yield stiffness curves with different slopes, the stiffness curve of the first mode being close to the theoretical curve at small displacements. Such a behaviour has already been observed experimentally, as shown in Figure 1.3.

The slope of the second mode may be explained by the stiffness force at the connection between DOF 1 and DOF 2. At mode 2, the two masses oscillate out-of-phase, which creates a large stiffness force between DOF 1 and DOF 2, the difference $q_1 - q_2$ being large, especially at the displacement extrema. More precisely, as the displacement amplitudes of both degrees of freedom are approximately equal and of opposite signs, as can be seen in Figure 3.7, $q_1 - q_2$ can be approximated as 2 q_1 since q_2 is almost equal to $-q_1$. The stiffness force $7\,(q_1 - q_2)$ can then be rewritten as 14 q_1. The total stiffness force applied to DOF 1, which is the sum of the stiffness force to the ground and to DOF 2, can thus be approximated by

$$f_{\text{s}} = q_1 + 14\, q_1 = 15\, q_1, \tag{3.7}$$

where the cubic stiffness term has been neglected since the displacement is small. As the mass of DOF 1 is equal to 1 kg, this results in a slope of the stiffness curve equal to 15 $\left(\text{m/s}^2\right)/\text{m}$, which corresponds to the estimated slope of the stiffness curve.

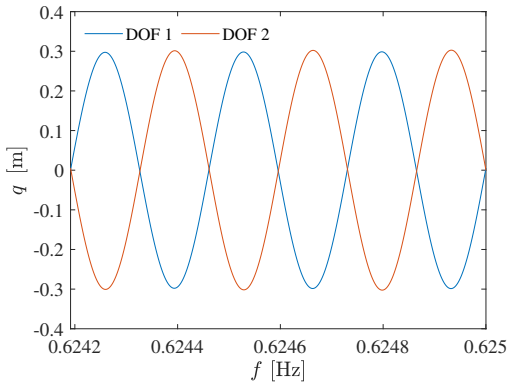

Figure 3.7: Displacement as a function of the excitation frequency of both degrees of freedom at the second mode of the 2 DOF system with a cubic stiffness and for a forcing amplitude of 0.1 N.

The damping curve of the second mode has a line that is similar to the one visible in the damping curve of the first mode. However, there are other loops in the damping curve, which are not present for the first mode. They are due to the beating phenomenon occurring after the main resonance peak. Indeed, each of these loops is due to a different peak of the beating, the first and largest peak being responsible for the largest loop, as it has the largest velocity and acceleration amplitudes. This beating phenomenon is shown in Figure 3.8.

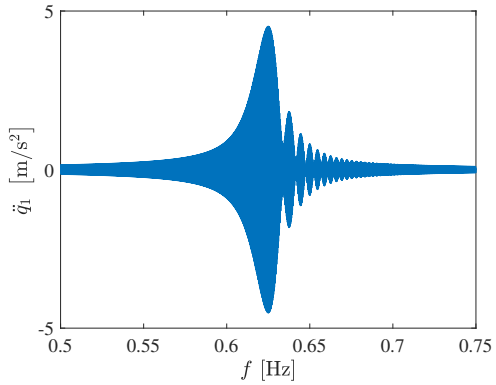

Figure 3.8: Acceleration of DOF 1 as a function of the excitation frequency at the second mode of the 2 DOF system with a cubic stiffness and for a forcing amplitude of 0.1 N.

3.1.2 Forcing amplitude of 1 N

A sine sweep excitation with a forcing amplitude of 1 N is now applied to the system. The nonlinearity ratio of the first mode is equal to 126 %, thus being very nonlinear, while the second mode has a ratio of 22.8 %, indicating that the cubic nature of the stiffness force between DOF 1 and the ground may also be deduced from the second mode, which is not possible for a forcing amplitude of 0.1 N. The stiffness and damping curves of the first mode are depicted in Figure 3.9.

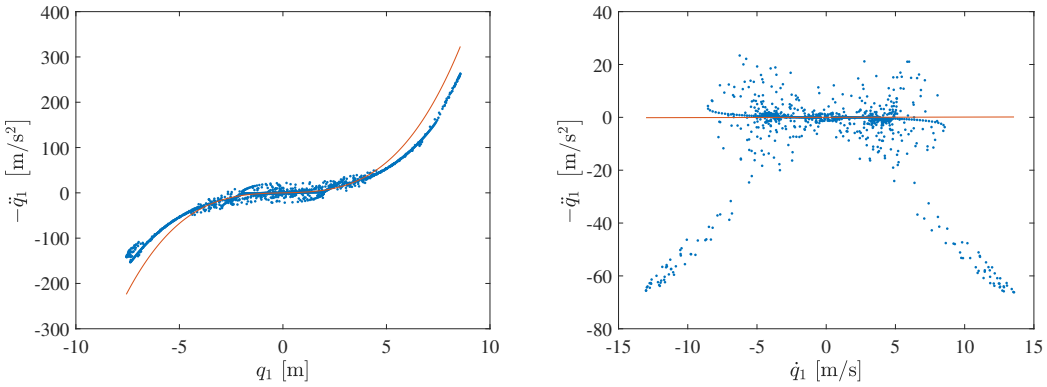

(a) Stiffness curve. (b) Damping curve.

Figure 3.9: Stiffness and damping curves for the first mode of the 2 DOF system with a cubic stiffness and for a forcing amplitude of 1 N. The curve obtained from the simulated measurements is shown in blue and the exact curve is depicted in orange.

At first sight, the stiffness and damping curves of the first mode obtained for a forcing level of 1 N are very different from those obtained for a forcing level of 0.1 N. While the cubic nature of the stiffness force is not detectable at a forcing amplitude of 0.1 N, it can be easily identified at an excitation of 1 N. The damping curve remains however difficult to interpret. This difference in the stiffness and damping curves is also accompanied by a large increase in the resonance frequency. Indeed, the resonance frequency is equal to 0.211 Hz for a forcing of 0.1 N and 0.388 Hz for a forcing of 1 N. This increase in the resonance frequency is due to an isola merging occurring at the frequency of the 3:1 modal interaction. Furthermore, the different parts of the stiffness and damping curves are related to different dynamical regimes corresponding to different frequency ranges. These frequency ranges are represented in Figure 3.10. The stiffness and damping curves with the points of the different dynamical regimes shown in the corresponding colours are depicted in Figure 3.11.

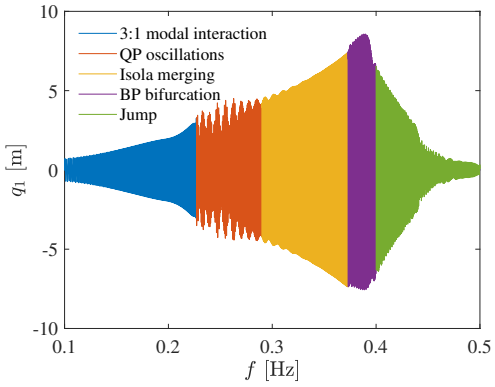

Figure 3.10: Displacement of DOF 1 as a function of the excitation frequency at the first mode of the 2 DOF system with a cubic stiffness and for a forcing amplitude of 1 N. The different dynamical regimes are indicated in different colours.

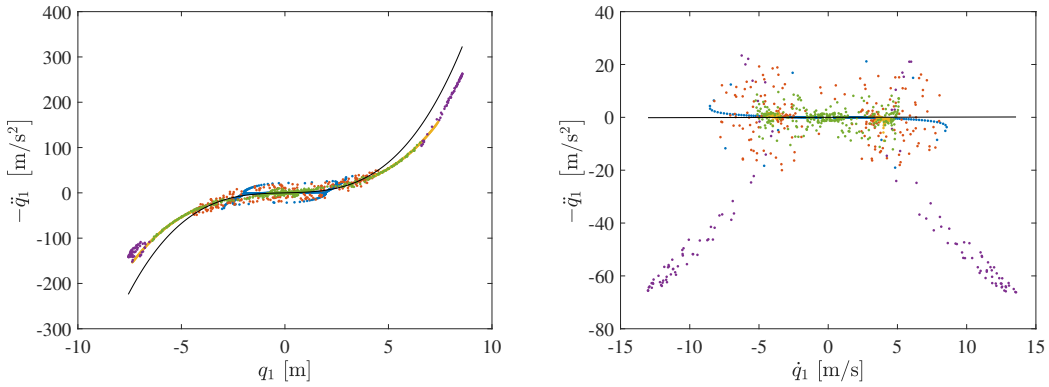

(a) Stiffness curve. (b) Damping curve.

Figure 3.11: Stiffness and damping curves for the first mode of the 2 DOF system with a cubic stiffness and for a forcing amplitude of 1 N. The points related to the different dynamical regimes are shown in the corresponding colour and the exact curve is depicted in black.

The first frequency range shown in blue corresponds to the 3:1 modal interaction, which is already present at a forcing of 0.1 N. The second frequency range indicated in orange corresponds to quasiperiodic (QP) oscillations due to a Neimark-Sacker bifurcation occurring at these frequencies. This Neimark-Sacker bifurcation likely results from the isola merging, as it has already been established that it can occur at the merging region between the main branch of the frequency response curve and an isola [21]. The third frequency range depicted in yellow results from the isola merging, as it corresponds to the isola that has merged with the main branch of the nonlinear frequency response curve. The fourth frequency range illustrated in purple corresponds to a branch-point (BP) bifurcation and the last frequency range represented in green corresponds to the jump from the upper branch of the nonlinear frequency response curve to the lower branch. The identification of the Neimark-Sacker and the branch-point bifurcations has been obtained by performing a harmonic balance continuation with the NI2D software.

Having a closer look at the region corresponding to the 3:1 modal interaction, the stiffness curve and the damping curve obtained only for this region are shown in Figure 3.12.

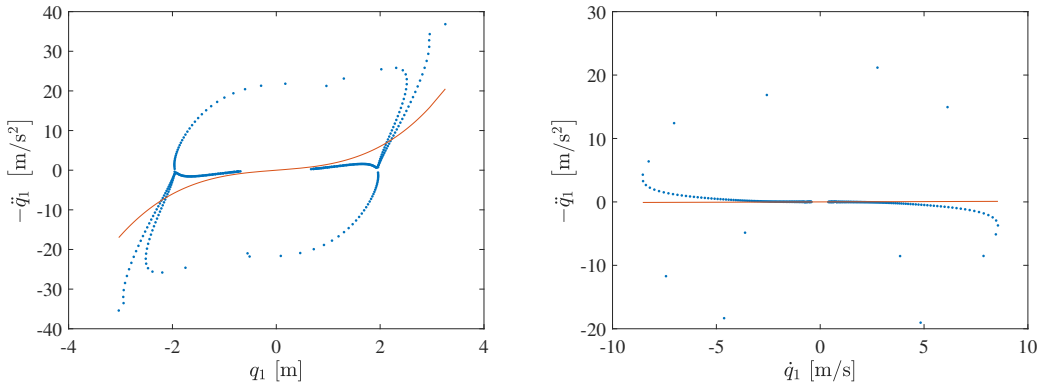

(a) Stiffness curve. (b) Damping curve.

Figure 3.12: Stiffness and damping curves for the 3:1 modal interaction of the first mode of the 2 DOF system with a cubic stiffness and for a forcing amplitude of 1 N. The curve obtained from the simulated measurements is shown in blue and the exact curve is depicted in orange.

It can be seen that the stiffness curve is similar to the one obtained at a forcing amplitude of 0.1 N, the curve separating in different parts at high displacement amplitudes. However, there are three clearly separated lines visible in this case, while there are only two at the lower forcing, two of them being combined to form a single one. These different lines are again due to the two maxima of one period responsible for the two lines increasing for a positive displacement and the decreasing line is due to the minimum for which the displacement is positive. The line linked to the local minimum also tends towards smaller displacements until it becomes negative. This is due to the presence of the third order harmonic component which becomes stronger as the system approaches the resonance. This increasing importance of the harmonic component reduces the displacement of the local minimum until it eventually becomes negative. The displacement of one of the two maxima is also reduced, which is visible on the stiffness curve. This phenomenon is illustrated in Figure 3.13.

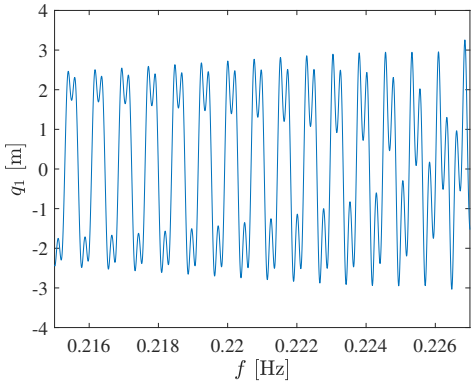

Figure 3.13: Displacement of DOF 1 as a function of the excitation frequency at the 3:1 modal interaction of the first mode of the 2 DOF system with a cubic stiffness and for a forcing amplitude of 1 N.

Focusing on the points of the stiffness curve due to the branch-point bifurcation shown in purple in Figure 3.11a, it can be seen that there is no symmetry between the points at a

positive displacement and those at a negative displacement, as has been observed for all the other studied systems. Indeed, while the points related to the branch-point bifurcation follow the stiffness curve for positive displacements, they are situated above the curve for negative displacements. The absolute value of the displacement and of the acceleration is smaller at negative displacements, creating these points. Furthermore, the amplitude of the acceleration is more strongly reduced as that of the displacement, which is the reason why the points of the stiffness curve for negative values of the displacement are situated above the rest of the curve, the acceleration having a lower amplitude for the same displacement. This asymmetry in the displacement is the result of the branch-point bifurcation and can be seen in Figure 3.10. The nonlinear frequency response curve including the different branches of the branch-point bifurcation, computed through harmonic balance continuation on the NI2D software, and the evolution of the displacement with the excitation frequency are superimposed in Figure 3.14. It can be seen that at a positive displacement, the response of the system to the excitation follows the main branch, while at a negative displacement, it follows the lower branch that appears due to the branch-point bifurcation.

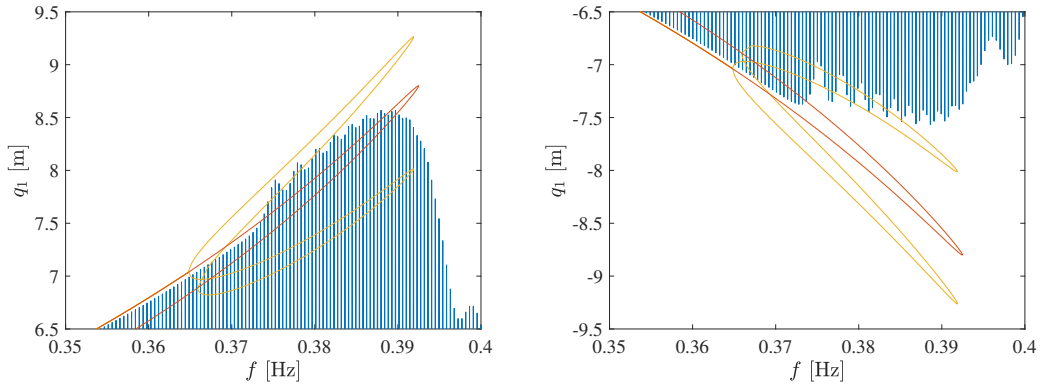

(a) Positive displacement. (b) Negative displacement.

Figure 3.14: Displacement of DOF 1 as a function of the excitation frequency and nonlinear frequency response curve at the branch-point bifurcation of the first mode of the 2 DOF system with a cubic stiffness and for a forcing amplitude of 1 N at positive and negative displacements. The displacement is shown in blue, the main branch of the frequency response curve is depicted in orange and the branches resulting from the branch-point bifurcation are represented in yellow.

Due to the branch-point bifurcation, harmonics of even order and a constant term appear in the response of the system. The presence of these harmonics can be put in evidence by the computation of the Fast Fourier Transform (FFT) of the displacement and the acceleration, which are depicted in Figure 3.15. The FFT reveals the presence of second and fourth order harmonics in the response, as well as a constant term, the peak at 0.38 Hz corresponding to the fundamental frequency. These harmonics of even order are responsible for the asymmetry in the displacement. The stronger asymmetry of the acceleration as that of the displacement can be explained by the higher importance of the even harmonics in the acceleration time series than in the displacement time series.

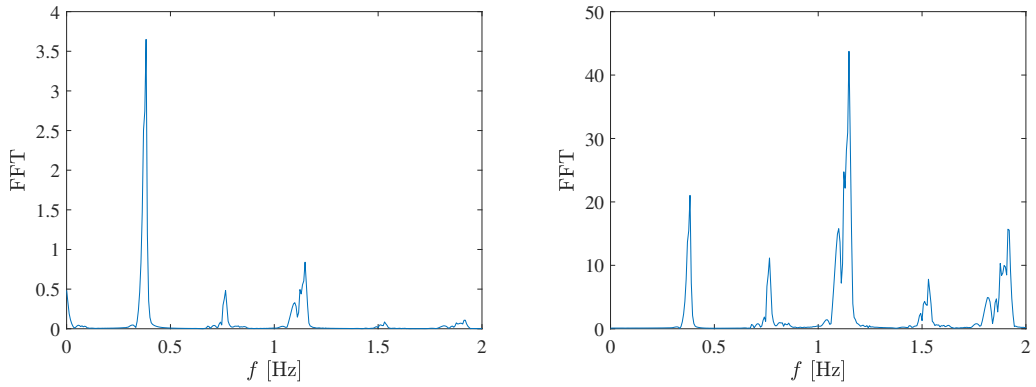

(a) FFT of the displacement.

(b) FFT of the acceleration.

Figure 3.15: Fast Fourier transform of the displacement and the acceleration of DOF 1 at the branch-point bifurcation of the first mode of the 2 DOF system with a cubic stiffness and for a forcing amplitude of 1 N.

The effect of the branch-point bifurcation on the damping curve is the appearance of two parts with negative values of $-\ddot{q}_1$ for both positive and negative velocities. This can be explained by the presence of harmonics of even order and the asymmetry resulting from it. Due to this asymmetry, for all the points at which the displacement is equal to 0 m and which thus correspond to the points of the damping curve, the acceleration is always positive, and therefore $-\ddot{q}_1$ is always negative. This is shown in Figure 3.16a. However, as the excitation frequency increases, the acceleration becomes always negative when the displacement is null, thus creating a few points for which $-\ddot{q}_1$ is always positive. This is shown in Figure 3.16b.

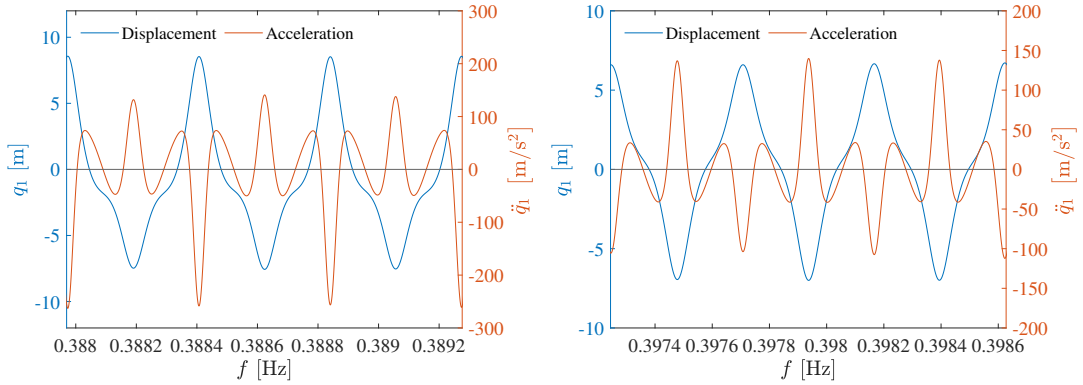

(a) Positive acceleration when the displacement is null.

(b) Negative acceleration when the displacement is null.

Figure 3.16: Displacement and acceleration of DOF 1 as a function of the excitation frequency at the branch-point bifurcation of the first mode of the 2 DOF system with a cubic stiffness and for a forcing amplitude of 1 N.

It has been shown that different dynamical regimes can exhibit different behaviours in the stiffness and damping curves that may make the curves more difficult to analyse. While the damping curve always remains difficult to interpret, one possible solution to improve the stiffness curve could be to filter the response, harmonics being present for different dynamical

regimes. This method has already proven to be adequate when there is a strong presence of harmonics. However, due to the large frequency range of the first mode, filtering does not improve the stiffness curve. Instead of filtering the data, another possibility is to simply select the dynamical regimes producing the best points on the stiffness curve and excluding those creating the points that make the stiffness curve more difficult to interpret, such as those related to the 3:1 modal interaction and the branch-point bifurcation. The frequency ranges of the excitation force that have been retained are those related to the isola merging and the jump to the lower branch of the frequency response curve. They are indicated in Figure 3.10 in yellow and green respectively. The resulting stiffness curve is shown in Figure 3.17.

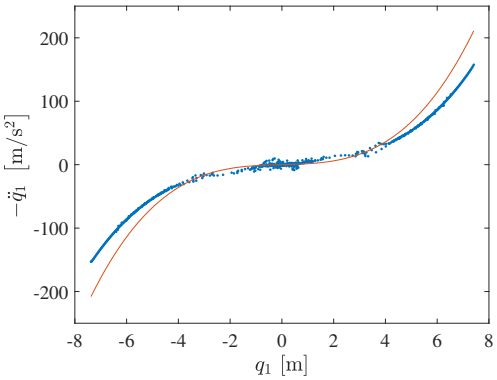

Figure 3.17: Stiffness curve for the isola merging and the jump of the first mode of the 2 DOF system with a cubic stiffness and for a forcing amplitude of 1 N.

The stiffness curve and the damping curve obtained for the second mode are represented in Figure 3.18.

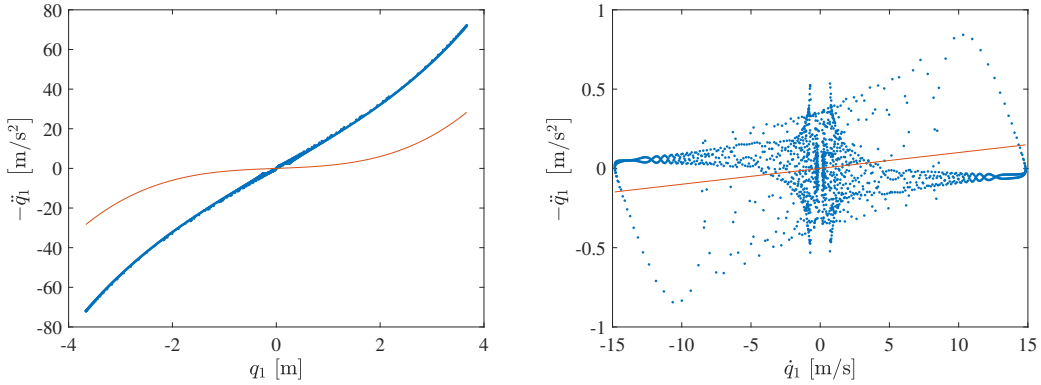

(a) Stiffness curve. (b) Damping curve.

Figure 3.18: Stiffness and damping curves for the second mode of the 2 DOF system with a cubic stiffness and for a forcing amplitude of 1 N. The curve obtained from the simulated measurements is shown in blue and the exact curve is depicted in orange.

The cubic nature of the stiffness force can be deduced from the stiffness curve, although there is a linear stiffness force higher than expected. The linear coefficient obtained through a least-squares estimation for which the two unknowns are the cubic and the linear coefficients

is equal to 14.5 $\left(\mathrm{m/s^2}\right)/\mathrm{m}$, which is close to 15 $\left(\mathrm{m/s^2}\right)/\mathrm{m}$, such as in the case of a forcing amplitude of 0.1 N. The origin of this overestimation of the linear stiffness force is the same as for a smaller forcing. However, as the displacement amplitude is larger at a higher excitation level, the cubic component of the stiffness force is not negligible anymore and can be seen in the stiffness curve. On the other hand, the linear expression of the damping curve is still impossible to deduce from the damping curve.

3.2 Second system with a cubic stiffness

The system described by

$$\begin{bmatrix} 1 & 0 \\ 0 & 1 \end{bmatrix} \begin{pmatrix} \ddot{q}_1 \\ \ddot{q}_2 \end{pmatrix} + 0.01 \begin{bmatrix} 2 & -1 \\ -1 & 2 \end{bmatrix} \begin{pmatrix} \dot{q}_1 \\ \dot{q}_2 \end{pmatrix} + \begin{bmatrix} 2 & -1 \\ -1 & 2 \end{bmatrix} \begin{pmatrix} q_1 \\ q_2 \end{pmatrix} + \begin{pmatrix} 0.5\, q_1^3 \\ 0 \end{pmatrix} = \begin{pmatrix} 0 \\ p(t) \end{pmatrix} \tag{3.8}$$

is now considered. The only difference with the previous system is the stiffness between DOFs 1 and 2, which is now equal to 1 N/m instead of 7 N/m. The external force $p(t)$ consists of a sine sweep excitation with a starting frequency of 0 Hz and an ending frequency of 0.5 Hz, the natural frequencies of the linear system being equal to 0.159 Hz and 0.276 Hz, and a sweep rate of 0.005 Hz/min, the amplitude being specified in each case.

3.2.1 Forcing amplitude of 0.1 N

The forcing amplitude of the excitation is first equal to 0.1 N. At this forcing level, the first mode is already strongly nonlinear as $r_{\mathrm{nl}} = 79.6$ %, but there is no modal interaction. On the other hand, at the second mode, $r_{\mathrm{nl}} = 6.26$ % and the mode is only weakly nonlinear.

The acceleration time series is depicted in Figure 3.19.

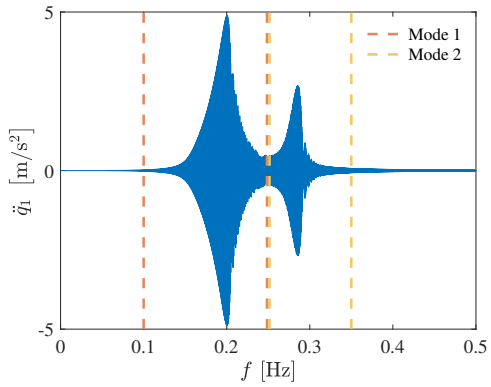

Figure 3.19: Acceleration of DOF 1 as a function of the excitation frequency for the second 2 DOF system with a cubic stiffness and for a forcing amplitude of 0.1 N and the frequency windows of the first and second modes.

The stiffness and damping curves obtained for the first mode are shown in Figure 3.20.

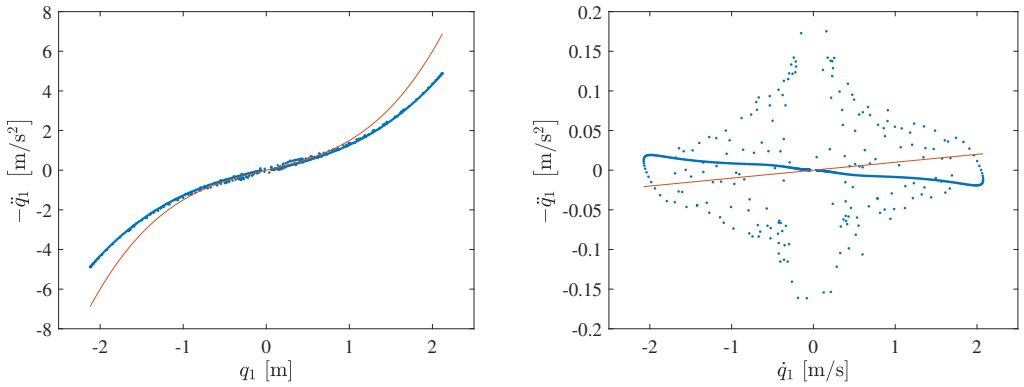

(a) Stiffness curve. (b) Damping curve.

Figure 3.20: Stiffness and damping curves for the first mode of the second 2 DOF system with a cubic stiffness and for a forcing amplitude of 0.1 N. The curve obtained from the simulated measurements is shown in blue and the exact curve is depicted in orange.

While for the previous system with a cubic stiffness and a forcing amplitude of 0.1 N, the stiffness curve gets separated in different parts, this does not happen for this system and the curve is cubic. It is thus easier to interpret the stiffness curve for this system. This is due to the fact that there is no modal interaction creating strong third order harmonics in this case, which is the reason for the shape of the stiffness curve of the other system. Indeed, for this system, the 3:1 modal interaction occurs at higher energy levels, such that it does not appear for this forcing amplitude, while the system is already nonlinear. This can be seen in the frequency-energy plot represented in Figure 3.21. The modal interaction occurs at an energy of around 300 J, while it occurs at an energy of approximately 30 J for the first system. A modal interaction can thus be created more easily and with low forcing amplitudes for the first system, while more energy needs to be added to the second system in order to detect a modal interaction.

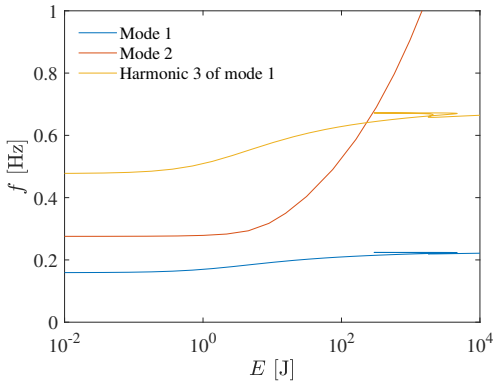

Figure 3.21: Frequency-energy plots of both nonlinear normal modes as well as the third harmonics of mode 1 of the second 2 DOF system with a cubic stiffness.

While the stiffness curve of the first mode significantly differs to that of the first mode of the previous system, the stiffness curve of the second mode is similar for both systems, with

a linear curve having a higher slope than the theoretical curve due to the linear stiffness force between DOFs 1 and 2.

3.2.2 Forcing amplitude of 2 N

In order to detect the 3:1 modal interaction, a forcing amplitude of 2 N is now considered. The first mode is such that $r_{\text{nl}} = 121$ % and the second mode has a nonlinearity ratio of 58.9 % and is thus clearly nonlinear, which is not the case for a forcing amplitude of 0.1 N.

The stiffness and damping curves for the first mode are depicted in Figure 3.22.

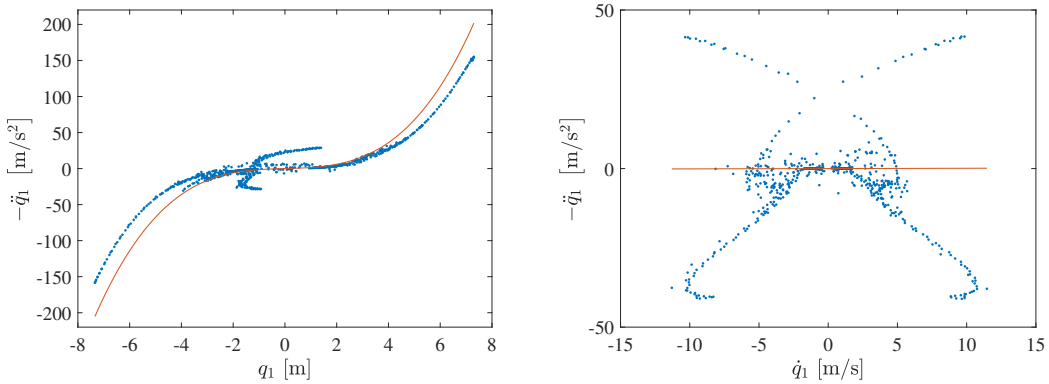

(a) Stiffness curve. (b) Damping curve.

Figure 3.22: Stiffness and damping curves for the first mode of the second 2 DOF system with a cubic stiffness and for a forcing amplitude of 2 N. The curve obtained from the simulated measurements is shown in blue and the exact curve is depicted in orange.

It can be seen that two lines appear in the stiffness curve at a displacement q_1 close to 0 m, one of them having a negative acceleration and the other one a positive acceleration. These lines result from the presence of harmonics of third order due to the 3:1 modal interaction between the two vibration modes. However, unlike for the first system, the stiffness curve still has a cubic shape and the lines appear at small displacements, not changing significantly the rest of the curve. This can be explained by the displacement time series shown in Figure 3.23. Indeed, while for the previous system, new displacement extrema are created close to the existing extrema, they appear here at displacements close to 0 m. As both maxima, respectively minima, close to 0 m have a similar amplitude, they form points in the stiffness curve that are also close to each other. Each of the two lines appearing in the stiffness curve, corresponding to either the maxima or the minima at small displacements, is thus composed of two lines corresponding to the two distinct extrema. However, due to the similar displacement and acceleration values of these extrema, the two lines cannot be distinguished from each other. Furthermore, an asymmetry can be observed in the displacement time series, which is due to the presence of even order harmonics and a constant term, resulting from a branch-point bifurcation. This explains why the lines start to differ from the main curve at a negative displacement and not at a displacement equal to 0 m.

The different lines in the damping curve can be explained by a similar reasoning, the points of the damping curve corresponding to the different points for which the displacement of DOF 1 is null.

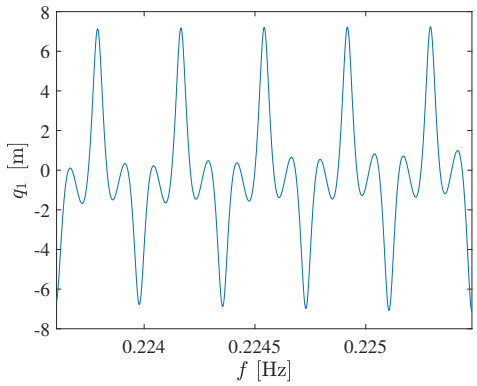

Figure 3.23: Displacement of DOF 1 as a function of the excitation frequency for the second 2 DOF system with a cubic stiffness and a forcing amplitude of 2 N at the first resonance mode.

The stiffness curve of the second mode is cubic, but with slightly higher absolute values of $-\ddot{q}_1$ than the exact curve due to the stiffness force between the masses 1 and 2.

3.3 Piecewise linear stiffness

In this section, a trilinear stiffness force representing an impact is added to the linear system. The equation of motion of the first mass is thus expressed as

$$\begin{cases} \ddot{q}_1 + 0.01\,\dot{q}_1 + q_1 + 0.01\,(\dot{q}_1 - \dot{q}_2) + 7\,(q_1 - q_2) = 0 & \text{if } |q_1| \leq 1 \text{ m} \\ \ddot{q}_1 + 0.01\,\dot{q}_1 + (1 + k_{\text{nl}})\,q_1 + 0.01\,(\dot{q}_1 - \dot{q}_2) + 7\,(q_1 - q_2) = 0 & \text{if } |q_1| > 1 \text{ m} \end{cases}, \tag{3.9}$$

where k_{nl} is the increase in stiffness due to the impact occurring at displacements of -1 and 1 m. Different coefficients k_{nl} are considered, a constant forcing amplitude of 0.1 N being applied to the system for all the studied cases. At this forcing level, the displacement amplitude is higher than 1 m for the first mode, which is therefore nonlinear, but smaller than 1 m for the second mode, which is thus perfectly linear.

3.3.1 Increase in stiffness of 2 N/m

First, an increase in stiffness of 2 N/m, with $k_{\text{nl}} = 2$ N/m, is considered. The stiffness and damping curves obtained for the first mode are shown in Figure 3.24.

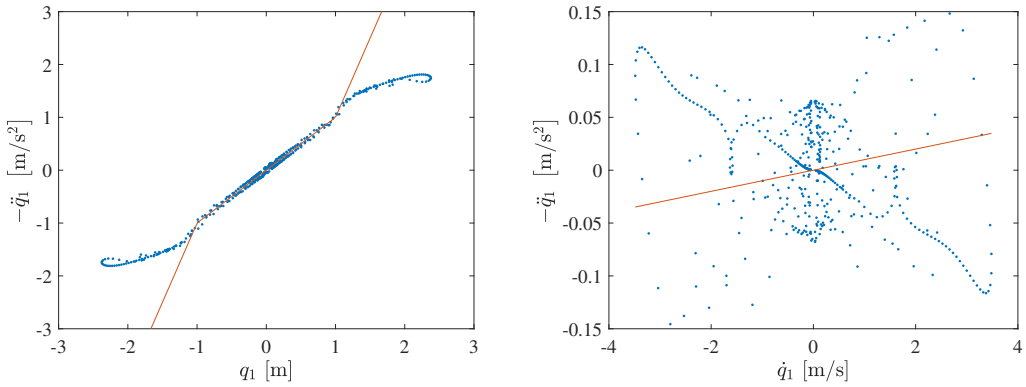

(a) Stiffness curve. (b) Damping curve.

Figure 3.24: Stiffness and damping curves for the first mode of the 2 DOF system with a trilinear stiffness with an increase in stiffness of 2 N/m. The curve obtained from the simulated measurements is shown in blue and the exact curve is depicted in orange.

Between displacements of -1 and 1 m, the stiffness curve corresponds almost exactly to the theoretical curve, but diverges from it as the displacement amplitude increases. For $|q_1| > 1$ m, the curve is not linear anymore and is not close to the theoretical linear curve. This is due to the stiffness force $7\,(q_1 - q_2)$, which increases as $|q_1|$ becomes greater than 1 m, since the amplitude of q_2 becomes larger than that of q_1 while they were close to each other at lower displacements. For a positive displacement q_1, $q_1 - q_2$ is thus negative and the stiffness force between DOF 1 and DOF 2 is also negative, which is the reason why the obtained stiffness curve is below the exact one for positive displacements. Furthermore, the presence of third order harmonics in the response of DOF 1 results in a local minimum of the acceleration at the points where the displacement amplitude is maximum, as shown in Figure 3.25. The points of the stiffness curve corresponding to the displacement maxima, this may explain the lower amplitude of the stiffness curve compared to the exact curve.

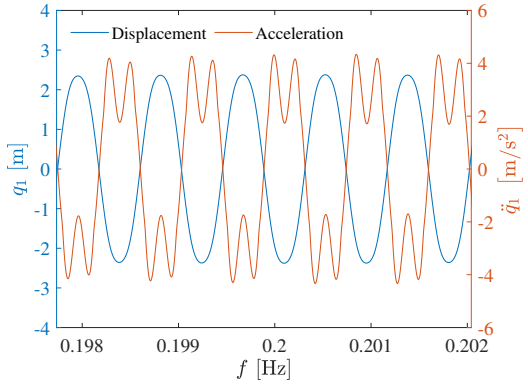

Figure 3.25: Displacement and acceleration of DOF 1 as a function of the excitation frequency for the first mode of the 2 DOF system with a trilinear stiffness with an increase in stiffness of 2 N/m.

One possible improvement of the results is thus to filter the displacement, velocity and acceleration time series of both degrees of freedom before applying the ASM. A low-pass

filter removing the harmonic components is used. The stiffness and damping curves obtained after filtering the data are depicted in Figure 3.26.

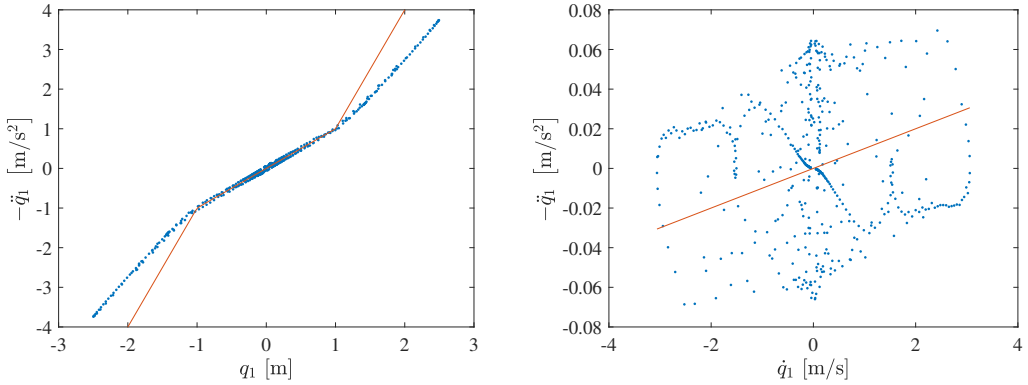

(a) Stiffness curve. (b) Damping curve.

Figure 3.26: Stiffness and damping curves for the first mode of the 2 DOF system with a trilinear stiffness with an increase in stiffness of 2 N/m obtained after filtering the data. The curve obtained from the simulated measurements is shown in blue and the exact curve is depicted in orange.

The stiffness curve is now clearly piecewise linear, but the damping curve is not modified significantly. The use of a filter thus again improves the stiffness curve, but not the damping curve.

The second mode displays a stiffness curve and a damping curve identical to those obtained for a cubic stiffness and for a forcing amplitude of 0.1 N, which are illustrated in Figure 3.6. Furthermore, as the displacement amplitude is smaller than 1 m, the system behaves perfectly linearly for this mode.

3.3.2 Increase in stiffness of 5 N/m

An increase in stiffness $k_{\text{nl}} = 5$ N/m is now considered. The acceleration time series for this system is represented in Figure 3.27.

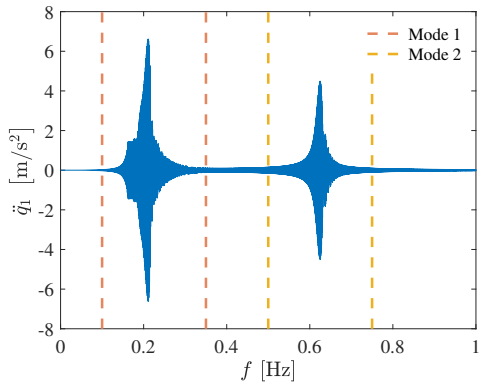

Figure 3.27: Acceleration of DOF 1 as a function of the excitation frequency for the second 2 DOF system with a trilinear stiffness with an increase in stiffness of 5 N/m and the frequency windows of the first and second modes.

The stiffness and damping curves obtained for the first mode are shown in Figure 3.28.

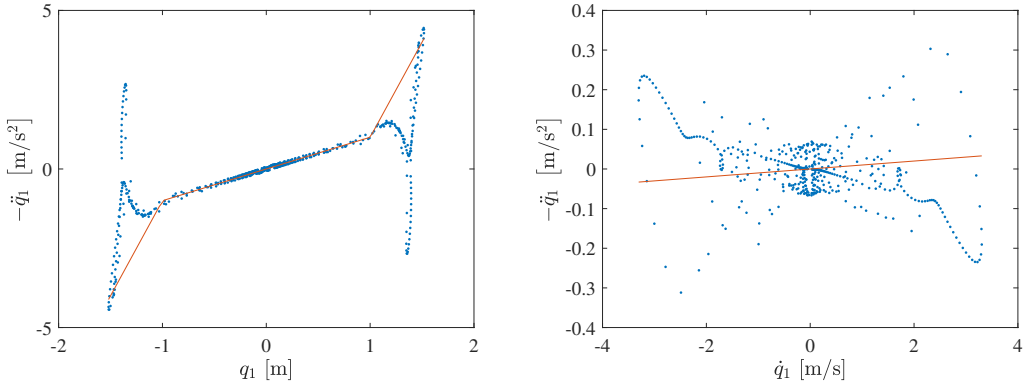

(a) Stiffness curve. (b) Damping curve.

Figure 3.28: Stiffness and damping curves for the first mode of the 2 DOF system with a trilinear stiffness with an increase in stiffness of 5 N/m. The curve obtained from the simulated measurements is shown in blue and the exact curve is depicted in orange.

The damping curve is similar to that resulting from a trilinear stiffness with a stiffness increase of 2 N/m and depicted in Figure 3.24b. The stiffness curve, on the other hand, is almost identical to the one obtained for a cubic stiffness and a forcing amplitude of 0.1 N, which is shown in Figure 3.2a. The origin of the shape of the curve is also similar and is due to the harmonic components of the response of the system to the excitation. This illustrates that two different types of nonlinearities can exhibit the same stiffness curve, making it difficult to correctly predict from the curve which type of nonlinearity is present in the system.

As has already been shown in the case of a cubic stiffness whose stiffness curve is identical to the one obtained here, filtering the data before applying the acceleration surface method to it may improve the stiffness curve such that the functional form of the nonlinear force can be retrieved from it. A filter is thus also used here to remove the harmonics from the response and only keep the fundamental frequency. The stiffness and damping curves resulting from it are represented in Figure 3.29.

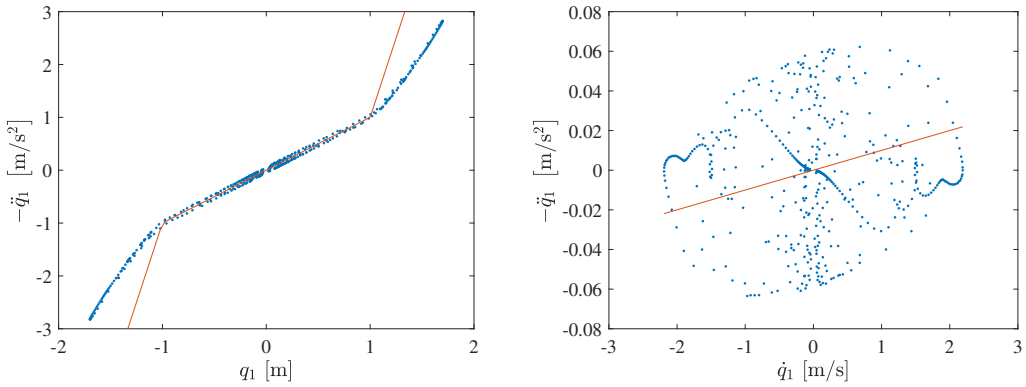

(a) Stiffness curve. (b) Damping curve.

Figure 3.29: Stiffness and damping curves for the first mode of the 2 DOF system with a trilinear stiffness with an increase in stiffness of 5 N/m obtained after filtering the data. The curve obtained from the simulated measurements is shown in blue and the exact curve is depicted in orange.

The piecewise linear expression of the nonlinear stiffness force can now be deduced from the stiffness curve, although it is not perfectly linear for $|q_1| > 1$ m and the observed increase in stiffness is lower than it should be. Despite this, it can be concluded that filtering the data helps distinguish a cubic stiffness from a piecewise linear stiffness. However, the characterisation of the damping force remains a difficult task when using the ASM, even when filtering the data.

The stiffness and damping curves of the second mode are identical to those for a lower increase in stiffness $k_{\text{nl}} = 2$ N/m, since the system is linear at this mode.

3.3.3 Increase in stiffness of 30 N/m

The nonlinearity in the system now consists in an increase in stiffness of $k_{\text{nl}} = 30$ N/m when $|q_1| > 1$ m. The stiffness and damping curves are illustrated in Figure 3.30.

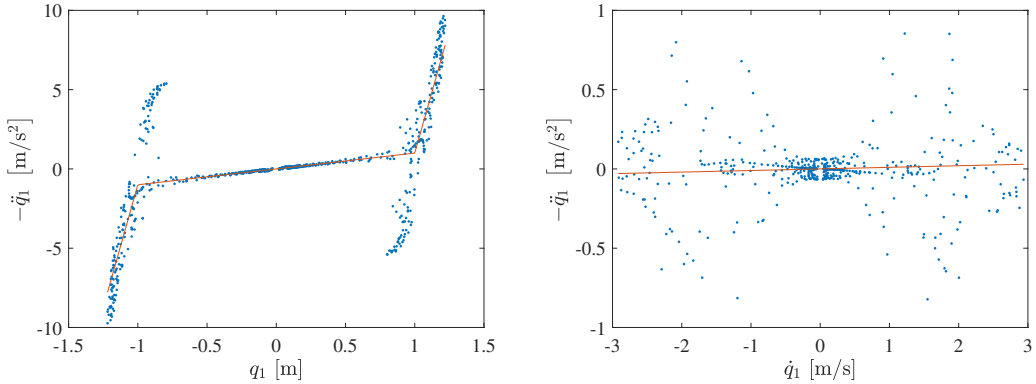

(a) Stiffness curve. (b) Damping curve.

Figure 3.30: Stiffness and damping curves for the first mode of the 2 DOF system with a trilinear stiffness with an increase in stiffness of 30 N/m. The curve obtained from the simulated measurements is shown in blue and the exact curve is depicted in orange.

It can be seen that the stiffness curve follows the theoretical curve, even at high displacements. However, there is another branch of the curve appearing at displacements of 1 and -1 m. Following the same reasoning as previously, the presence of this branch is due to the harmonics of order 3. While in all the previous cases, no branch of the stiffness curve corresponds to the exact curve, this can be observed here. This is a particular case for which q_2 is almost equal to q_1 when q_1 reaches a maximum, the stiffness force between DOF 1 and DOF 2 being therefore small, allowing the stiffness curve to follow the exact curve. A similar behaviour of the stiffness curve has already been observed experimentally for the SmallSat structure [2], as shown in Figure 1.2, and an aircraft Piccolo tube [12]. Furthermore, the presence of harmonics in the response of the SmallSat structure to the excitation has been put in evidence, leading to the creation of new extrema of the relative displacement of the nonlinear connection [3]. This might thus explain the appearance of additional branches in the stiffness curve of the SmallSat structure.

As there is a strong presence of harmonics in the response of the system to the excitation, a filter can be used to remove these harmonics and improve the stiffness curve. The stiffness and damping curves obtained after using a low-pass filter are shown in Figure 3.31.

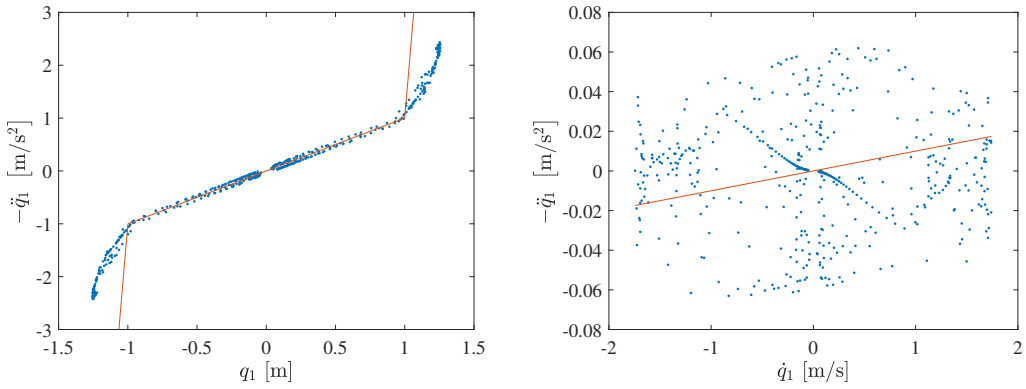

(a) Stiffness curve. (b) Damping curve.

Figure 3.31: Stiffness and damping curves for the first mode of the 2 DOF system with a trilinear stiffness with an increase in stiffness of 30 N/m obtained after filtering the data. The curve obtained from the simulated measurements is shown in blue and the exact curve is depicted in orange.

Filtering the data again does not improve the damping curve, but improves the stiffness curve. Indeed, the branch which was previously present has disappeared and the piecewise linear expression of the stiffness force can be more easily recognised. However, for a displacement amplitude above 1 m, the curve is not exactly linear and does not follow the theoretical curve as previously.

As has already been observed for all the cases with a piecewise linear stiffness for the first mode, the stiffness curve is linear between the positions of the impact. This always holds true, whether a filter is used or not. This can be explained by the fact that before the change in stiffness occurs, the system is perfectly linear. There are thus no harmonics appearing which may influence the shape of the stiffness curve. Furthermore, at these small displacements, q_1 and q_2 are almost equal, such that the stiffness force at the connection between both masses is small. However, q_1 and q_2 are not perfectly equal and the amplitude of motion of DOF 2

is slightly larger than that of DOF 1. There is thus a small negative stiffness force $7\,(q_1 - q_2)$ for positive displacements and the stiffness curve lies slightly below the exact curve. This is illustrated in Figure 3.32a for the case where $k_{\text{nl}} = 30$ N/m and for which a filter is used. It can be seen that the points follow a straight line situated just below the theoretical curve, and above for negative displacements. The other points are due to the jump after the resonance peak, for which $q_1 - q_2$ changes sign with time, being positive at some points and negative at others. This behaviour is similar to the one observed for 1 DOF systems and depicted in Figure 2.3a and can also be seen for systems with a cubic stiffness.

A similar observation can be made for the out-of-phase mode, where two distinct lines are visible at small displacements, as shown in Figure 3.32b. The lower line, for positive displacements, is due to the points before the resonance peak for which the amplitude of motion of DOF 1 is slightly larger than that of DOF 2, the stiffness force between DOF 1 and DOF 2 thus being slightly smaller than 14 q_1. The upper line is due to the points after the resonance and for which the amplitude of motion of DOF 1 is slightly smaller than that of DOF 2, the stiffness force between DOF 1 and DOF 2 thus being larger than 14 q_1 for positive displacements. A similar phenomenon has also been put in evidence experimentally on the SmallSat structure [13], as illustrated in Figure 1.3.

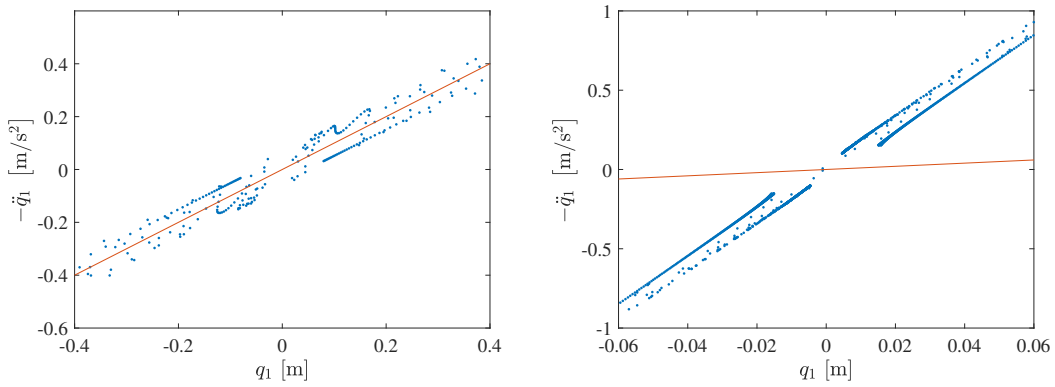

(a) Mode 1. (b) Mode 2.

Figure 3.32: Close-up of the stiffness curve for both modes of the 2 DOF system with a trilinear stiffness with an increase in stiffness of 30 N/m. The curve obtained from the simulated measurements is shown in blue and the exact curve is depicted in orange.

3.4 First system with Coulomb friction

After having studied two types of nonlinear stiffness, nonlinear damping is now considered. Coulomb friction is thus added to the linear system and Equation 3.3 can be expressed as

$$0.01\,\dot{q}_1 + q_1 + 0.01\,(\dot{q}_1 - \dot{q}_2) + 7\,(q_1 - q_2) + \text{sign}\,(\dot{q}_1) = -\ddot{q}_1, \tag{3.10}$$

where

$$\text{sign}\,(\dot{q}_1) = \begin{cases} 1 & \text{if } \dot{q}_1 > 0 \text{ m/s} \\ 0 & \text{if } \dot{q}_1 = 0 \text{ m/s} \\ -1 & \text{if } \dot{q}_1 < 0 \text{ m/s} \end{cases}. \tag{3.11}$$

3.4.1 Forcing amplitude of 10 N

First, the system is subjected to an excitation level of 10 N, at which both modes are close to having a linear behaviour, the nonlinearity ratios of the modes being respectively equal to 3.60 % and 1.44 %, the Coulomb friction only having a little influence on the dynamics of the system. The stiffness and damping curves obtained for the first mode are illustrated in Figure 3.33.

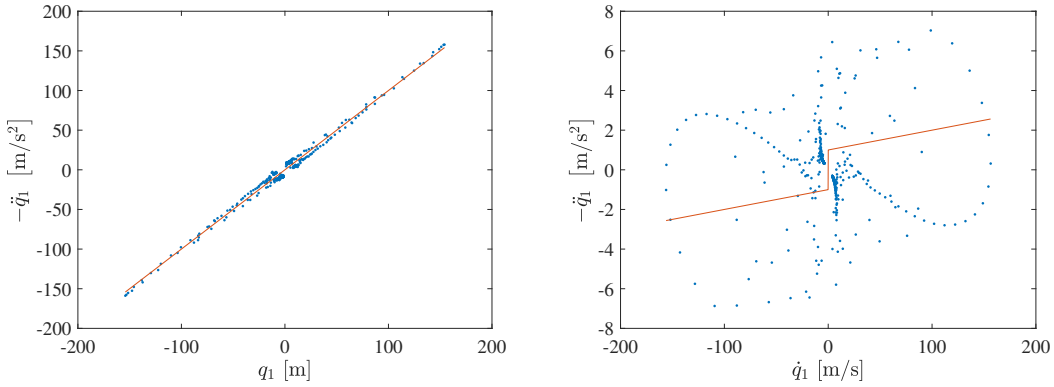

(a) Stiffness curve. (b) Damping curve.

Figure 3.33: Stiffness and damping curves for the first mode of the 2 DOF system with Coulomb friction and for a forcing amplitude of 10 N. The curve obtained from the simulated measurements is shown in blue and the exact curve is depicted in orange.

The stiffness curve is linear and close to the theoretical curve, but the damping curve does not correspond to the expression of the damping force. The presence of Coulomb friction in the system is thus difficult to detect from this curve, as the curve is mainly dominated by the stiffness force between DOF 1 and DOF 2 and is also influenced by the damping force between DOF 1 and DOF 2.

The stiffness and damping curves of the second mode are represented in Figure 3.34.

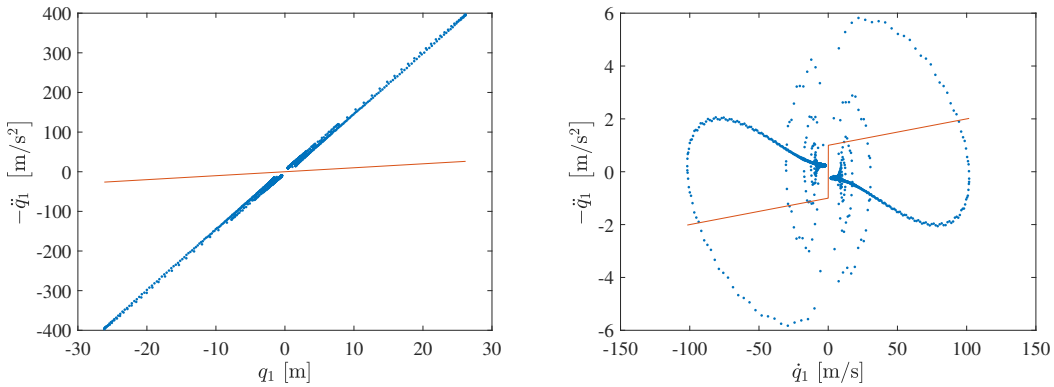

(a) Stiffness curve. (b) Damping curve.

Figure 3.34: Stiffness and damping curves for the second mode of the 2 DOF system with Coulomb friction and for a forcing amplitude of 10 N. The curve obtained from the simulated measurements is shown in blue and the exact curve is depicted in orange.

It can be seen that the stiffness curve is very similar to the stiffness curves of the previous cases for the second mode. The damping curve is also similar, as different pairs of lines related to the different peaks of the beating phenomenon can be observed. However, there is one difference. Indeed, while for all the other cases, the two large lines related to the main resonance peak seem to join each other at the centre of the curve, this does not happen here and there is a jump between them, which can be linked to the jump of the damping force at zero velocity due to the Coulomb friction. While this jump is smaller than on the theoretical curve and goes from the positive to the negative values of $-\ddot{q}_1$ as the velocity becomes positive, it may still hint at the presence of Coulomb friction.

3.4.2 Forcing amplitude of 2 N

In order to better detect the existence of Coulomb friction in the system, a lower forcing amplitude of 2 N is applied to the system, such that the Coulomb friction is not negligible anymore with respect to the other forces acting on DOF 1, the two modes having a ratio r_{nl} of 36.1 % and 13.8 % respectively. This enhances the nonlinear behaviour of the system. The stiffness and damping curves of the first mode are shown in Figure 3.35.

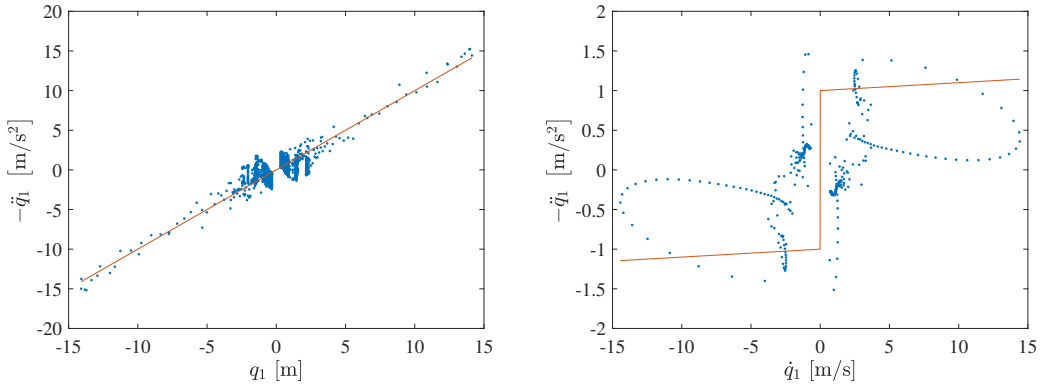

(a) Stiffness curve. (b) Damping curve.

Figure 3.35: Stiffness and damping curves for the first mode of the 2 DOF system with Coulomb friction and for a forcing amplitude of 2 N. The curve obtained from the simulated measurements is shown in blue and the exact curve is depicted in orange.

The damping curve for this mode does not allow the determination of the expression of the damping force. The stiffness curve is linear and follows the exact curve, but exhibits points with a large error compared to the theoretical curve for small displacements. Replacing $-\ddot{q}_1$ by $-\ddot{q}_1 - 0.01\,(\dot{q}_1 - \dot{q}_2) - 7\,(q_1 - q_2)$ when applying the ASM to remove the contribution of the forces between DOF 1 and DOF 2, all the points should be perfectly situated on the theoretical curve. This is true for all the studied nonlinearities, but not for Coulomb friction, where these points remain. This is due to the nature of the Coulomb friction force, which is discontinuous at a velocity of 0 m/s. However, the points of the stiffness curve correspond to the points at which the velocity is null. Since the displacement and acceleration values of these points are obtained through linear interpolation between the points with velocities of opposite signs, the Coulomb friction impacts the acceleration of these points, but the error induced by

the Coulomb friction in the stiffness force is never larger than 1 $\left(\mathrm{m/s^2}\right)/\mathrm{m}$, the Coulomb friction having an intensity of 1 N and the mass of DOF 1 being equal to 1 kg.

The stiffness and damping curves of the second mode are displayed in Figure 3.36.

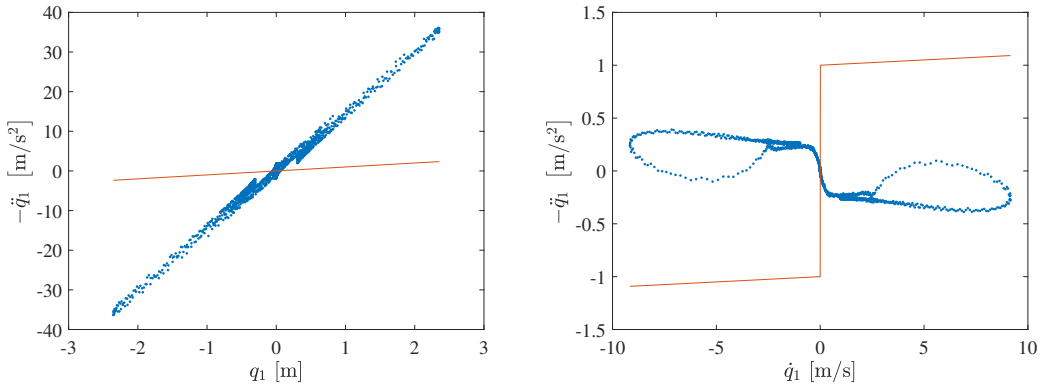

(a) Stiffness curve.

(b) Damping curve.

Figure 3.36: Stiffness and damping curves for the second mode of the 2 DOF system with Coulomb friction and for a forcing amplitude of 2 N. The curve obtained from the simulated measurements is shown in blue and the exact curve is depicted in orange.

As for all the other cases studied previously, the stiffness curve of the second mode is linear with a slope close to 15 $\left(\mathrm{m/s^2}\right)/\mathrm{m}$. The damping curve, on the other hand, has a different shape. There is a jump in acceleration at zero velocity, which is expected for Coulomb friction. However, when going from a negative to a positive velocity, $-\ddot{q}_1$ jumps from a positive to a negative value, which is the opposite of the Coulomb friction force indicated in orange. This is due to the stiffness force between DOFs 1 and 2, which is negative for positive velocities and positive for negative velocities. The linear parts of the curve result from the points occurring before the resonance and the loop is due to the points occurring after the resonance peak. The jump at zero velocity in the damping curve only appearing for Coulomb friction, it can be seen as an evidence for the presence of Coulomb friction in the system, although it does not correspond to the curve one might expect for Coulomb friction.

3.5 Second system with Coulomb friction

Another system with Coulomb friction is now studied. It is described by the system of equations

$$\begin{bmatrix} 0.1 & 0 \\ 0 & 1 \end{bmatrix} \begin{pmatrix} \ddot{q}_1 \\ \ddot{q}_2 \end{pmatrix} + 0.01 \begin{bmatrix} 2 & -1 \\ -1 & 2 \end{bmatrix} \begin{pmatrix} \dot{q}_1 \\ \dot{q}_2 \end{pmatrix} + \begin{bmatrix} 2 & -1 \\ -1 & 2 \end{bmatrix} \begin{pmatrix} q_1 \\ q_2 \end{pmatrix} + \begin{pmatrix} \mathrm{sign}\left(\dot{q}_1\right) \\ 0 \end{pmatrix} = \begin{pmatrix} 0 \\ p\left(t\right) \end{pmatrix}, \tag{3.12}$$

where the external force $p\left(t\right)$ consists of a sine sweep excitation with an amplitude of 5 N, a starting frequency of 0 Hz and an ending frequency of 1 Hz, the eigenfrequencies of the linear system being equal to 0.192 Hz and 0.721 Hz, and a sweep rate of 0.01 Hz/min. The acceleration time series of DOF 1 is depicted in Figure 3.37.

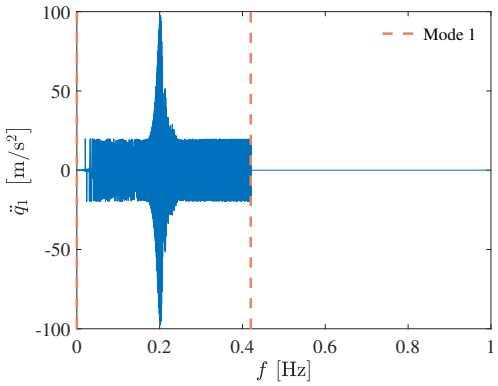

Figure 3.37: Acceleration of DOF 1 as a function of the excitation frequency of the second 2 DOF system with Coulomb friction and the frequency window of mode 1.

The second mode is not visible in the time series and the ASM therefore cannot be applied to this mode. At this mode, the motion of DOF 1 is very small since the forces between DOF 1 and the ground and between DOF 1 and DOF 2 act in opposite directions and are small. On the other hand, the first mode is easily detected and has a nonlinearity ratio of 75.6 %, indicating a strong nonlinear behaviour of the mode. It can also be observed that for lower and higher frequencies than the resonance frequency, the acceleration has a constant amplitude of around 20 m/s^2, which is due to the presence of Coulomb friction in the system.

Applying the method to the first mode, the stiffness and damping curves illustrated in Figure 3.38 are obtained.

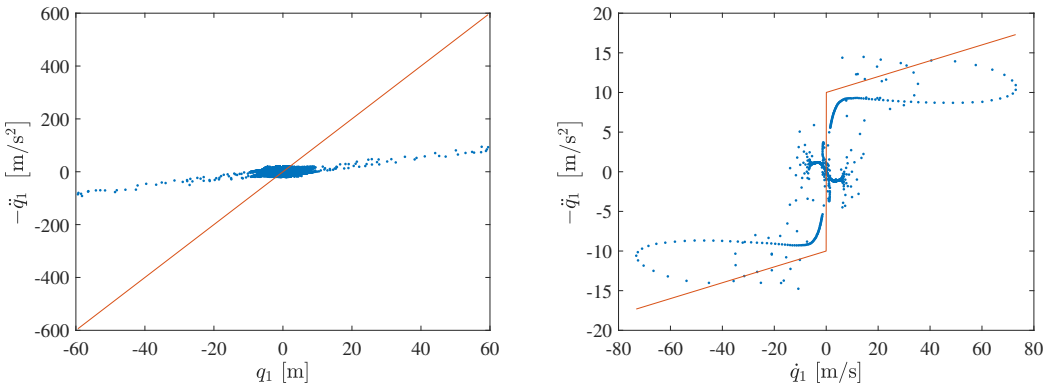

(a) Stiffness curve.

(b) Damping curve.

Figure 3.38: Stiffness and damping curves for the first mode of the second 2 DOF system with Coulomb friction and for a forcing amplitude of 5 N. The curve obtained from the simulated measurements is shown in blue and the exact curve is depicted in orange.

The presence of Coulomb friction can be deduced from the damping curve as there is a jump from negative to positive values of $-\ddot{q}_1$ as the velocity is equal to 0 m/s. The damping curve is thus close to the exact curve since the damping force between DOF 1 and the ground is large compared to the stiffness and damping forces between DOFs 1 and 2. This is due to the fact that q_2 is close to 0 m when $q_1 = 0$ m, such that the stiffness force $1 \times (q_1 - q_2)$ is small for the points of the damping curve. Additionally, the velocities of DOFs 1 and 2 are

also close to each other and the damping force between the two degrees of freedom is thus also small. For this system, the damping force between DOF 1 and the ground can therefore be correctly characterised using the acceleration surface method, which proved to be difficult for the other studied systems.

Furthermore, the stiffness curve is linear as expected, but has a lower slope than the theoretical curve. This is due to the stiffness force between DOFs 1 and 2, which is negative for a positive displacement of DOF 1, the displacement amplitude of DOF 2 being larger than the displacement amplitude of DOF 1.

3.6 Conclusion

The study of nonlinear 2 DOF systems has revealed a lot of different artefacts that may appear in the stiffness and damping curves and may cause problems for the accurate determination of the functional form of the nonlinear force. These can be the result of harmonic components appearing in the response of the system to the excitation or to specific dynamical regimes such as branch-point bifurcations. In particular, a cubic stiffness and a piecewise linear stiffness can produce similar stiffness curves, making the identification of the type of nonlinearity in the system challenging. Furthermore, the characterisation of the damping force is always difficult due to its small importance compared to the stiffness force.

One solution to improve the results when applying the acceleration surface method is to filter the measurement data to remove the contribution of the harmonics. This has proven to be useful to distinguish between a cubic and a piecewise linear stiffness, both resulting in a similar stiffness curve due to the presence of harmonics. In the case of the presence of several dynamical regimes in the response of the system, a careful selection of the dynamical regimes to take into account in the ASM can improve the stiffness curve by excluding those for which the obtained curves are not satisfactory. Finally, the choice of the resonance mode to which to apply the method is of crucial importance in order to get the best stiffness and damping curves. This will be highlighted more particularly in the next chapter, where 10 DOF systems will be studied.

Chapter 4

10 DOF systems

It has been shown in the previous chapter that different modes yield different stiffness and damping curves and that the nonlinearities are easier to characterise using one mode instead of another. In particular, for 2 DOF systems, the first mode, which is the in-phase mode, enables a better identification of the nonlinear force due to the lower stiffness and damping forces between both masses. The aim of this chapter is thus to analyse on systems with more vibration modes which of these modes results in the best stiffness and damping curves. Systems consisting of 10 degrees of freedom are therefore considered, having 10 vibration modes.

4.1 First system with a cubic stiffness

The system represented in Figure 4.1 is first studied. It has a cubic stiffness at the connection between DOF 5 and DOF 6, the degrees of freedom being numbered in the increasing order from the left to the right. The excitation consists of a sine sweep excitation with an amplitude of 0.2 N, a starting frequency of 0 Hz, an ending frequency of 0.35 Hz and a sweep rate of 0.001 Hz/min. The ending frequency has been chosen such as to detect all the modes of the system, the 10th mode of the linear system having a natural frequency of 0.338 Hz. Different excitation positions are considered to study their influence on the results.

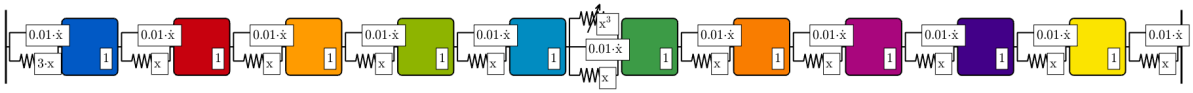

Figure 4.1: 10 DOF system with a cubic stiffness as represented in the NI2D software.

The equations of motion of the system are given by

$$\mathbf{M}\ddot{\mathbf{q}} + \mathbf{C}\dot{\mathbf{q}} + \mathbf{K}\mathbf{q} + \mathbf{f}_{\mathrm{nl}}(\mathbf{q}, \dot{\mathbf{q}}) = \mathbf{p}(t). \tag{4.1}$$

The response of the system to the excitation is simulated on the NI2D software using a Newmark integration scheme with a sampling frequency of 200 Hz, which is more than 200 times the highest frequency of the excitation of 0.35 Hz, $\gamma = \frac{1}{2}$ and $\beta = \frac{1}{4}$. The acceleration surface method is then applied in a similar way as for the 1 DOF and 2 DOF systems.

4.1.1 Excitation applied to DOF 1

The sine sweep excitation is applied to the first mass and the ASM is applied to all the modes in order to study the difference in the results between the different modes. Furthermore, the method is successively applied to the degrees of freedom 5 and 6 to analyse whether one extremity of the nonlinear connection yields better results than the other.

ASM applied to DOF 5

The ASM is first applied to DOF 5, for which the equation of motion can be expressed as

$$0.01\left(\dot{q}_5-\dot{q}_6\right)+\left(q_5-q_6\right)+\left(q_5-q_6\right)^3+0.01\left(\dot{q}_5-\dot{q}_4\right)+\left(q_5-q_4\right)=-\ddot{q}_5, \tag{4.2}$$

where q_i represents the displacement of the mass i.

The acceleration time series of DOF 5 is shown in Figure 4.2. The 10 modes of the system are visible in the time series and they are well separated from each other, although the four last modes are closer to each other than the other modes. The acceleration surface method can thus be applied to each of the modes separately.

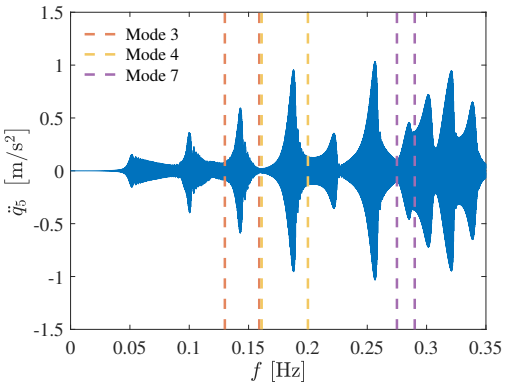

Figure 4.2: Acceleration of DOF 5 as a function of the excitation frequency of the 10 DOF system with a cubic stiffness and an excitation at DOF 1 and the frequency windows of modes 3, 4 and 7.

For 2 DOF systems, it has been shown that the best mode to which to apply the ASM corresponds to the mode for which the stiffness and damping forces of the linear connection are the smallest in comparison with the forces at the nonlinear connection. To verify that this observation holds true for more complex systems such as 10 DOF systems, the ratio between the root mean square (RMS) values of the relative displacements q_5-q_6 and q_5-q_4 is computed for each mode. It is then verified whether the mode with the highest ratio gives the best results. For all the modes, the displacement ratio

$$r_\mathrm{d}=\frac{\mathrm{RMS}\left(q_5-q_6\right)}{\mathrm{RMS}\left(q_5-q_4\right)} \tag{4.3}$$

is thus calculated and indicated in Table 4.1.

Mode	r_d [-]
1	0.382
2	1.13
3	0.335
4	4.54
5	0.525
6	0.994
7	1.79
8	0.774
9	1.15
10	0.526

Table 4.1: Displacement ratio of all the modes of the 10 DOF system with a cubic stiffness for which the excitation is applied to DOF 1 and the ASM is applied to DOF 5.

However, another important aspect regarding the selection of the best mode is the importance of the nonlinear force to the motion of the system. Indeed, for a cubic stiffness for example, if the relative displacement is too low, the nonlinear force will remain small and the system will be almost linear. The ASM should therefore not be applied to modes which are only weakly nonlinear. To identify the modes for which the nonlinearity is significantly activated, the time series of the acceleration for different forcing levels are compared. A shift in the resonance frequency of a mode towards a higher frequency indicates a nonlinear behaviour and thus enables to identify the nonlinear modes of the system. The acceleration time series of DOF 5 for different forcing amplitudes is represented in Figure 4.3.

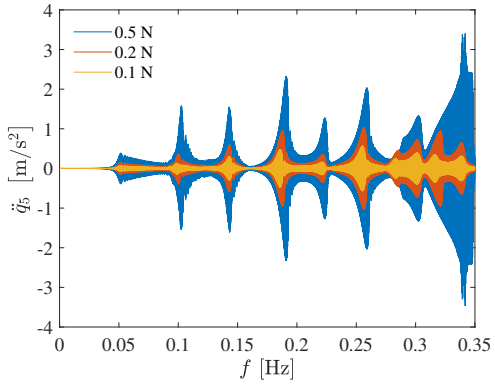

Figure 4.3: Acceleration of DOF 5 as a function of the excitation frequency of the 10 DOF system with a cubic stiffness and an excitation at DOF 1 with amplitudes of 0.1, 0.2 and 0.5 N.

The 4th mode is the mode for which the displacement ratio is the highest. Furthermore, this mode exhibits an increase in the resonance frequency as the forcing level increases, indicating a nonlinear behaviour of this mode. When analysing the displacements q_4, q_5 and q_6 at this mode, such as depicted in Figure 4.4, it can be seen that the masses 4 and 5 oscillate in phase while the mass 6 is out-of-phase compared to them. Furthermore, the displacement amplitudes of DOFs 4 and 5 are close to each other. The relative displacement between masses 4 and 5 is thus small in comparison with the relative displacement between masses 5 and 6, explaining

the high ratio. The nonlinear behaviour of this mode can be explained by the high relative displacement $q_5 - q_6$, which is maximum for this mode and for which the nonlinear force is not negligible.

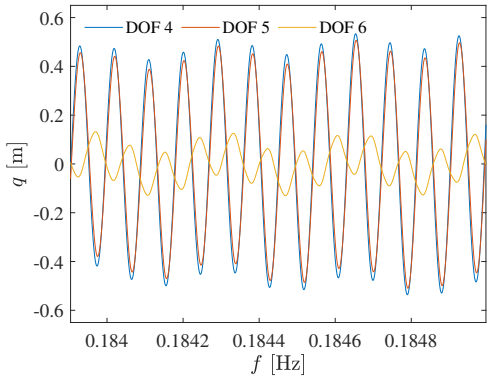

Figure 4.4: Displacement of DOFs 4, 5 and 6 as a function of the excitation frequency for the 4th mode of the 10 DOF system with a cubic stiffness and an excitation at DOF 1.

Applying the ASM to this mode, the stiffness and damping curves shown in Figure 4.5 are obtained.

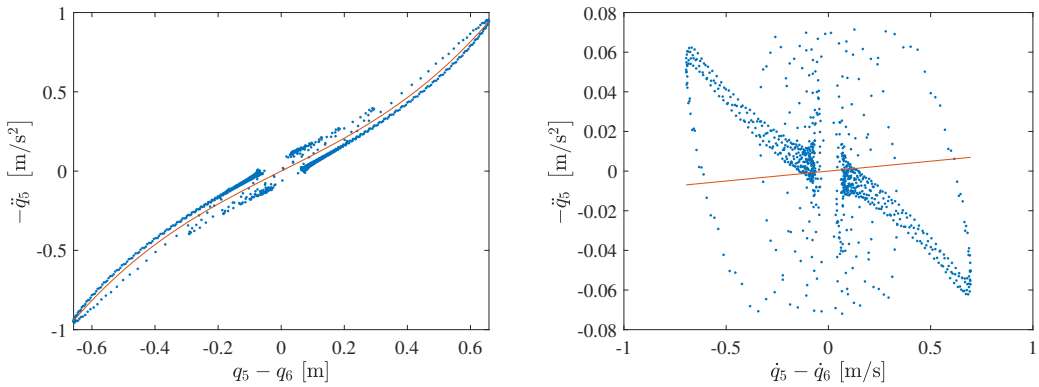

(a) Stiffness curve.

(b) Damping curve.

Figure 4.5: Stiffness and damping curves for the 4th mode of the 10 DOF system with a cubic stiffness and an excitation at DOF 1 and for which the ASM is applied to DOF 5. The curve obtained from the simulated measurements is shown in blue and the exact curve is depicted in orange.

The stiffness curve is close to the theoretical curve and has a cubic shape. This mode thus produces a good stiffness curve, as predicted by the ratio r_d and the analysis of the displacements illustrated in Figure 4.4. Among all the 10 vibration modes of the system, this mode results in the best stiffness curve. However, as in most previous cases, the damping curve does not allow the proper characterisation of the damping force of the nonlinear connection.

It can also be observed that both curves have similar features as those obtained for 2 DOF systems. Indeed, the damping curve consists of a set of points decreasing as the velocity increases before suddenly increasing at the resonance peak. The stiffness curve, on the other

hand, is composed of one line situated below the exact curve and one located above it for positive displacements. They are respectively due to the points before the resonance, for which q_4 has a greater amplitude than q_5, and the points after the resonance, for which q_5 has a greater amplitude than q_4.

Furthermore, some small oscillations are visible in the stiffness curve, which do not appear for 2 DOF systems. These oscillations are due to the presence of the harmonics 1/4 in the response of the system, as shown by the FFT of $\ddot{q}_5$ depicted in Figure 4.6.

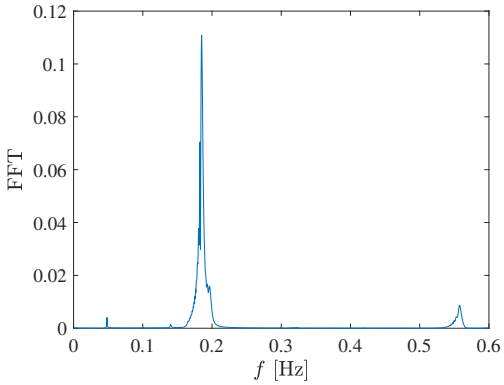

Figure 4.6: Fast Fourier transform of the acceleration of DOF 5 at the 4th mode of the 10 DOF system with a cubic stiffness and an excitation at DOF 1.

There is a small peak visible at 0.0483 Hz, which is close to the natural frequency of the first mode, which is equal to 0.0482 Hz. It thus results from a 1:4 modal interaction of mode 4 with the first mode of the system. A third order harmonics is also detected with the FFT, with a higher amplitude than the harmonics 1/4. However, this third order harmonic component is not responsible for the oscillations of the stiffness curve. Indeed, using a high-pass filter to only remove the harmonics 1/4, the oscillations of the stiffness curve disappear and the damping curve is also improved, as illustrated in Figure 4.7.

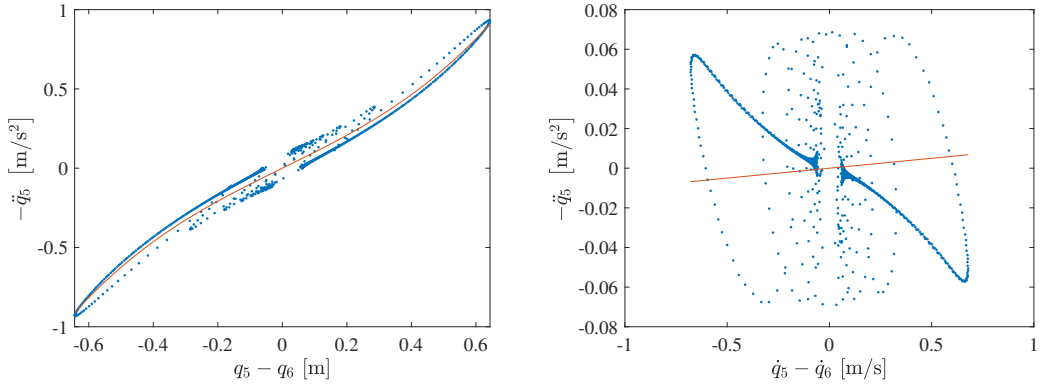

(a) Stiffness curve. (b) Damping curve.

Figure 4.7: Stiffness and damping curves for the 4th mode of the 10 DOF system with a cubic stiffness and an excitation at DOF 1 and for which the ASM is applied to DOF 5 obtained after filtering the data. The curve obtained from the simulated measurements is shown in blue and the exact curve is depicted in orange.

According to Table 4.1, another mode which may yield a good stiffness curve is the 7th mode, for which the displacement ratio is high compared to the other modes and a shift in the resonance frequency is clearly visible. At this mode, the degrees of freedom 4 and 5 vibrate in phase, although there is a small phase delay for DOF 5, while the degree of freedom 6 is out-of-phase. However, the difference in amplitude between q_4 and q_5 is larger than at mode 4. The stiffness and damping curves for this mode are shown in Figure 4.8.

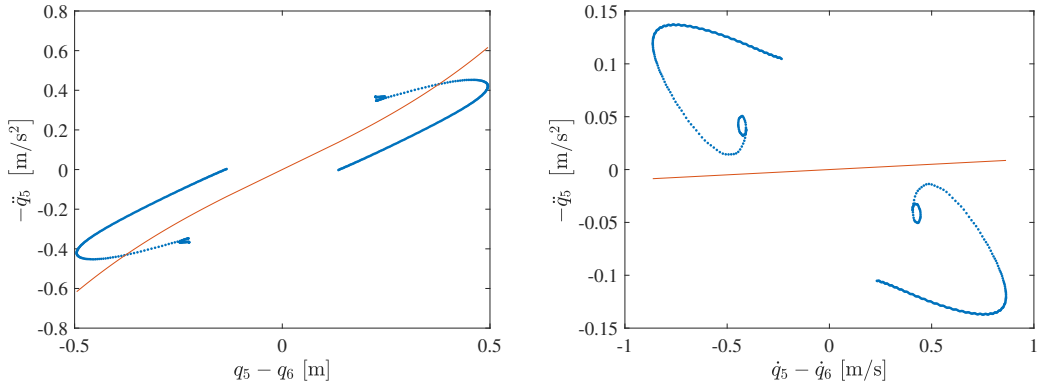

(a) Stiffness curve.

(b) Damping curve.

Figure 4.8: Stiffness and damping curves for the 7th mode of the 10 DOF system with a cubic stiffness and an excitation at DOF 1 and for which the ASM is applied to DOF 5. The curve obtained from the simulated measurements is shown in blue and the exact curve is depicted in orange.

The stiffness curve does not exactly follow the theoretical curve, although it remains close to it due to the small stiffness force between DOFs 1 and 2 compared to the stiffness force between DOF 1 and the ground. The cubic nature of the stiffness force therefore cannot be deduced from it. The other modes producing less good results, the 4th mode is the only one which can be used to determine the functional form of the stiffness force between DOF 5 and DOF 6. Some oscillations are again visible in the damping curve and the FFT of $\ddot{q}_5$ reveals some frequency content at the frequency of the first mode. The use of a high-pass filter removes these oscillations. In fact, such oscillations can also be detected at modes 5, 6, 8, 9 and 10. These oscillations thus occur for mode 4 and all the modes higher than mode 4. They are always due to a modal interaction with the first mode and can be removed by applying a high-pass filter to the data.

Now considering mode 3 for which DOFs 5 and 6 are in phase while being out-of-phase with DOF 4, the displacement ratio is the lowest for this mode. The stiffness and damping curves of this mode are indicated in Figure 4.9.

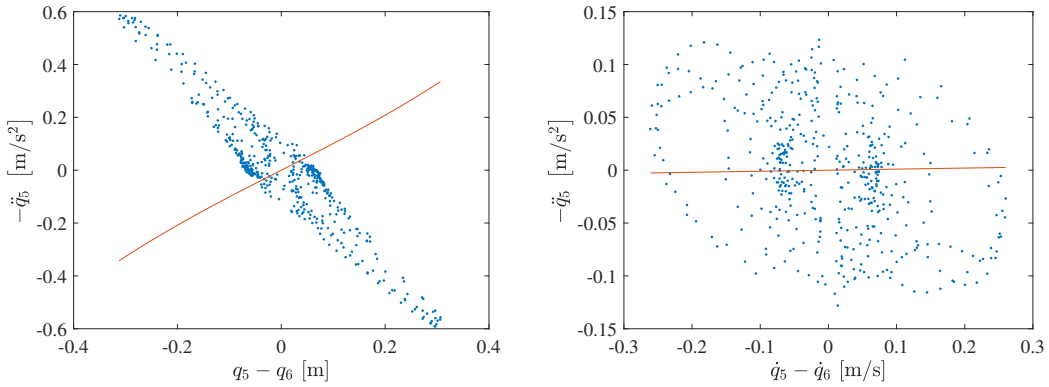

(a) Stiffness curve.

(b) Damping curve.

Figure 4.9: Stiffness and damping curves for the third mode of the 10 DOF system with a cubic stiffness and an excitation at DOF 1 and for which the ASM is applied to DOF 5. The curve obtained from the simulated measurements is shown in blue and the exact curve is depicted in orange.

As expected, the stiffness and damping curves do not correspond at all to the theoretical curves. The stiffness curve decreases as the relative displacement increases, which could be interpreted as a negative stiffness between degrees of freedom 5 and 6. The choice of the mode to select for using the ASM is thus of crucial importance in order to correctly characterise the nonlinearity.

ASM applied to DOF 6

The acceleration surface method is now applied to DOF 6, in order to study the influence on the results of the choice of the degree of freedom to which the method is applied. The equation of motion of DOF 6 is given by

$$0.01\left(\dot{q}_6 - \dot{q}_5\right) + \left(q_6 - q_5\right) + \left(q_6 - q_5\right)^3 + 0.01\left(\dot{q}_6 - \dot{q}_7\right) + \left(q_6 - q_7\right) = -\ddot{q}_6. \tag{4.4}$$

The stiffness and damping forces at the connection between the masses 6 and 7 now appear in the equation, while the forces between masses 4 and 5 are present when the ASM is applied to DOF 5. The computation of the displacement ratio r_d is thus adapted accordingly. Its values for all the 10 modes are indicated in Table 4.2. The comparison between the time series of $\ddot{q}_6$ for different forcing levels is illustrated in Figure 4.10.

Mode	r_d [-]
1	0.718
2	0.859
3	0.565
4	0.947
5	0.603
6	1.25
7	0.779
8	1.63
9	1.03
10	1.91

Table 4.2: Displacement ratio of all the modes of the 10 DOF system with a cubic stiffness for which the excitation is applied to DOF 1 and the ASM is applied to DOF 6.

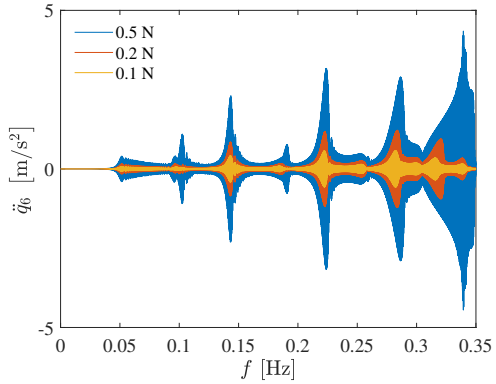

Figure 4.10: Acceleration of DOF 6 as a function of the excitation frequency of the 10 DOF system with a cubic stiffness and an excitation at DOF 1 with amplitudes of 0.1, 0.2 and 0.5 N.

Mode 8 has a high displacement ratio, but a low shift in the resonance frequency, indicating that the nonlinearity is not significantly activated for this mode. Applying the ASM to this mode thus does not allow the identification of the cubic nature of the stiffness force between degrees of freedom 5 and 6. While modes 4 and 6 have a good displacement ratio, they also do not enable the correct characterisation of the nonlinear force. Indeed, the only mode at which the cubic nature of the stiffness force is visible is the 9th mode. At this mode, the degrees of freedom 5 and 7 are in phase and the degree of freedom 6 is out-of-phase. However, there is a small phase delay for DOF 5 and the amplitude of q_7 is smaller than that of q_5, resulting in a relative displacement $q_6 - q_7$ which is smaller than $q_6 - q_5$, but not negligible. The small difference between $q_6 - q_7$ and $q_6 - q_5$ explains why the displacement ratio is only slightly higher than 1. The displacements of the DOFs 5, 6 and 7 at mode 9 are represented in Figure 4.11.

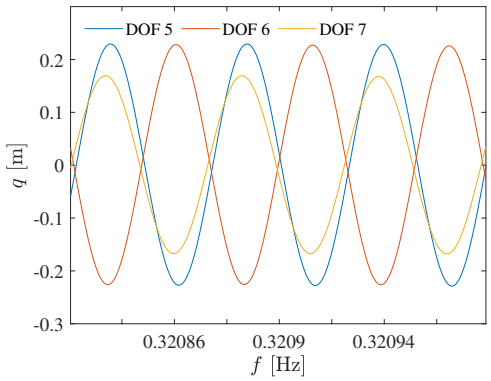

Figure 4.11: Displacement of DOFs 5, 6 and 7 as a function of the excitation frequency for the 9th mode of the 10 DOF system with a cubic stiffness and an excitation at DOF 1.

The stiffness and damping curves obtained for this mode are illustrated in Figure 4.12.

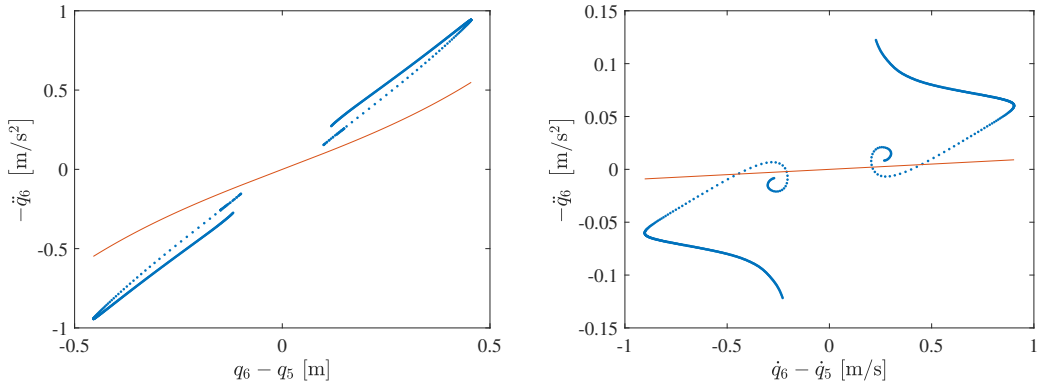

(a) Stiffness curve.

(b) Damping curve.

Figure 4.12: Stiffness and damping curves for the 9th mode of the 10 DOF system with a cubic stiffness and an excitation at DOF 1 and for which the ASM is applied to DOF 6. The curve obtained from the simulated measurements is shown in blue and the exact curve is depicted in orange.

The stiffness curve does not follow the theoretical curve and two different lines are visible. Similarly as for Figure 4.5a, the presence of these distinct lines is due to the fact that at the resonance peak, the amplitude of q_7 becomes larger than the amplitude of q_6 while it is smaller before the resonance peak is reached. The stiffness curve seems to be almost linear, but there is a small curvature visble at the highest displacement amplitude, indicating the presence of a cubic stiffness. There is no other mode for which the resulting stiffness curve is cubic.

4.1.2 Excitation applied to DOF 4

The sine sweep excitation is now applied to DOF 4, the other parameters of the excitation remaining unchanged. The ASM is again applied to DOF 5 and DOF 6 and to all the modes.

ASM applied to DOF 5

The acceleration surface method is first applied to DOF 5. The displacement ratios of the 10 modes are indicated in Table 4.3. The comparison between the time series of the acceleration of DOF 5 for different forcing levels is illustrated in Figure 4.13.

Mode	r_d **[-]**
1	0.293
2	0.614
3	0.460
4	3.13
5	0.392
6	1.51
7	1.41
8	0.875
9	1.51
10	0.461

Table 4.3: Displacement ratio of all the modes of the 10 DOF system with a cubic stiffness for which the excitation is applied to DOF 4 and the ASM is applied to DOF 5.

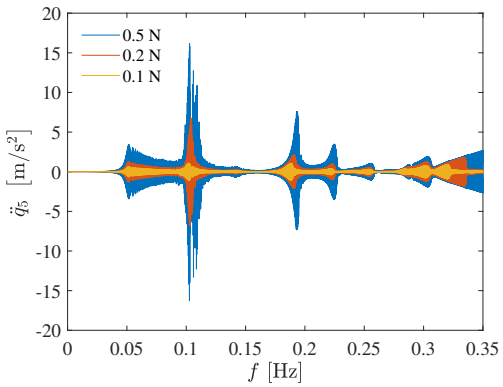

Figure 4.13: Acceleration of DOF 5 as a function of the excitation frequency of the 10 DOF system with a cubic stiffness and an excitation at DOF 4 with amplitudes of 0.1, 0.2 and 0.5 N.

Mode 4 has again the best displacement ratio and a significant shift in the resonance frequency as the forcing amplitude increases. It thus corresponds to the mode for which the expression of the nonlinear stiffness force is the easiest to determine. The stiffness and damping curve obtained for this mode are depicted in Figure 4.14.

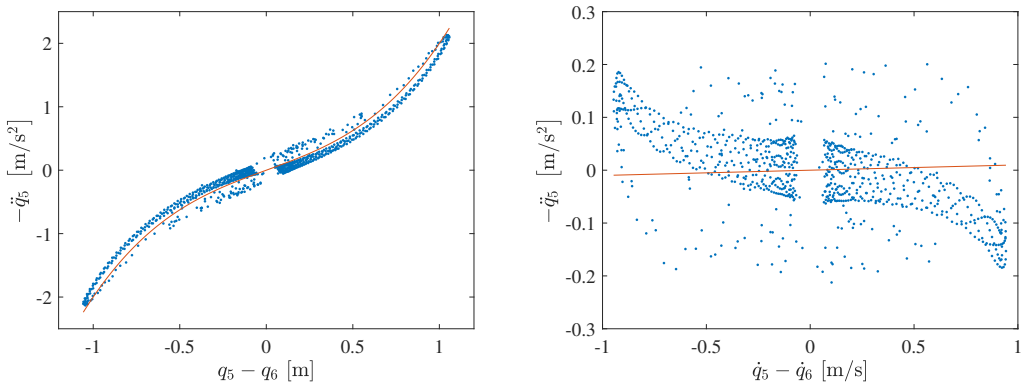

(a) Stiffness curve.

(b) Damping curve.

Figure 4.14: Stiffness and damping curves for the 4th mode of the 10 DOF system with a cubic stiffness and an excitation at DOF 4 and for which the ASM is applied to DOF 5. The curve obtained from the simulated measurements is shown in blue and the exact curve is depicted in orange.

Both curves are similar to those depicted in Figure 4.5, obtained for a forcing at DOF 1. However, the maximum values of the relative displacement and velocity and of the acceleration are higher, such that the cubic shape of the stiffness curve is more visible, which facilitates the characterisation of the nonlinearity. The higher amplitude of motion of this mode compared to the case of an excitation applied to DOF 1 can be explained by the fact that this mode is more excited for a force applied to DOF 4 than for a force applied to DOF 1. Furthermore, some oscillations are again present in the curves due to the presence of the harmonics 1/4. They can be removed by applying a high-pass filter to the data.

Another mode for which the ASM produces good results is the second mode. Indeed, although the displacement ratio is not very high, the analysis of the acceleration time series reveals a strong nonlinear behaviour. Furthermore, the amplitude of the relative displacement $q_5 - q_6$ and of the acceleration $\ddot{q}_5$ are maximum for this mode. The stiffness and damping curve obtained for this mode are shown in Figure 4.15.

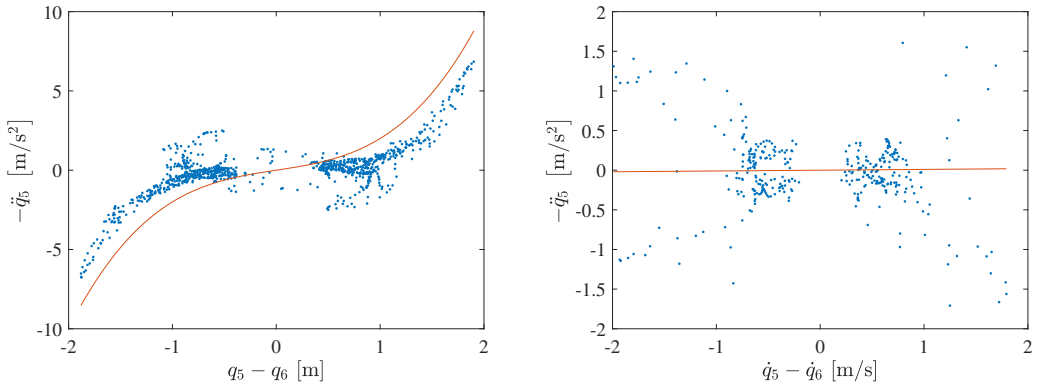

(a) Stiffness curve. (b) Damping curve.

Figure 4.15: Stiffness and damping curves for the second mode of the 10 DOF system with a cubic stiffness and an excitation at DOF 4 and for which the ASM is applied to DOF 5. The curve obtained from the simulated measurements is shown in blue and the exact curve is depicted in orange.

The cubic nature of the stiffness force can be deduced from the stiffness curve. However, similarly as for 2 DOF systems with a cubic stiffness, there is a separation of the curve in two distinct branches at a relative displacement of approximately -0.9 and 0.9 m. This is again due to the presence of harmonics in the response of the system. Since there are both harmonics of higher order and the harmonics 1/2, both a low-pass and a high-pass filter have to be successively applied to the data. The stiffness and damping curves obtained when filtering the data is represented in Figure 4.16.

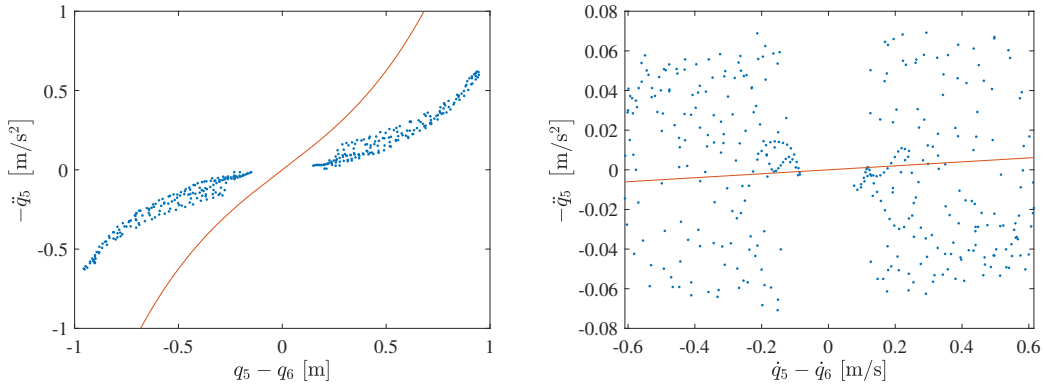

(a) Stiffness curve. (b) Damping curve.

Figure 4.16: Stiffness and damping curves for the second mode of the 10 DOF system with a cubic stiffness and an excitation at DOF 4 and for which the ASM is applied to DOF 5 obtained after filtering the data. The curve obtained from the simulated measurements is shown in blue and the exact curve is depicted in orange.

The different branches of the stiffness curve have disappeared and the curve is cubic, although it does not correspond to the theoretical curve. Once again, filtering the data before applying the acceleration surface method proves to be a good solution to improve the stiffness curve. On the other hand, the damping curve is still difficult to interpret.

An additional mode for which the functional form of the stiffness force may be found from the stiffness curve is the 9th mode. However, the cubic shape is less clearly visible as for modes 2 and 4, but it is more easy to identify as when the excitation is applied to DOF 1, for which the stiffness curve is shown in Figure 4.12a. While there is only one mode for which the cubic nature of the stiffness force between DOFs 5 and 6 can be identified when applying the excitation to DOF 1, there are three modes when applying the forcing to DOF 4. This highlights the influence of the position of the excitation on the results of the ASM.

ASM applied to DOF 6

The acceleration surface method is now applied to DOF 6. The displacement ratio

$$r_{\mathrm{d}} = \frac{\mathrm{RMS}\left(q_6 - q_5\right)}{\mathrm{RMS}\left(q_6 - q_7\right)} \tag{4.5}$$

is computed for each mode and indicated in Table 4.4.

Mode	r_{d} **[-]**
1	0.569
2	0.471
3	0.699
4	0.657
5	0.525
6	2.31
7	0.776
8	1.67
9	1.07
10	2.15

Table 4.4: Displacement ratio of all the modes of the 10 DOF system with a cubic stiffness for which the excitation is applied to DOF 4 and the ASM is applied to DOF 6.

Despite its low displacement ratio, mode 2 is the mode for which the resulting stiffness curve is the best. Similarly as when the ASM is applied to DOF 5, it can be explained by the high amplitude of $q_6 - q_7$ and $\ddot{q}_6$ at this mode. The stiffness and damping curves for the second mode are illustrated in Figure 4.17.

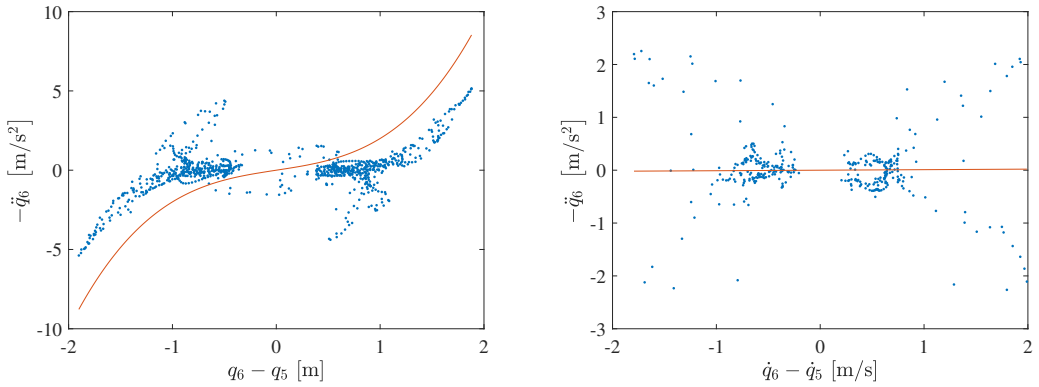

(a) Stiffness curve. (b) Damping curve.

Figure 4.17: Stiffness and damping curves for the second mode of the 10 DOF system with a cubic stiffness and an excitation at DOF 4 and for which the ASM is applied to DOF 6. The curve obtained from the simulated measurements is shown in blue and the exact curve is depicted in orange.

Both curves are similar to those obtained for the same mode when the ASM is applied to DOF 5. The stiffness curve is cubic, but there is the presence of two branches, one at the positive displacements and one at the negative displacements. These branches are more visible in this case than in Figure 4.15a. They are again due to the presence of harmonics. Applying a low-pass and a high-pass filter to remove all the harmonics and only keep the fundamental frequency, the stiffness and damping curves in Figure 4.18 are obtained.

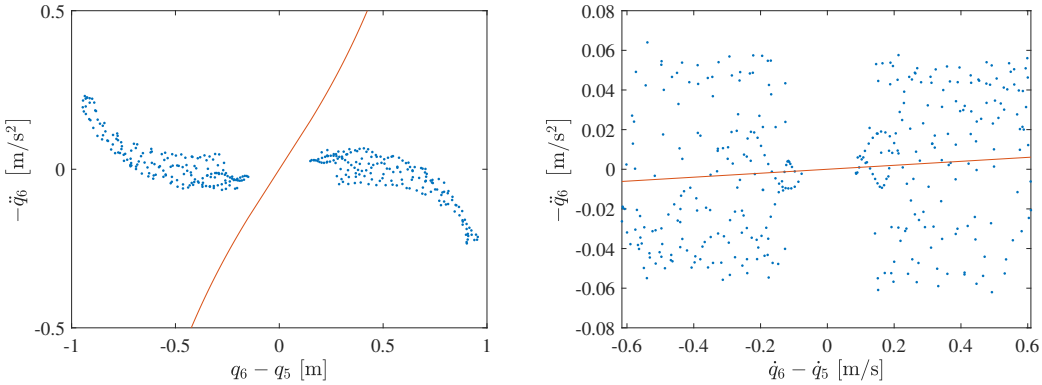

(a) Stiffness curve. (b) Damping curve.

Figure 4.18: Stiffness and damping curves for the second mode of the 10 DOF system with a cubic stiffness and an excitation at DOF 4 and for which the ASM is applied to DOF 6 obtained after filtering the data. The curve obtained from the simulated measurements is shown in blue and the exact curve is depicted in orange.

It can be seen that the stiffness curve is not composed of different branches anymore and has a cubic shape. However, unlike in Figure 4.16a, the cubic coefficient seems to be negative while it is in reality positive. The nonlinearity could thus be considered as a softening nonlinearity while it is actually hardening. This is due to the stiffness force between masses 6 and 7, which makes the stiffness curve decrease as the relative displacement increases. As the

acceleration surface method only intends at finding the functional form of the nonlinear force and not at determining its coefficients, the method could still provide useful information with such a stiffness curve, the correct cubic coefficient being afterwards determined accurately with a parameter estimation technique.

Despite their low displacement ratios, modes 5, 7 and 9 are also good candidates to apply the ASM as the stiffness curves exhibit a slightly cubic curve and are similar to the curve depicted in Figure 4.12a. Applying the excitation to DOF 4, there are thus again more modes for which the stiffness curve is cubic than when applying the excitation to DOF 1 and the ASM to DOF 6.

On the other hand, modes 6, 8 and 10, which have the highest displacement ratios, do not produce stiffness curves from which the cubic expression of the stiffness force can be recognised. For these modes, the curve is close to the theoretical curve, which can be explained by the high displacement ratio, the stiffness force of the nonlinear connection being high compared to that of the linear connection neglected in the ASM. As the neglected force is small, the curve is close to the exact curve obtained from the expression of the stiffness force of the nonlinear connection. However, the stiffness curve has a different shape and is not cubic due to the neglected forces that are small but not null. This is illustrated for mode 6 in Figure 4.19.

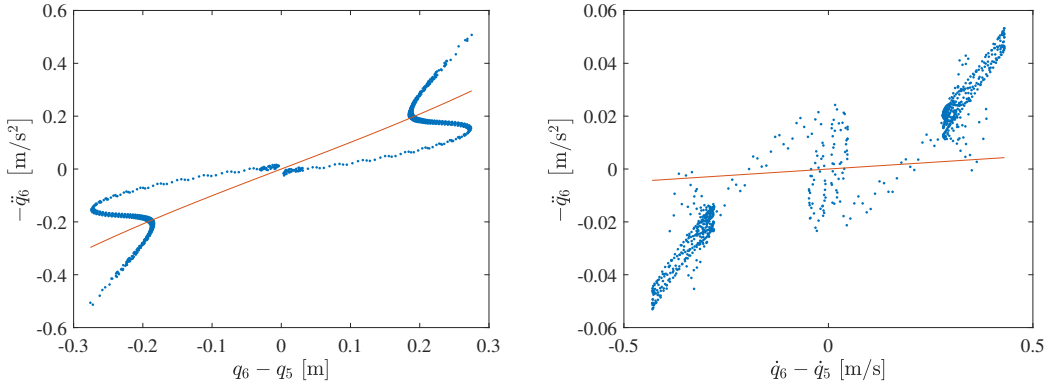

(a) Stiffness curve.

(b) Damping curve.

Figure 4.19: Stiffness and damping curves for the 6th mode of the 10 DOF system with a cubic stiffness and an excitation at DOF 4 and for which the ASM is applied to DOF 6. The curve obtained from the simulated measurements is shown in blue and the exact curve is depicted in orange.

The unexpected shape of the stiffness curve for these three modes may be explained by the fact that they cannot be clearly detected in the time series of the acceleration of DOF 6 as they are close to the previous mode, which also has a larger amplitude. These modes may therefore be impacted by the other modes, creating these stiffness and damping curves. The acceleration time series of DOF 6 and the frequency windows of modes 6, 8 and 10 used for the ASM are shown in Figure 4.20.

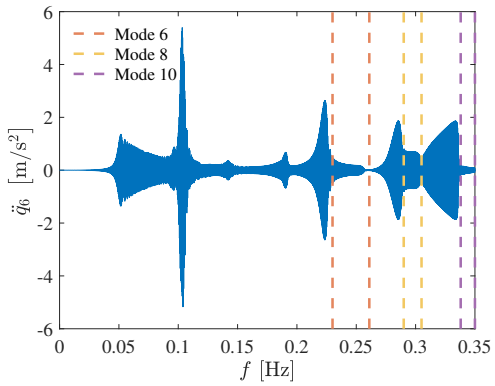

Figure 4.20: Acceleration of DOF 6 as a function of the excitation frequency of the 10 DOF system with a cubic stiffness and an excitation at DOF 4 and the frequency windows of modes 6, 8 and 10.

4.2 Second system with a cubic stiffness

Another system is now considered whose nonlinearity also consists of a cubic stiffness at the connection between DOFs 5 and 6. The stiffness coefficients on one side of the nonlinear connection are all equal to 1 N/m and are equal to 10 N/m on the other side. One side of the nonlinear connection thus has a higher stiffness than the other. This may occur in real-life structures for which the connection between two substructures may exhibit nonlinear characteristics [2, 10, 11]. Each of the two substructures being made of different materials and having a different geometry, they have a different stiffness, such that one side of the nonlinearity often has a higher stiffness than the other. The studied system is represented in Figure 4.21.

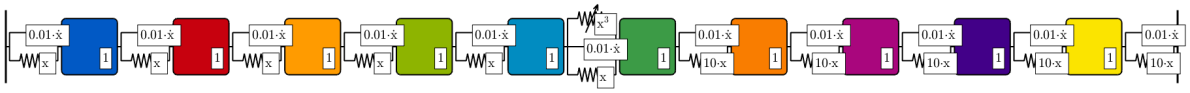

Figure 4.21: Second 10 DOF system with a cubic stiffness as represented in the NI2D software.

A sine sweep excitation is applied to the system having an amplitude of 0.2 N, a starting frequency of 0 Hz, an ending frequency of 1 Hz, which is higher than the frequency of the 10th linear mode equal to 0.966 Hz, and a sweep rate of 0.001 Hz/min. The parameters of the Newmark integration scheme are $\gamma = \frac{1}{2}$ and $\beta = \frac{1}{4}$ and the sampling frequency is equal to 200 Hz, which is 200 times the highest frequency of the excitation.

4.2.1 Excitation applied to DOF 4

The forcing is first applied to DOF 4 as this showed to provide good results for the previous 10 DOF system. The ASM is applied to the degrees of freedom 5 and 6 and to all the modes. The time series of the acceleration of DOFs 5 and 6 are depicted in Figure 4.22.

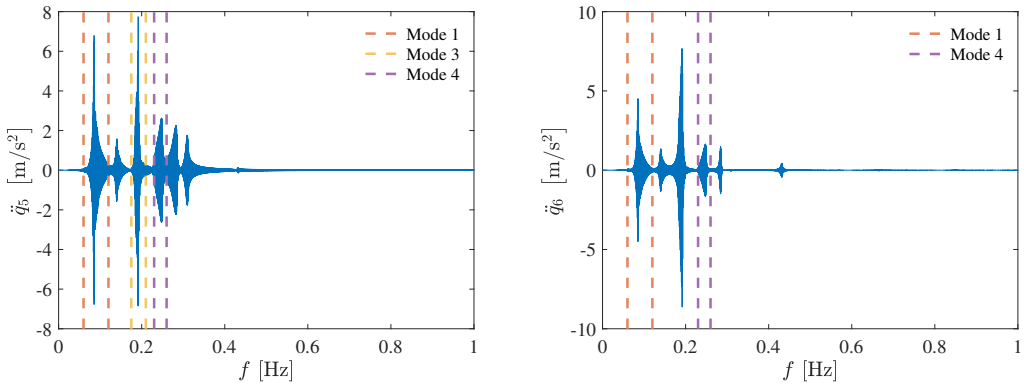

(a) DOF 5. (b) DOF 6.

Figure 4.22: Acceleration of DOF 5 and DOF 6 as a function of the excitation frequency of the second 10 DOF system with a cubic stiffness and an excitation applied to DOF 4 and the frequency windows of the studied modes.

At both degrees of freedom, the first seven modes can be detected, although mode 6 has a small amplitude at DOF 6 and mode 7 has a small amplitude at DOF 5. However, the modes 8, 9 and 10 have such a small amplitude that they are difficult to identify in the time series. The ASM can therefore not be applied to these modes, as the frequency band of a mode needs to be determined from the time series before applying the method to the data of this frequency band. Additionally, at such small amplitudes, the modes behave linearly and are therefore of little interest for the ASM.

ASM applied to DOF 5

The acceleration surface method is first applied to DOF 5 and to mode 1. The resulting stiffness and damping curves are illustrated in Figure 4.23.

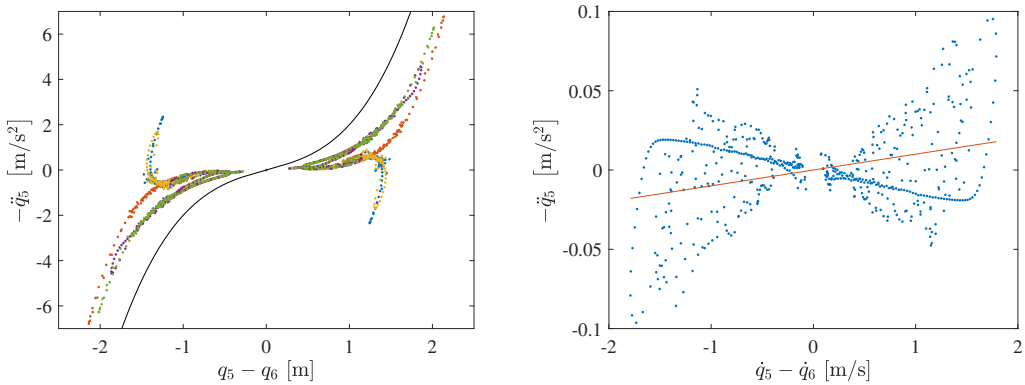

(a) Stiffness curve. The different pairs of lines are represented in different colours and the exact curve is depicted in black.

(b) Damping curve. The curve obtained from the simulated measurements is shown in blue and the exact curve is depicted in orange.

Figure 4.23: Stiffness and damping curves for the first mode of the second 10 DOF system with a cubic stiffness and an excitation at DOF 4 and for which the ASM is applied to DOF 5.

It can be seen that the stiffness curve is composed of 5 different pairs of lines indicated in different colours, which are due to the 5 maxima and 5 minima per period. These extrema are due to the presence of harmonic components, such as the harmonics of third and fifth order, in the response of the system to the excitation and can be seen in Figure 4.24. Three of these lines have a positive value of $-\ddot{q}_5$ for a positive relative displacement and are due to the three maxima for which $q_5 - q_6$ is positive, the two other lines corresponding to the two minima for which the relative displacement is positive. These different pairs of lines separate the stiffness curve in two different parts for which the value of $-\ddot{q}_5$ has opposite signs, making it more difficult to analyse the curve. This is similar to what can also be encountered for 2 DOF systems. While there are several extrema of the relative displacement per period, it is equal to 0 m at only two points, one for which the relative velocity is positive and one for which it is negative. The damping curve is therefore not composed of different curves such as the stiffness curve. Applying a low-pass filter to remove the harmonic components, the obtained stiffness and damping curves are shown in Figure 4.25.

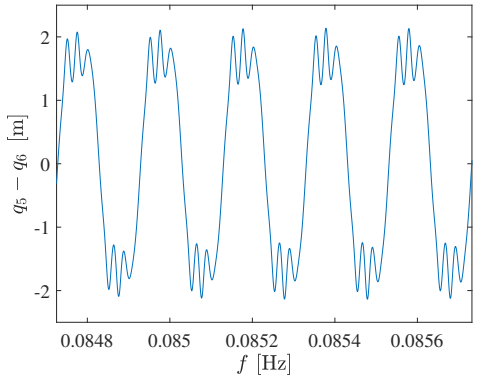

Figure 4.24: Relative displacement $q_5 - q_6$ as a function of the excitation frequency for the first mode of the second 10 DOF system with a cubic stiffness and an excitation at DOF 4.

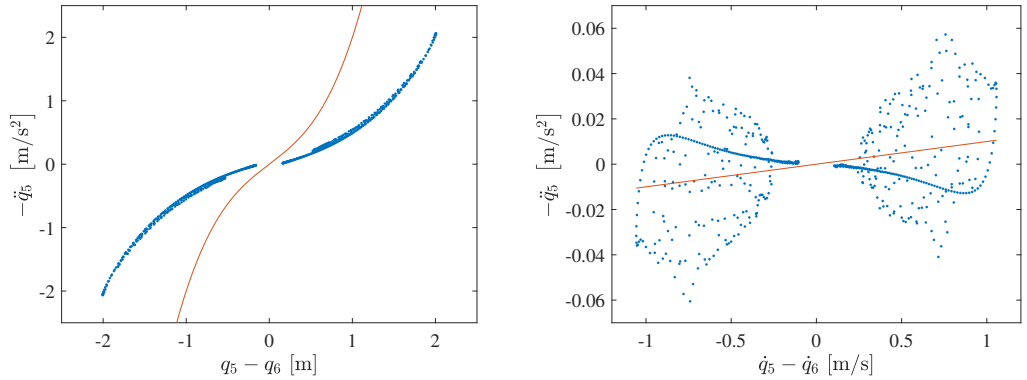

(a) Stiffness curve.

(b) Damping curve.

Figure 4.25: Stiffness and damping curves for the first mode of the second 10 DOF system with a cubic stiffness and an excitation at DOF 4 and for which the ASM is applied to DOF 5 obtained after filtering the data. The curve obtained from the simulated measurements is shown in blue and the exact curve is depicted in orange.

Filtering the data before applying the ASM improves the stiffness curve, as it is now cubic and not composed of different lines. It is thus easier to interpret the curve and deduce from it the cubic nature of the stiffness force between DOFs 5 and 6, although it does not correspond to the exact curve. However, applying a filter does not improve the damping curve, which remains impossible to interpret.

Applying the ASM to DOF 5 and to the other modes, it can be concluded that modes 3 and 4 also produce cubic stiffness curves, which are however less good than that of mode 1 obtained after filtering the data.

ASM applied to DOF 6

The ASM is now applied to DOF 6. When considering the first mode, the stiffness curve is similar to the curve obtained when the ASM is applied to DOF 5. However, at small relative displacements when the curve is not separated in different curves, the curve is decreasing as the relative displacement increases. This is due to the stiffness force between the masses 6 and 7, which decreases as the relative displacement $q_6 - q_5$ increases. Using a low-pass filter to remove the harmonic components, the resulting stiffness curve is cubic such as the one represented in Figure 4.25a, but it seems to have a negative cubic coefficient, such as in Figure 4.18a. This is again due to the linear stiffness force between DOFs 6 and 7, which decreases as a cubic function of the relative displacement $q_6 - q_5$, as depicted in Figure 4.26. A similar reasoning explains the stiffness curve shown in Figure 4.18a.

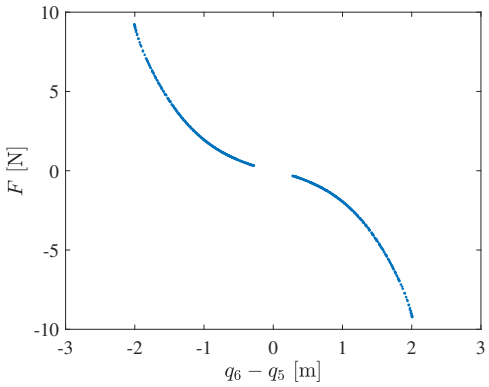

Figure 4.26: Stiffness force between DOFs 6 and 7 as a function of the relative displacement $q_6 - q_5$ for the first mode of the second 10 DOF system with a cubic stiffness and an excitation at DOF 4 and for which a low-pass filter has been used.

Applying the acceleration surface method to mode 4, the obtained stiffness and damping curves are depicted in Figure 4.27.

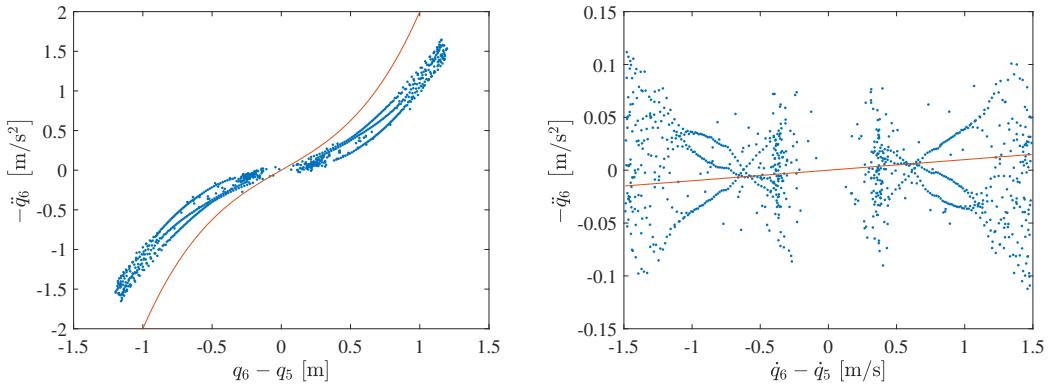

(a) Stiffness curve. (b) Damping curve.

Figure 4.27: Stiffness and damping curves for the 4th mode of the second 10 DOF system with a cubic stiffness and an excitation at DOF 4 and for which the ASM is applied to DOF 6. The curve obtained from the simulated measurements is shown in blue and the exact curve is depicted in orange.

Both in the stiffness curve and in the damping curve, three distinct curves can be observed for small relative displacements and velocities. They are due to the presence of the harmonics 3 and 1/3 in the response of the system to the excitation, the presence of the harmonics of third order being due to a 3:1 modal interaction with mode 8, as indicated by the frequency-energy plots represented in Figure 4.28.

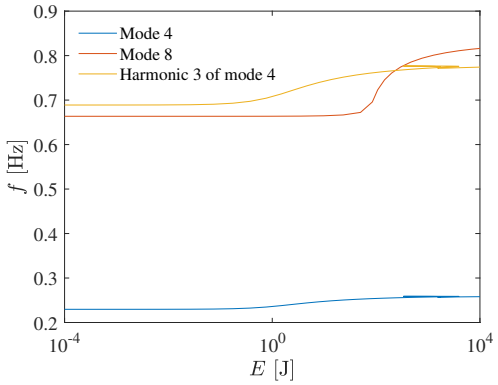

Figure 4.28: Frequency-energy plots of the nonlinear normal modes 4 and 8 of the second 10 DOF system with a cubic stiffness as well as the third harmonics of mode 4.

These harmonics create small variations in amplitude of the maxima of the relative displacement, such as already illustrated for another system in Figure 4.4. As these oscillations are small, the different curves resulting from the different maxima, for the stiffness curve, and the different zeros, for the damping curve, are close to each other, unlike in cases for which there are stronger harmonic components creating additional maxima. As these different lines result from harmonic components, a low- and a high-pass filter are applied to the data to remove all the harmonic components. The obtained stiffness and damping curves are shown in Figure 4.29.

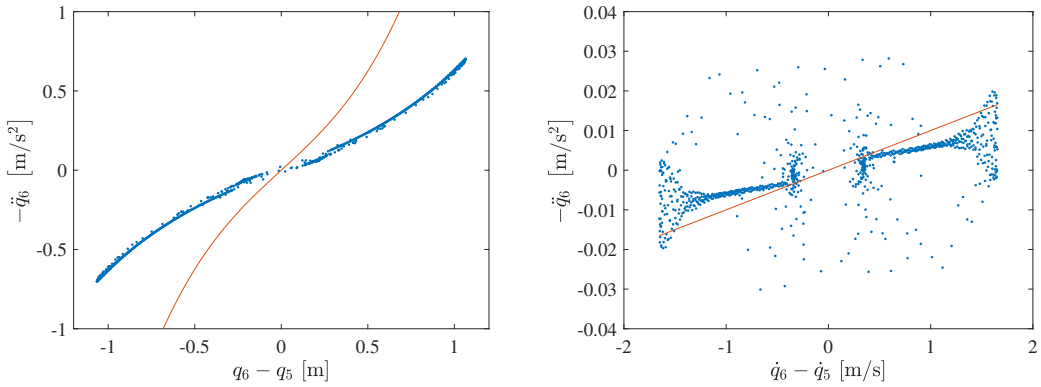

(a) Stiffness curve. (b) Damping curve.

Figure 4.29: Stiffness and damping curves for the 4th mode of the second 10 DOF system with a cubic stiffness and an excitation at DOF 4 and for which the ASM is applied to DOF 6 obtained after filtering the data. The curve obtained from the simulated measurements is shown in blue and the exact curve is depicted in orange.

4.2.2 Excitation applied to DOF 7

The sine sweep excitation is now applied to DOF 7, which is situated in the part of the system with the highest stiffness. The time series of the acceleration of DOFs 5 and 6 are depicted in Figure 4.30.

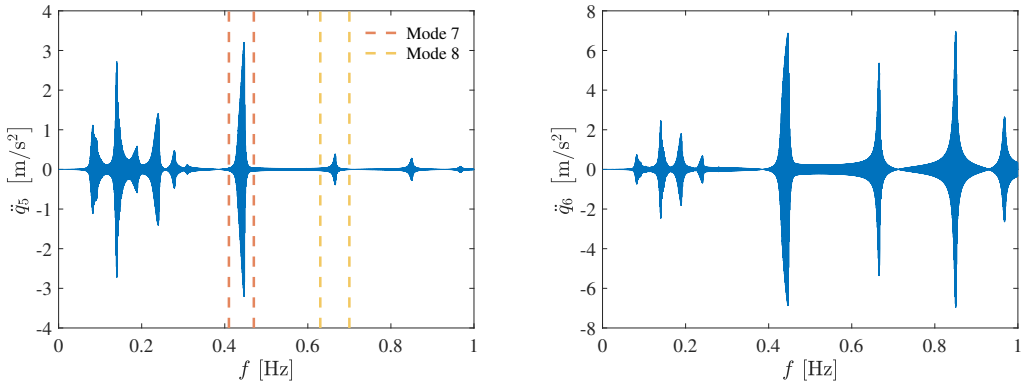

(a) DOF 5. (b) DOF 6.

Figure 4.30: Acceleration of DOF 5 and DOF 6 as a function of the excitation frequency of the second 10 DOF system with a cubic stiffness and an excitation at DOF 7 and the frequency windows of the studied modes.

While for an excitation at DOF 4, modes 8, 9 and 10 were not detectable and mode 7 was only weakly visible, these modes can now easily be detected in both time series. The ASM can therefore be applied to these modes. On the other hand, modes 5 and 6 cannot be detected in the time series of $-\ddot{q}_6$.

The acceleration surface method is applied to DOF 5 and to mode 7. The resulting stiffness and damping curves are illustrated in Figure 4.31.

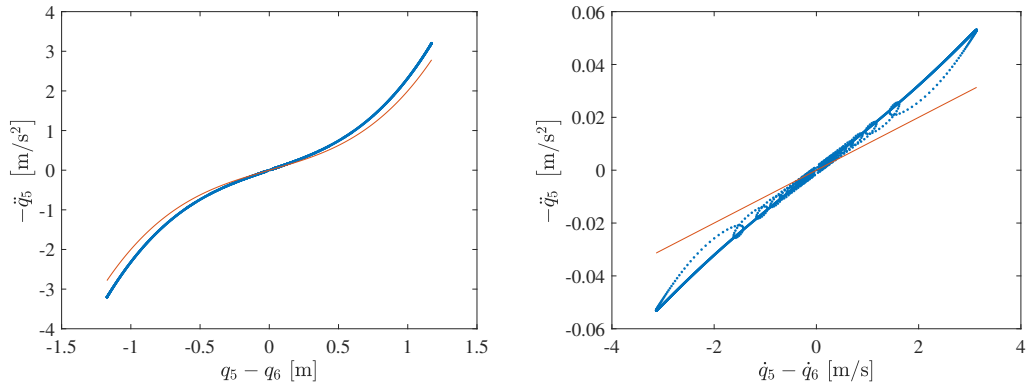

(a) Stiffness curve. (b) Damping curve.

Figure 4.31: Stiffness and damping curves for the 7th mode of the second 10 DOF system with a cubic stiffness and an excitation at DOF 7 and for which the ASM is applied to DOF 5. The curve obtained from the simulated measurements is shown in blue and the exact curve is depicted in orange.

The stiffness curve is cubic and close to the theoretical curve and the damping curve is linear as it should be. However, the damping curve does not exactly correspond to the theoretical curve obtained from the analytical expression of the damping force between DOFs 5 and 6. Furthermore, some loops can be observed around the linear part of the damping curve. These loops are due to the beating phenomenon occurring after the main resonance peak. Despite these loops in the damping curve, this mode allows the correct identification of the functional forms of both the stiffness and the damping force between DOFs 5 and 6, the stiffness force being cubic and the damping force being linear.

The ASM is now applied to mode 8. The stiffness and damping curves obtained for this mode are represented in Figure 4.32.

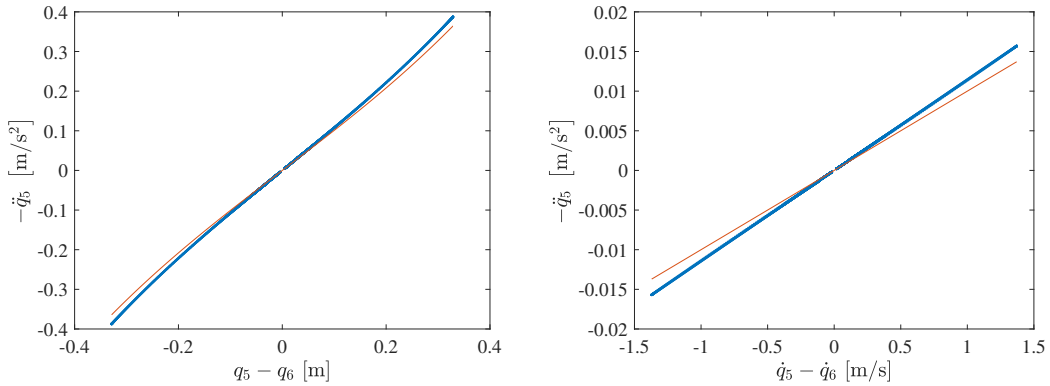

(a) Stiffness curve. (b) Damping curve.

Figure 4.32: Stiffness and damping curves for the 8th mode of the second 10 DOF system with a cubic stiffness and an excitation at DOF 7 and for which the ASM is applied to DOF 5. The curve obtained from the simulated measurements is shown in blue and the exact curve is depicted in orange.

Both the stiffness curve and the damping curve are close to the theoretical curve. However,

due to the small relative displacement $q_5 - q_6$ at this mode, the stiffness curve is only weakly cubic and may be mistaken for a linear stiffness curve. The determination of the cubic nature of the stiffness force is thus more difficult when applying the ASM to mode 8 than when applying it to mode 7. On the other hand, the damping curve is closer to the theoretical curve than the damping curve of mode 7 and the loops in the curve are less visible, although still present. The linear expression of the damping force can thus be recognised from this mode, but not the cubic expression of the stiffness force.

The fact that the damping curve is linear and close to the theoretical curve is due to the stiffness force between DOFs 4 and 5 which is small for mode 8. Indeed, the damping curve corresponds to the points for which the relative displacement $q_5 - q_6$ is equal to zero and thus $q_5 = q_6$, both displacements being close to 0 m. The degrees of freedom 4, 5 and 6 reaching 0 at almost the same moment, meaning that they are perfectly in phase, respectively out-of-phase, the displacement of DOF 4 is also close to q_5 when $q_5 = q_6$, such that the stiffness force $1 \times (q_5 - q_4)$ is small and only has a small influence on the damping curve, while it is larger for other modes. Similar observations with linear stiffness and damping curves can also be made for modes 9 and 10. Applying the ASM to DOF 6 does not produce a linear damping curve for any mode, such that the nonlinear connection cannot be accurately characterised.

4.3 Coulomb friction

A 10 DOF system with Coulomb friction is considered in this section. The system is similar to the system studied in Section 4.2, the cubic stiffness force being replaced by Coulomb friction with an intensity of 0.1 N located at the connection between the masses 5 and 6. The forcing again consists of a sine sweep excitation with an amplitude of 0.2 N, a starting frequency of 0 Hz, an ending frequency of 1 Hz and a sweep rate of 0.001 Hz/min. The parameters of the Newmark integration scheme are the same as previously. As the damping curve yields good results for the system in Section 4.2 and an excitation applied to DOF 7, the forcing is again applied to DOF 7.

4.3.1 ASM applied to DOF 5

The ASM is applied to DOF 5 and mode 8, as this results in good stiffness and damping curves for the previous system. The stiffness and damping curves are depicted in Figure 4.33.

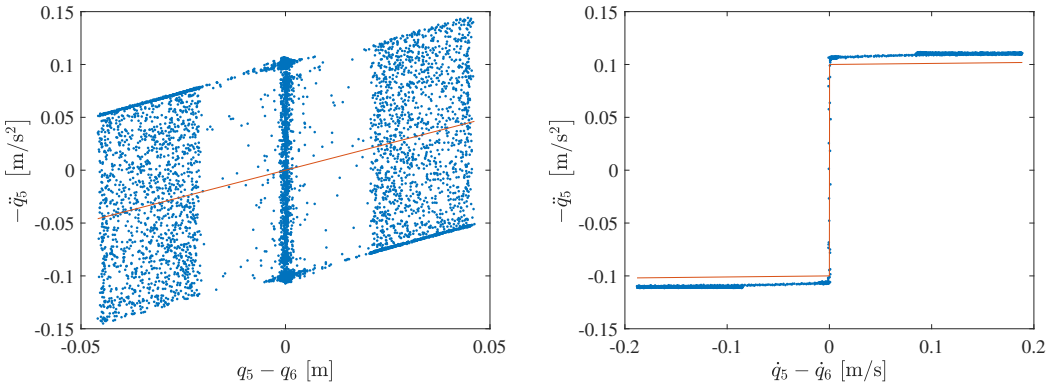

(a) Stiffness curve.

(b) Damping curve.

Figure 4.33: Stiffness and damping curves for the 8th mode of the 10 DOF system with Coulomb friction and an excitation at DOF 7 and for which the ASM is applied to DOF 5. The curve obtained from the simulated measurements is shown in blue and the exact curve is depicted in orange.

The damping curve is close to the theoretical curve and the presence of Coulomb friction in the system can be deduced from it, as the jump in $-\ddot{q}_5$ at zero relative velocity is clearly visible. Similarly as for the previous system, this is due to the low stiffness force between DOFs 4 and 5 at the points of the damping curve, which is only responsible for a small increase in amplitude of $-\ddot{q}_5$ in the damping curve. On the other hand, the points composing the stiffness curve are not concentrated on a line, but a linearly increasing trend can be seen. Indeed, all the points of the curve seem bounded by an upper and a lower limit, which are both linearly increasing with the same slope as the theoretical curve. Furthermore, these limits are located 0.1 m/s^2 above, respectively below, the exact curve. This is due to the Coulomb friction, having an intensity of 0.1 N, thus creating an acceleration of 0.1 m/s^2, the mass of DOF 5 being equal to 1 kg. As the points of the stiffness curve are obtained through linear interpolation, they are not always situated on the lower or upper limit, but are always located between them. The distribution of the points is thus not due to the linear stiffness and damping forces between DOFs 4 and 5, but to the discontinuity in the damping force between DOFs 5 and 6 resulting from the presence of Coulomb friction. Similar stiffness and damping curves are obtained for modes 9 and 10.

4.3.2 ASM applied to DOF 6

The ASM is now applied to DOF 6 and mode 9. The stiffness and damping curves are shown in Figure 4.34.

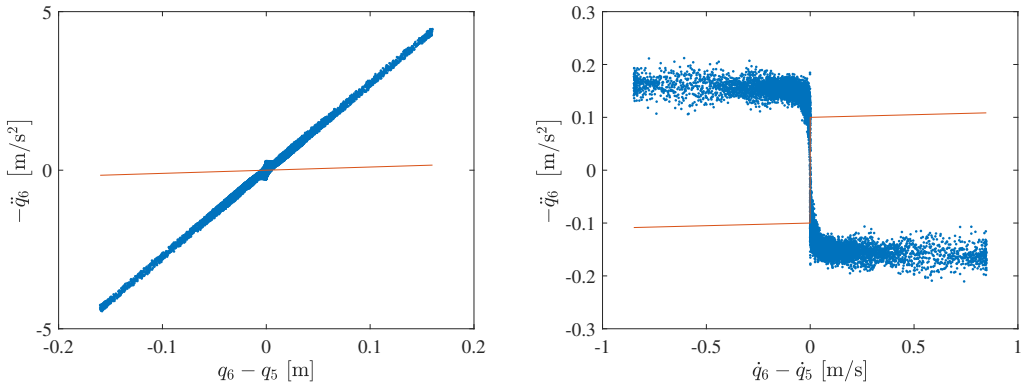

(a) Stiffness curve.

(b) Damping curve.

Figure 4.34: Stiffness and damping curves for the 9th mode of the 10 DOF system with Coulomb friction and an excitation at DOF 7 and for which the ASM is applied to DOF 6. The curve obtained from the simulated measurements is shown in blue and the exact curve is depicted in orange.

A jump can be seen in the damping curve. However, as the relative velocity becomes positive, $-\ddot{q}_6$ jumps from a positive to a negative value, while it should be the opposite. A similar behaviour has already been observed in Chapter 1 for a stiffness curve obtained from experimental measurements on an F-16 aircraft. The shape of the damping curve is mainly due to the stiffness force between DOFs 6 and 7. Indeed, the representation of this stiffness force as a function of the relative velocity $\dot{q}_6 - \dot{q}_5$ at the points of the damping curve is almost identical to the actual damping curve, the difference being mainly due to the Coulomb friction having an amplitude of 0.1 N. This is illustrated in Figure 4.35.

The stiffness curve is linear, but with a higher slope than the theoretical curve. This is again due to the stiffness force between DOFs 6 and 7, the masses 6 and 7 oscillating perfectly out-of-phase, resulting in a linear stiffness curve with a higher slope than it should. Such stiffness curves have already been encountered at the out-of-phase mode of 2 DOF systems.

Similar stiffness and damping curves can also be observed for modes 8 and 10.

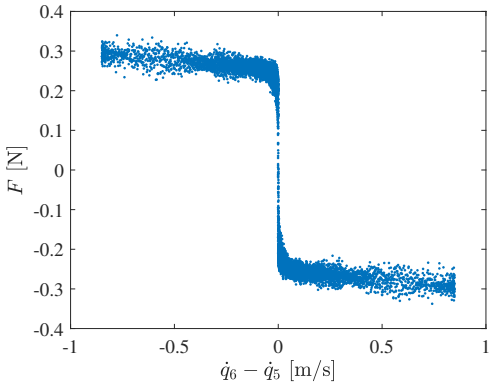

Figure 4.35: Stiffness force between DOFs 6 and 7 as a function of the relative velocity $\dot{q}_6 - \dot{q}_5$ for the 9th mode of the 10 DOF system with Coulomb friction and an excitation at DOF 7.

4.4 Cubic stiffness and Coulomb friction

Since the functional form of both the stiffness and the damping force can be correctly identified using the ASM for the previous systems with only a cubic stiffness or only Coulomb friction, a system with both a cubic stiffness and Coulomb friction is now considered. Such a system with both a nonlinear stiffness and Coulomb friction can also be encountered in real-life structures [10]. The system is the same as in Section 4.2 to which Coulomb friction with an intensity of 0.1 N has been added between DOFs 5 and 6. A sine sweep excitation with a starting frequency of 0 Hz, an ending frequency of 1 Hz and a sweep rate of 0.001 Hz/min is applied to DOF 7, as this enables an accurate characterisation of both the stiffness and the damping force of the nonlinear connection. The forcing amplitude is equal to 1 N, such that both the cubic stiffness and the Coulomb friction are not negligible with respect to the linear force terms. Applying the ASM to DOF 5 and to mode 8 as for the system with only Coulomb friction, the stiffness and damping curves depicted in Figure 4.36 are obtained.

The stiffness curve is cubic and a jump at zero relative velocity can be seen in the damping curve, indicating the presence of Coulomb friction. Both the cubic stiffness and the Coulomb friction can thus be identified from the curves, leading to an accurate characterisation of the nonlinear forces.

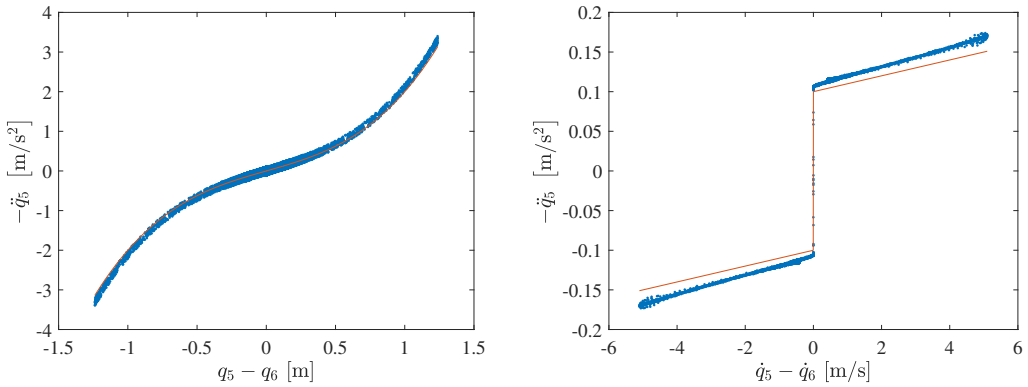

(a) Stiffness curve. (b) Damping curve.

Figure 4.36: Stiffness and damping curves for the 8th mode of the 10 DOF system with a cubic stiffness and Coulomb friction and an excitation at DOF 7 and for which the ASM is applied to DOF 5. The curve obtained from the simulated measurements is shown in blue and the exact curve is depicted in orange.

4.5 Conclusion

It has been demonstrated that the choice of the mode used in the acceleration surface method is of high importance, as only some modes allow the accurate characterisation of the nonlinear force. In particular, the modes for which the relative displacements of the linear connections of the degree of freedom to which the ASM is applied are low with respect to those of the nonlinear connection are of high interest for the acceleration surface method. These modes mostly correspond to modes for which the degrees of freedom at each extremity of the nonlinear connections vibrate out-of-phase while those of the linear connections oscillate in phase

and have a similar amplitude. On the other hand, the considered modes also need to have a nonlinear behaviour in order to determine the expression of the nonlinear forces.

Furthermore, the selection of the extremity of the nonlinear connection to which to apply the method also influences the results, as different modes should be considered depending on the selected degree of freedom. One of these degrees of freedom may also yield better results and simplify the characterisation of the nonlinearity. The selection of the location at which to apply the excitation is also of crucial importance, as the activation of the modes depends on the position of the force on the structure, some excitation positions enabling a correct characterisation of the stiffness and damping forces and others not.

Oscillations in the stiffness and damping curves have been detected, resulting from a modal interaction with the first mode of the system. These oscillations can easily be removed by using a high-pass filter. It has also been shown that the presence of harmonics of higher order can have an influence on the stiffness and damping curves, but the curves can be improved by applying a low-pass filter to the data.

Chapter 5

Conclusion

The acceleration surface method has been applied to 1 DOF, 2 DOF and 10 DOF systems with different types of nonlinearities, such as a cubic stiffness, a trilinear stiffness and Coulomb friction. The systems were subjected to sine sweep excitations at different forcing levels. The response of the system was obtained through numerical integration using a Newmark integration scheme on the NI2D software.

It has been shown that the ASM works well for the characterisation of the stiffness force of the nonlinear connection while the characterisation of the damping force remains a difficult task. Nonetheless, some artefacts may appear in the stiffness curve as well as in the damping curve which may complicate the determination of the functional forms of the stiffness and damping forces. These artefacts can result from the presence of harmonics in the response of the system to the external force. These harmonics especially appear at some dynamical regimes, such as superharmonic resonances or modal interactions. This may even lead to similar stiffness and damping curves for different types of nonlinearities, making the characterisation of the nonlinear force more challenging. One solution to improve the results and enable a better characterisation of the nonlinearity is to filter the measurement data in order to remove the harmonic components. This method has proven to work well for the identification of the stiffness force.

Finally, the choice of the degree of freedom and the mode to which to apply the ASM is of crucial importance, as the results can significantly differ between modes and the considered degrees of freedom. In particular, modes for which the relative displacement of the nonlinear connection is large in comparison with the relative displacement of the linear connection are of high interest for the ASM. Such modes mostly correspond to modes for which the extremities of the nonlinear connection oscillate out-of-phase, while those of the linear connection have a similar amplitude and vibrate in phase. The importance of the position where the force is applied to the structure has also been highlighted.

In some future work, it might be worth trying to improve the results obtained with the acceleration surface method for experimental measurements on a real-life structure by filtering the measurement data, as this proved to work well for numerical simulations of simple systems. Furthermore, it could be investigated in more details why the method works well to characterise the damping force in some cases, but not in others, and why the quality of the results strongly depends on the location of the external force applied to the system and the degree of freedom to which the method is applied.

Bibliography

[1] G. Kerschen, K. Worden, A.F. Vakakis, and J.C. Golinval. "Past, present and future of nonlinear system identification in structural dynamics". In: *Mechanical Systems and Signal Processing* 20 (2006), pp. 505–592.

[2] J.P. Noël, L.Renson, and G. Kerschen. "Complex dynamics of a nonlinear aerospace structure: Experimental identification and modal interactions". In: *Journal of Sound and Vibration* 333 (2014), pp. 2588–2607.

[3] J.P. Noël and G. Kerschen. "Nonlinear system identification in structural dynamics: 10 more years of progress". In: *Mechanical Systems and Signal Processing* 83 (2017), pp. 2–35.

[4] T. Dossogne, L. Masset, B. Peeters, and J.P. Noël. "Nonlinear dynamic model upgrading and updating using sine-sweep vibration data". In: *Proceedings of the Royal Society A* 475 (2019).

[5] G. Kerschen and G. Raze. *Nonlinear vibrations of aerospace structures - Lecture notes*. University of Liège, 2024.

[6] K. Worden. "Data processing and experiment design for the restoring force surface method, part I: integration and differentiation of measured time data". In: *Mechanical Systems and Signal Processing* 4 (1990), pp. 295–319.

[7] S.F. Masri and T.K. Caughey. "A Nonparametric Identification Technique for Nonlinear Dynamic Problems". In: *Journal of Applied Mechanics* 46 (1979), pp. 433–447.

[8] D. Anastasio, S. Marchesiello, G. Gatti, P.J.P. Gonçalves, A.D. Shaw, and M.J. Brennan. "An investigation into model extrapolation and stability in the system identification of a nonlinear structure". In: *Nonlinear Dynamics* 111 (2023), pp. 17653–17665.

[9] U. Gogilan, A. Oveisi, and T. Nestorović. "Detection and characterization of local nonlinearity in a clamped-clamped beam with state space realization". In: *Proceedings in Applied Mathematics and Mechanics* 23 (2023).

[10] T. Dossogne, J.P. Noël, L. Masset, G. Kerschen, and B. Peeters. "Understanding and Modeling Nonlinear Behaviors in Aerospace Structures using Sine-Sweep Testing". In: *AerospaceLab Journal* 14 (2018).

[11] G. Kerschen, M. Peeters, J.C. Golinval, and C. Stéphan. "Nonlinear Modal Analysis of a Full-Scale Aircraft". In: *Journal of Aircraft* 50 (2013), pp. 1409–1419.

[12] T. Dossogne, P. Trillet, M. Schoukens, B. Bernay, J.P. Noël, and G. Kerschen. "Nonlinearities of an Aircraft Piccolo Tube: Identification and Modeling". In: *Model Validation and Uncertainty Quantification, Volume 3*. Springer International Publishing, 2019, pp. 57–59.

[13] J.P. Noël, G. Kerschen, and A. Newerla. “Application of the Restoring Force Surface Method to a Real-life Spacecraft Structure”. In: *Topics in Nonlinear Dynamics, Volume 3*. Springer New York, 2012, pp. 1–19.

[14] J.P.Noël and M. Schoukens. *F-16 Aircraft Benchmark Based on Ground Vibration Test Data*. 2020. URL: https://data.4tu.nl/articles/dataset/F-16_Aircraft_Benchmark_Based_on_Ground_Vibration_Test_Data/12954911/1.

[15] K. Worden. “Data processing and experiment design for the restoring force surface method, part II: choice of excitation signal”. In: *Mechanical Systems and Signal Processing* 4 (1990), pp. 321–344.

[16] NOLISYS. *NI2D*. URL: https://nolisys.com/?page_id=97.

[17] N.M. Newmark. “A method of computation for structural dynamics”. In: *Journal of the Engineering Mechanics Division* 85 (1959), pp. 67–94.

[18] M. Géradin and D.J. Rixen. *Mechanical Vibrations: Theory and Application to Structural Dynamics*. 3rd ed. John Wiley & Sons Ltd, 2015. ISBN: 978 1 118 90020 8.

[19] G. Duffing. *Erzwungene Schwingungen bei veränderlicher Eigenfrequenz und ihre technische Bedeutung*. Vieweg, Braunschweig, 1918.

[20] K. Worden and G.R. Tomlinson. *Nonlinearity in structral dynamics: Detection, Identification and Modelling*. Institute of Physics Publishing, Bristol and Philadelphia, 2001. ISBN: 0 7503 0356 5.

[21] T. Detroux, J.P. Noël, L.N. Virgin, and G. Kerschen. “Experimental study of isolas in nonlinear systems featuring modal interactions”. In: *PLOS ONE* 13 (2018), pp. 1–25.